

Chapter 9

Medical Applications of X-Ray Nanochemistry



All living things have inertia too – once they start, it is hard to stop

9.1 Introduction

Medical applications have been the central theme of X-ray nanochemistry from the very beginning. Prior to the conception of the idea of using nanoparticles to improve X-ray imaging or radiotherapy, many efforts had been given to studying how to increase radiation effects using various materials. One of the most noticeable therapeutic efforts involving ionizing radiation and new materials was Auger therapy using iodine labeled nucleotides such as IUdR, as discussed by Kasis [1]. However, the enthusiasm of employing IUdR quickly dissipated after the first wave of demonstrations using nanomaterials to improve radiotherapy that began in 2004 and 2005, and little happened until a recent theoretical work by Ye et al. [2] showed that it is possible to combine Auger therapy with X-ray nanochemistry. Other therapeutic methods, such as proton therapy using boron species, will not be discussed here, though it is perceivable that discoveries made within X-ray nanochemistry will help these methods as well.

The original idea of using nanomaterials to enhance radiotherapy was straightforward, meaning no special care was needed except for passively mixing nanoparticles with, or delivering them to, targets that receive X-ray irradiation. The first account on record describing X-ray enhancement through the use of nanomaterials in medical applications was an ACS annual meeting report in August 2004 by Guo [3] in which the phrase “nanoparticle-enhanced X-ray therapy” (NEXT) was mentioned. Guo [4] used the same term in a patent application. The first publication of using nanoparticles under X-ray irradiation to improve the effectiveness of X-rays was contributed by Hainfeld et al. [5], who reported the first case of using gold nanoparticles to treat tumors in mice. Their patent was issued in 2009, with the priority date set in 1998; the earlier date was more than a decade after the authors had been exploring gold nanoparticles as a transmission electron microscope contrast agent. The work by Hainfeld et al. made a clear and strong case

of supporting the concept of nanoparticle-enhanced X-ray therapy. Based on the idea proposed by Guo in 2001, Guo et al. [6] published their result in early 2005 using strand breaks of plasmid DNA as the reporter reaction to measure enhanced damage to supercoiled plasmid DNA molecules in the presence of gold nanoparticles irradiated with X-rays. The original intention of works by Hainfeld et al. and Guo et al. was to use relatively simple nanomaterials (i.e., first-generation nanomaterials in Roco's NNI definition [7]) to increase X-ray absorption and improve the efficacy of radiotherapy for cancer treatment. It is fair to say that these works marked the beginning of X-ray nanochemistry research, even though X-ray nanochemistry was not formally established until about 8 years later.

In the medical field, the most direct way to prove that a method or a drug can effectively destroy cancer cells without lethal side effects is to run clinical trials. However, it is difficult to do so for new ideas like nanomaterial-assisted or nanomaterial-enhanced X-ray therapy. This is because the therapeutic method, as it stood a decade ago, was too primitive and was far from being understood, let alone optimized. A more appropriate approach would be to first carry out careful work in chemistry and biology laboratories to assure that materials or methods are optimized before performing animal studies. In this sense, what Hainfeld et al. did as described in their first publication of using small gold nanoparticles to increase the efficacy of X-ray treatment of cancerous mice was both premature and revolutionary because such a novel idea was never tested anywhere, not even in a chemistry research lab. The idea was only proposed starting in 2001 by Guo and no work was done in chemistry laboratories until 2003. However, as Chap. 2 shows, a relatively simple calculation would suggest that there should be detectable physical enhancement with a sufficient amount of gold in the target volume. If one has enough experience working with nanomaterials in animals, then a biological experiment using the animal model seemed reasonable.

In reality and as shown in Chaps. 2, 3, 4, and 5, even the enhancement to the yield of a relatively simple chemical reaction can be quite complex to understand, let alone damaging cells or treating tumors in animals with nanomaterials under X-ray irradiation. The latter two systems contain many more reactions and pathways. It seems unfathomable to directly use animal models before understanding every possible pathway. However, in biology and medical practices, focusing on the destruction of cells is often much simpler to do than understanding mechanisms. To many researchers, the most accessible and prudent or even scientifically sound method to show an enhancement is to prove that neither nanomaterials nor radiation is too toxic to cells and that the combination of the two causes significantly more destruction than the sum of the two acting alone. Many works have shown that gold nanoparticles indeed help improve the destruction of cells when irradiated with X-rays. Unfortunately, this does not mean that enhanced destruction is actually caused by enhanced absorption of X-rays by the added gold nanoparticles. The observed enhancement may arise from other mechanisms, such as biological enhancement shown in Chap. 4, that have little to do with X-ray absorption by the added nanomaterials. That being said, the experimental outcomes are still true and impactful, even if the results may or may not be completely caused by the expected

mechanisms. Understanding of the enhancement mechanisms and optimization of enhancement may progress slowly and demand greater efforts over many years. Readers should be aware that explanations or interpretations of the results may be complex, and proper experiments, new nanomaterials, and methodologies have to be developed before the true origins of enhancement can be identified.

Considering X-rays can both image and treat tumors, it is reasonable to deploy X-ray nanochemistry in both areas. Many methods have been developed, and much progress has been made in nanomaterial-assisted X-ray imaging. In addition, new imaging methodologies are being developed as well. Studying imaging also promotes exploration of delivering nanomaterials to target tumors, as shown in Sect. 9.3, which helps current treatment methods and future use of X-ray nanochemistry in cancer treatment. These publications lay the foundation to guide the use of primitive nanomaterials in radiotherapy and X-ray imaging. As discussed in Sect. 9.8, future use of X-ray nanotechnology will probably rely much more on X-ray-triggered release than on the current radiotherapy.

For the purpose of cancer treatment, many *in vitro* and *in vivo* enhancement measurements have been performed using relatively simple nanomaterials or nanochemistry. IUdR and BUdR were also used to improve radiosensitization, but their contribution to cancer therapy has been limited. While nanomaterials have not yet met the same fate as other originally promising materials such as BUdR and IUdR, little value has been added to the overall cancer treatment paradigm so far through the use of nanomaterials under X-ray irradiation. This is probably why only incremental improvements have been made more than a decade after several important papers were published and a first round of patents were granted. The main advantage of using nanomaterials to date seem to be that moderate gains in the effectiveness of radiotherapy can be achieved from using high loadings of these nanomaterials without severe toxicities.

Publications to date suggest that the original hypothesis of using gold nanoparticles to enhance radiotherapy is largely validated, but the exact technologies as they stand now have not generated the impact originally envisioned. Fortunately, unlike IUdR that had limited potential but significant cytotoxicity, gold nanoparticles have much less cytotoxicity, and there are many ways to improve their performance. Currently, efforts are being devoted to developing nanomaterials for various enhancements, and some of the developments have been used clinically. Movement from using nanoparticles to enhance radiotherapy in research labs to practical medical applications including clinical settings is happening, albeit slowly. The review of these works presented here and elsewhere using nanomaterials under X-ray irradiation for medical applications might inspire new approaches.

The intent of this chapter is therefore to discuss publications that apply X-ray nanochemistry to medicine. Among the topics covered in this chapter is a section that discusses theoretical studies related to medical applications of X-ray nanochemistry, which is given in Sect. 9.4. The rest of the chapter are divided into three main sections.

The first section of this chapter, i.e. Sect. 9.3, intends to systematically discuss papers in the area of imaging using nanomaterials under X-ray irradiation. Imaging

work has been expanded in many directions by researchers, and many findings are reviewed and discussed in this section.

The second section, Sect. 9.5–9.7, deals with the treatment of cells and tumors. As shown in Chaps. 2, 3, 4, and 5, it is even difficult to perform clean physical enhancement studies in controlled environments of pure water. It is conceivable that high loadings of small metallic or semiconductor nanoparticles in cells or animals may have many unintended consequences. For cellular work, this chapter only covers work using cancer cell lines. The results of studying healthy cell lines are given in Chap. 8, despite the fact that results on healthy cells are equally useful in medical applications. Instead of assigning different categories of enhancement to the results, this chapter summarizes all the efforts of using nanomaterials to enhance imaging or treatment of cancer cell lines (in vitro) and tumors (in vivo) under X-ray irradiation. Several methods of treating cancer cell lines with drugs and X-ray radiation are included as well. In addition, clinical trials are mentioned in this section. Although a majority of work published to date in the area of enhancing the effectiveness of X-ray irradiation with nanomaterials only scratches the surface of X-ray nanochemistry, the field is advancing. It is expected that increasingly advanced nanoscale systems will help advance medicine in the next decade, much more than simple nanomaterials did in the past decade.

The third section of this chapter, Sect. 9.8, covers X-ray-triggered release of drugs. Most of the work in the area of medical applications of X-ray nanochemistry intends to use nanomaterials to directly enhance the effectiveness of X-ray irradiation, e.g., to use nanomaterials to cause more damage to cancer tissues than X-rays alone. In this regard, current X-ray nanochemistry may have a limited impact. A more promising approach is to use X-ray nanochemistry to support the use of a subacute dose of X-rays to trigger the release of a lethal dose of drugs to annihilate tumors. In this area of research, X-ray nanochemistry may help uncover underlying mechanisms and push for more advanced chemical systems for cancer treatment. One such work was shown by Guo et al. [8] in which X-rays were used to trigger the release of doxorubicin from the surface of gold nanoparticles, by way of radicals produced in cells reacting with and cleaving DNA linkers to which the drug molecules were attached. Their work represented the first attempt to use nanomaterials in a sophisticated manner to achieve enhancement. Several other publications demonstrated a similar proof of concept. For example, Xu and Zhang et al. [9] created a diselenide nanomaterial responsive to ionization radiation. X-ray-triggered release of drugs, as defined in X-ray nanochemistry, may reshape the landscape of radiotherapy by largely eliminating it and replacing it with X-ray-triggered therapy, a new approach sans any radiation side effects. X-ray nanochemistry may also change chemotherapy by allowing the triggered release of extremely potent chemotherapy drugs at designated locations in the body. Although there are still many obstacles to overcome, future work in this area is exciting.

An X-ray nanochemistry application closest to creating a real therapy uses rare earth nanomaterials for physical enhancement and cancer treatment. Maggiorrella et al. [10] published the results, and a company, Nanobiotix Inc., was formed and has been carrying out clinical trials using these nanomaterials. Future work will need to identify the actual mechanisms and causes of the enhancement.

9.2 General Approaches and Procedures Used in Medical Applications

In vitro and in vivo works are laborious and difficult to perform, with many variables being able to affect the outcome. In this section, generic guidelines on cell and animal work are described to help reduce inconsistencies due to ambiguities among works by different research groups. Enhancements are often measured using assays that probe endpoints, and both assays and endpoints are discussed. This discussion is placed before the main sections of imaging and treatment so that these practices can help guide readers and researchers to navigate through many different results reported in the literature and discussed in this book. Due to largely varying procedures and conditions throughout the literature, we try to briefly summarize all the major and most relevant information and conditions.

9.2.1 Cell Work

9.2.1.1 Types of Cells

Many cell lines have been used in medical applications of X-ray nanochemistry. They have different dose response curves, and there are advantages or disadvantages for using a specific cell line. Table 9.1 lists many cell lines used in X-ray nanochemistry works and their lethal dose, LD₃₇, either directly available from their work or calculated by the author of this book based on the survival fraction curve. As tumor cells divide faster than healthy cells, one would expect that tumor cells might have lower LD₃₇ values. The difference is not obvious, however, possibly because the standard deviations associated with each of the two categories of cells are large, hence making such a differentiation difficult. Nonetheless, the difference exists between some of these two types of cell lines, as shown in Chap. 8.

9.2.1.2 Cell Preparation

The cells are generally incubated in CO₂ (5%) at 37 °C prior to treatment with nanoparticles and X-rays. In many studies, the cells are placed at the bottom of a Petri dish for a few days prior to incubation with nanoparticles and X-ray irradiation. The incubation concentration of nanoparticles ranges from nanomolar to micromolar of nanoparticles, depending on the type and size of nanoparticles. Instead of reporting nanoparticle concentrations, many researchers use the concentration of gold atoms or ions (salt), which ranges from micromolar to millimolar. However, in many cases it is preferable to provide nanoparticle concentrations as well as atomic or ionic concentrations. After incubation, nanoparticles outside cells are washed away before irradiation.

Table 9.1 Cell lines used in X-ray nanochemistry work. Only one reference is given to each cell line. The results are ordered alphabetically according to the cell names. Cell type, name, and their LD₃₇ (1/e) dose are also given

Cell name	Cell type	LD ₃₇ (Gy) ^b	Ref.
4T1	Murine breast cancer	4.0	Yang et al. [11]
9L	Brain cancer	3.5	Tehei et al. [12]
A375	Skin cancer		Chen et al. [13]
A-431/MDA-MB-231/DU-145/PC-3	Various cancers		Mikkelsen et al. [14]
A549	Lung cancer	2.0	Jiang et al. [15]
A549/KB	Human epidermal	>10	Yan et al. [16]
Bovine aortic endothelial cell	Endothelial	>10	Geso et al. [17]
C3H 10T1/2	Fibroblast	–	Regulla et al. [18]
C6	Glioma	6.1 ^a	Kotler et al. [19]
CHO-K1 /EMT-6 / DU-145	Hamster ovary	2–4	Das et al. [20]
CT26	Colon cancer	–	Choi et al. [21]
CT26	Colorectal	3.0	Hwu et al. [22]
CT26	Colon cancer	–	Guo et al. [23]
DU145	Prostate	40	Juzenas et al. [24]
DU145/HaCaT	Prostate	6–8/2–4	Geso et al. [25]
Du145/MDA-MB-231/T98G	Prostate	6.0	Taggart et al. [26]
<i>E. coli</i>	Bacteria	100	Liu et al. [27]
EMT-6/CT26	Murine breast cancer	6.0/3.0	Hwu et al. [28]
F98 and B16	Glioma	4.0	Pradhan et al. [29]
GBM (MCF-7)	Human glioblastoma	–	Krishnan et al. [30]
GL261	Brain tumor		Hallahan et al. [31]
H1299-Luc	Lung, lymph	8	Xie et al. [32]
H460	Lung cancer	3.5	Sheng et al. [33]
HCT116/HT1080	Colorectal tumor/ fibrosarcoma	5.0	Maggiorella et al. [10]
HCT116	Colorectal tumor	3.0	Paquette et al. [34]
HeLa	Cervical cancer	4.0	Chirthrani et al. [35]
HeLa/BEL-7402	Cervical cancer/liver carcinoma	10	Zhao et al. [36]
HepG2	Liver	1.0	Li et al. [37]
HT1080	Human fibrosarcoma	3.0	Tsourkas et al. [38]
HT29	Colorectal cancer	6.0	Arab-Bafrani et al. [39]
HTB-72	Skin melanoma	4.2	Kim et al. [40]
K562	Glioma	–	Su et al. [41]
KB	Cervical cancer	6.0	Chen et al. [42]
MCF-7	Breast cancer	4.0	Liu et al. [43]
MCF-7	Breast cancer		Chen et al. [44]
MCF-7 (nine total)	Breast cancer (eight others)	2.0	Butterworth et al. [45]

(continued)

Table 9.1 (continued)

Cell name	Cell type	LD ₃₇ (Gy) ^b	Ref.
MCF-7/Caco-2/3T3	Breast cancer	–	Kryschi et al. [46]
MCF-7/Hep G2	Breast cancer, human liver cancer	–	Ito et al. [47]
MCF-7/SKOV-3	Breast/ovarian cancer	–	Cook et al. [48]
MCG803	Gastric carcinoma	–	Cui et al. [49]
MDA-231 (nine)	Breast cancer	4.5	Jain et al. [50]
MDA-MB-231	Breast cancer	4.3	McMahon et al. [51]
MDA-MB-231/T47D	Breast cancer	5/4	Latimer [52]
CT26	Colon cancer	–	Kim et al. [53]
OECM1	Human cancer	–	Hwu et al. [54]
OVCAR-3	Ovarian	–	Chen et al. [55]
Panc1	Pancreas	>50 ^a	Goldys et al. [56]
PC-3	Prostate	–	Vo-Dinh et al. [57]
RG2	Glioma	~10	Geso et al. [58]
S2	Glioblastoma	–	Weland et al. [59]
U251	Brain cancer	–	Wen et al. [60]
U87	Glioblastoma	14 ^a	Retif et al. [61]

^aPredicted by the author of the book based on the data in the report

^bLD₅₀ = 0.70 × LD₃₇

9.2.1.3 Uptake

Most of the published works only specify incubation concentrations and times. However, it is important to have the uptake measured so that experimentally measured enhancements can be calibrated against theoretically predicted enhancement values, at least for physical enhancement. Uptake is usually determined with the help of atomic absorption spectroscopy (AA) or other mass spectrometry methods, such as inductively coupled plasma mass spectrometry (ICP-MS). The difference between incubation and uptake concentrations is often significant. Table 9.2 summarizes results for studies that have measured uptake. The size dependency of uptake is also studied and the results are given in the table as well.

Two of the most important parameters affecting the uptake of nanoparticles by cells are the size and surface coating (surfactant) of nanoparticles. With regard to size, several studies focused on the effect of size. Chan et al. [75] studied the uptake of five different sizes of gold nanoparticles, ranging from 14 to 100 nm for three different cell lines. They found that 50 nm gold nanoparticles had the highest uptake. Chithrani et al. [35] studied the radiation damage enhancing capability of gold nanoparticles ranging from 14 to 74 nm in diameter. The authors also found that 50 nm nanoparticles had the highest uptake. Chang et al. [76] showed that among

Table 9.2 Uptake of nanoparticles for different cell lines. The works are arranged based on the magnitude of uptake, from the lowest (1 ppm or 0.0001 WP) to highest (40 WP). Ligands or surfactants on the surface of nanoparticles are shown as well

Composition	Size (nm)	Ligand name	Cell name	Uptake amount (WP)	Ref.
Au/Fe ₃ O ₄	50	Folic acid	A549	0.0001	Mei et al. [62]
Au	14, 50, 74	CTAB	HeLa	0.00005, 0.005, 0.016	Chan et al. [63]
Van-GQD/PpIX	100	Vancomycin	<i>E. coli</i>	0.01	Liu et al. [27]
Au	7	Glucose	Du145	0.023	Xing et al. [64]
Au	10	Cysteamine	MCF-7	0.03	Xing et al. [65]
AuNPs	1.9/28–142	Micelles	HT1080	0.057	Tsourkas et al. [38]
Au	10.8	Thiol-glucose	DU-145	0.081	Roa et al. [64]
Au	10.8	6-Deoxy-6-fluoro-1-thio-D-glucose	DU-145	0.081	Roa et al. [66]
Bismuth oxide	µm plates	PEG	9L	0.1	Tehet et al. [12]
Au	1.4	pHLIP	A549	0.11	Reshtenyak et al. [67]
Au@SiO ₂	45.97/1.16	CTAB	MCG-803	0.3	Cui et al. [49]
Au	47.3 ± 8.7	HS-mPEG	MDA-MB-231 MDA-MB-436	0.44 and 0.20	Allen et al. [68]
Se	100–500	PEG	HeLa	0.46 µM/10 cells	Chen et al. [69]
Pt	–	Terpyridine	F98 B16	0.7	Pradhan et al. [29]
Au	14–74	Citrate	HeLa	0.7	Chirthrani et al. [35]

Au	2–50 nm	–	MDA-MB-231	0.88	McMahon et al. [70]
Gd ₂ O ₃	42 ± 3	Polysiloxane	CT26	0.9	Kim et al. [53]
Au	3000	–	EMT-6	1	Das et al. [20]
Au	1.9	–	Du145, MDA-MB-231, T98G 4 T1	0.07–1.5	Taggart et al. [26]
Bi	3.6	LyP-1	A375	1.72	Li et al. [71]
Au-Se	100	Chitosan	A375	2	Chen et al. [72]
Au	3	Tiopronin	HCT116	3.3	Paquette et al. [34]
Au	47	Folate	HeLa	3.4	Khoshgard et al. [73]
Au	50	(Purchased from sigma-Aldrich)	HT29	5	Arab-Bafрани et al. [39]
Au	4–5	Glucose	A549, KB	6	Yan et al. [16]
Au	16–17	Thioctic acid-β-cyclodextrin	HeLa, A549	12	Yan et al. [74]
FeO _x	13	Alginate	CT26	17	Choi et al. [21]
Au	15	DNA/DOX	MCF-7	30	Guo et al. [8]
Au	30	CPP-PEG	MDA-MB-231 T47D	5–40	Latimer [52]

CPP cell-penetrating peptides, CTAB cetyltrimethylammonium bromide, DNA deoxyribonucleic acid, DOX doxorubicin, PEG polyethylene glycol, pHLIP pH low-insertion peptides.

3 to 50 nm gold nanoparticles, 13 nm gold nanoparticles were found to be the best for maximum uptake. Xing et al. [77] studied the uptake of several gold nanoparticles by two cancer cell lines. They discovered that cysteamine covered 10 nm gold nanoparticles had the highest uptake rate of 1.2×10^5 nanoparticles/cell, corresponding to approximately 0.1 WP of gold in the cell.

Many works have studied the effect of surfactants on uptake. For example, Mukherjee et al. [78] showed the uptake of gold nanoparticles on the order of 0.2 WP at different locations after incubation/circulation. Their nanoparticles were coated with various ligands, including antibodies and gemcitabine. Su et al. [79] used polyelectrolyte ligands on gold nanoparticles to improve nanoparticle internalization. No quantitative results were presented, although increased damage to nuclear DNA was observed with positively charged ligands on the surface of gold nanoparticles. Latimer [52] found that cell-penetrating peptides (CPPs) improved uptake. The author used clonogenic assays to determine the enhancement, and values between 1.3 and 2.1 DEU were measured using between 0.03 and 1.6 million ca. 30 nm gold nanoparticles per cell. These uptake levels corresponded to 0.8 to 43 WP of gold in a cell, and physical enhancement of 0.8 to 43 DEU is expected for such uptake. Coatings of other ligands could also improve uptake. Although no absolute uptake data was given, an acidity sensing peptide, pHLIP (pH low-insertion peptide), was found by Cooper and Reshetnyak et al. [67] to significantly improve uptake. TEM images showed the presence of significant amounts of 1.4 nm pHLIP functionalized gold nanoparticles in the cell. Kim et al. [40], however, found no 1.9 nm gold nanoparticles in the cell. In contrast, significant uptake of 50 nm gold nanoparticles was observed in the same work. Further studies are needed to reconcile all these diverging uptake results.

9.2.1.4 Endpoints and Assays

Endpoints and assays are two closely connected concepts. Many endpoints can be used to estimate the enhancement, and the results of enhancement measurements can be quite different, depending on the endpoint. Table 9.3 shows several endpoints and assays used to measure the enhancement. Some endpoints are easier to employ than others. For example, MTT assay is much less time consuming than clonogenic assay. However, data from clonogenic assays can be more reliable in terms of assessing the viability of the cell because the cell has adequate time to respond to the treatment.

Table 9.3 Endpoints and assays used in X-ray nanochemistry to inspect enhancement

Endpoint	Assay
Apoptosis, sub-G1	Flow cytometry
Cell death	Clonogenic
Cell viability	Clonogenic, MTT, MTS, caspase-3
DNA SSBs	γ -H2AX, gel electrophoresis
DNA damage	Comet assay
Oxidative stress	Fluorescence dye/flow cytometry

9.2.1.5 Cytotoxicity

After selecting the cell line, incubation conditions, and the assay to probe an endpoint, it is important to assess the cytotoxicity of a nanomaterial to the cell before enhancement can be measured. Nanoparticles and especially surfactants may pose toxicity to cells. It is possible, for example, for nanoparticles themselves to be nontoxic, while the ligands on the surface exhibit toxicity. As a result, cell viability may be reduced when ligands are detached from the surface of nanoparticles in the cell. Depending on the assay used to measure enhancement, this toxicity may or may not be evident before irradiation. Rotello and Vachet et al. [80] studied the stability of gold nanoparticles in cells using mass spectrometry. Their study found that biothiols on gold nanoparticles were more stable in cells, which may render thiol-protected gold nanoparticles more stable in cells. Even if nanoparticles themselves and their surfactants are not toxic, nanoparticles may disintegrate in cells, releasing toxic ions or atoms. Selenium or cadmium nanomaterials belong to this category.

9.2.1.6 Irradiation with X-Rays and Enhancement Measurements

Cells are typically irradiated for up to tens of minutes to obtain a total dose of 1–10 Gy. Typical cell survivability curves, with and without gold nanoparticles, are shown in Fig. 9.1. This can be obtained from clonogenic, MTT or other assays, and different assays usually generate different surviving fraction curves and hence enhancement values. DNA damage curve is different, counting the damaged DNA rather than the percentage of intact DNA after irradiation. Enhancement values are derived by comparing the curve with nanoparticles under X-ray irradiation to the

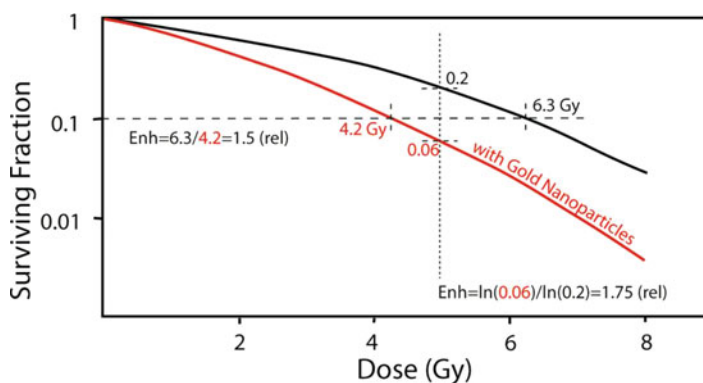


Fig. 9.1 Two typical cell survival curves, with and without nanoparticles are shown here. There are two ways to calculate the magnitude of enhancement. One uses the ratio of survival fractions at the same dose (shown here at 5 Gy, marked by the dotted line), and the other uses the ratio of doses at the same survival fraction (shown here at 0.1 surviving fraction, marked by the dashed line). The two values should be close, although there is no guarantee for them to be identical. Other methods have also been used to determine the magnitude of enhancement

curve without nanoparticles under X-ray irradiation. If nanoparticles are toxic, then the toxicity has to be included as well. Figure 9.1 shows two quick methods of calculating the magnitude of enhancement using *in vitro* data. Similar methods of enhancement calculation have been discussed in the literature. The first method uses the doses without and with gold nanoparticles at the same surviving fraction. For example, if 10% surviving fraction is used, as shown by the horizontal dashed line in Fig. 9.1, the dose without gold nanoparticles needed to cause this amount of damage is 6.3 Gy, while the dose needed to cause the same magnitude of damage with gold nanoparticles is 4.2 Gy. The enhancement is $6.3/4.2 - 1 = 0.50$ DEU. The second method, shown by the vertical dotted line in Fig. 9.1, is to use surviving fractions at the same dose of X-ray irradiation to compute the enhancement. The enhancement value is calculated as the ratio of the natural log of the surviving fraction with nanomaterials under X-ray irradiation to X-rays without nanomaterials minus 1, which is $\ln(0.06)/\ln(0.2) - 1 = 0.75$ DEU. It is worth pointing out that ratios of doses or surviving fractions give rise to relative enhancement. Absolute enhancement is equal to relative enhancement minus one. The two enhancement values obtained using these two methods are close. Although these methods are simple to use, they are dependent of the surviving fraction or dose of choice and therefore need to be used with caution. For the purpose of destruction of tumor cells, 10% or even 1% surviving fraction should be used.

A third method of enhancement computation using the survival curves is to use ratios of α or β or both, the coefficients of the fitted survival fraction exponential equations. The enhancement is the ratio of α or β with nanoparticles to without nanoparticles, whichever has the larger coefficients in front of them. This method also yields different results due to the choice of doses and survival fractions. Subiel et al. [81] reviewed and discussed several standard methodologies used to determine the enhancement factor based on survival fraction data. Several different ways were provided, and two of them, radiation enhancement factor and radiation enhancement ratio, are similar to those given here. At least two additional methods of evaluating enhancement using the survival fraction curves exist in the literature, which can be derived from (1) linear-quadratic model and (2) mean inactive dose.

9.2.2 *Animal Work*

There are similarities between the use of cellular models and animal models for enhancement studies. In general, animals are infected with tumor cells and then treated with nanoparticles and radiation. The tumor sizes or life span changes at the end of treatment are commonly used to obtain the magnitude of enhancement or improvement. Compared with cellular models, animal models have even more variables. The established procedures, regardless of their effectiveness and validity in simulating human diseases, are given here so that researchers have a general guideline to follow as they go through the rest of this chapter.

9.2.2.1 Animals

Mice or rats are most frequently employed, although other animals such as swine are used as well. There are two general methods to infect animals with tumor cells. One is to purchase the infected animals and then treat them with nanoparticles and radiation. The other is to purchase healthy animals and then infect them with cancerous cells. Tumors are allowed to grow to a certain size before the planned treatment experiments.

9.2.2.2 Nanoparticle Delivery/Tracking

There are several methods to deliver nanomaterials to tumors in animals. One is through intravenous injection, usually through the tail veins. The other is to inject nanomaterials directly into the tumor, a method employed less often. Irradiation follows, after which animals are euthanized and tumor size is measured. Nanoparticles are generally in aqueous solutions, but in several cases, they are in serum. The method of delivery, however, is the same for these different solutions.

9.2.2.3 Targeting

X-ray nanochemistry benefits from and contributes to delivery and targeting of nanomaterials to biological targets because applications of X-ray nanochemistry rely on the development of these chemical and biological methods. For example, nanodrugs should not only be triggered by X-rays to release payloads but also be easily taken up by tumors or be actively targeting tumors and other biological entities. Other factors include that the release of drugs from nanomaterials uses bio-orthogonal chemistries so that drugs are not released without external triggering. These are important aspects of X-ray nanochemistry.

Tumors may be targeted both actively and passively. In active targeting, ligands such as peptides or antibodies are coated on the surface of nanoparticles so that nanomaterials can seek and bind to tumor cell surfaces and eventually, preferentially enter tumor cells. For example, Hallahan et al. [82] reported the use of a recombinant peptide, HVGGSSV, that binds to irradiated tumors to help improve the delivery of nab-paclitaxel to tumors. Even without these targeting agents, passive targeting is possible because the size and charge of the nanoparticles may be suitable to facilitate their entry into tumors by relying on the so-called epidermal permeation and retention (EPR) effect. These processes are important to both imaging and treatment of tumors. Although targeting and delivery are not a central topic in X-ray nanochemistry, these two aspects are of paramount importance to X-ray nanochemistry applications in medicine. A list of the surfactants, including targeting and delivery reagents, is given in Table 6.2. There are several review articles on this topic as well. For example, El-Sayed et al. [83] examined a targeting mechanism through the use of nuclear localization signal (NLS) peptide, a popular method.

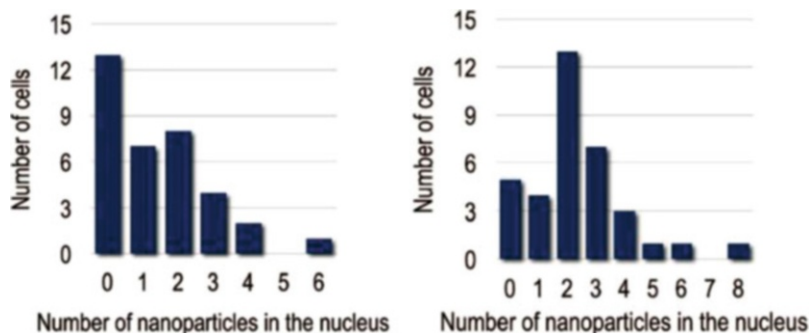


Fig. 9.2 Uptake and nuclear targeting studied by Brust et al. [84]. The numbers of gold nanoparticles per nucleus with only cell-penetrating peptide (CPP) ligands are less than those with both CPP and nuclear location signal (NLS) ligands on gold nanoparticles. Those with CPP are shown in the left panel, and those having both CPP and NLS ligands are shown in the right panel. (Reprinted with permission from Brust et al. [84]. Copyright (2008) American Chemical Society.)

Cell-penetrating peptide (CPP) was another example. Brust et al. [84] studied the uptake and intracellular fate of gold nanoparticles with several different types of surfactants, including NLS peptides. They used HeLa cells as the platform and 16 nm gold nanoparticles, which were close to the size limit of nanoparticles that can move through nuclear envelope pores of less than 20 nm in diameter. Figure 9.2 shows typical results obtained with NLS but without CPP (left panel) and those obtained with both CPP and NLS (right panel). The authors showed the result of increased occurrence of cell nuclei containing gold nanoparticles when both CPP and NLS ligands were conjugated to the surface of these gold nanoparticles. Jon et al. [85] provided an extensive review of the current literature on targeting for imaging and therapy. More recently, Su et al. [86] employed CPP-modified gold nanoparticles to improve the effectiveness of radiotherapy.

Although nuclear targeting is different from cell or tumor targeting, many groups found that the surfactant on nanoparticles can affect both cell uptake and nuclear penetration. For instance, Hainfeld et al. [87] and Su et al. [79] found that positively charged ligands on gold nanoparticles increase their uptake by cells and nuclei.

9.2.2.4 Biodistribution of Nanomaterials in Animals

Similar to the importance of uptake data to cellular work and enhancement measurements, it is important to know the biodistribution information of nanomaterials in animals. Mass spectrometry is usually used to determine biodistribution of nanomaterials in animals. Biodistribution in animal work is also discussed in Sect. 9.3 using X-ray imaging tools, which require adequate amounts of nanomaterials within the targeted volume in animals. Biodistribution and pharmacokinetics are critical to the study of the fate and effect of nanomaterials in animals.

9.2.2.5 Irradiation Protocols

Animals are irradiated with X-rays, either by single irradiations or in fractionations, depending on the required dose. If a dose of less than 10 Gy is needed, then a single irradiation is commonly used. For greater doses, fractionations may be used by administering a moderate dose multiple times. Many researchers, especially those performing *in vitro* studies, used a single dose of irradiation. X-ray filters are used to remove low-energy X-rays when needed. Other important factors are irradiation timing and duration, as nanoparticles may quickly clear the tumor, as shown in Fig. 4.3.

9.2.2.6 Enhancement Measurements and Calculations

Delayed tumor growth is often used to evaluate the effectiveness of treatment. The method shown in Fig. 7.1 is used to determine enhancement in *in vivo* work. If there is no toxicity from the nanomaterials, the magnitude of the enhancement can be calculated using the formula:

$$\frac{\ln(\text{tumor size without any intervention}) - \ln(\text{tumor size with X-ray + nanoparticles})}{\ln(\text{tumor size without any intervention}) - \ln(\text{tumor size with X-ray only})} \quad (9.1)$$

An example is given here for a tumor that has grown to 11 times its original size at the time of inspection. If the size is reduced to seven times its original size after X-ray irradiation alone and to two times its original size after irradiation with X-rays in the presence of nanomaterials, then the enhancement is:

$$\frac{\ln(11) - \ln(2)}{\ln(11) - \ln(7)} = \frac{2.40 - 0.69}{2.40 - 1.95} = 3.80 \text{ DEU (rel)} \quad (9.2)$$

The absolute enhancement is 2.8 DEU. This calculation assumes there is no toxicity from the nanomaterial and the growth of tumor follows an exponential function. The results shown here are consistent with the magnitude of enhancement calculated using Eq. 7.1.

9.2.3 Clinical Work

There are several cases of clinical work involving nanomaterials in the context of X-ray nanochemistry. Stage II/III clinical trials are being conducted by a French company Nanobiotix Inc. using hafnium oxide nanoparticles and X-rays for enhanced cancer treatment. The work is described in this chapter as well.

9.3 Imaging and Detection of Tumors with X-Rays Assisted by Nanomaterials

Imaging with X-rays has been an important tool in medical research and medicine for more than a century since the discovery of X-rays by Röntgen in 1895. Enhanced absorption by the added nanoparticles made of heavy elements can further improve imaging contrast when nanoparticles are delivered to tumor sites through active or passive targeting.

Many new nanomaterials have been developed to improve X-ray imaging. Even though most of the current imaging studies use only the most straightforward principles of X-ray attenuation by nanomaterials as the basis for guiding their imaging improvement, it is foreseeable that other enhancement mechanisms, such as X-ray-induced energy transfer (XIET) discussed in Chap. 2, may be used in the future to enrich nanomaterial-assisted X-ray imaging.

In practice, the sensitivity of X-ray imaging is moderate, whereas state-of-the-art positron emission tomography (PET) and magnetic resonance imaging (MRI) offer better sensitivity. Nonetheless, computed tomography (CT) and regular transmission imaging such as chest X-rays are popular and useful because of their low costs and adequate sensitivity. The number of studies using nanoparticle-based contrast agents to improve CT and other X-ray imaging techniques has grown quickly in the past decade. Figure 9.3 shows the number of works published per year for the last 20 years that have the combination of keywords of “nanoparticle + X-ray + imaging.” A similar graph is presented by Cormode et al. [88]. The growth rate is similar to the number of publications in the area of X-ray nanochemistry shown in Fig. 1.1. It is worth noting that Fig. 1.1 is obtained through the papers cited in this book, whereas Fig. 9.3 is obtained through literature searches using keywords.

Five areas related to imaging are briefly reviewed and discussed in this section. The first is the method of imaging. Several new imaging methods are included. The second is the object of imaging, ranging from mice to swine. The third area

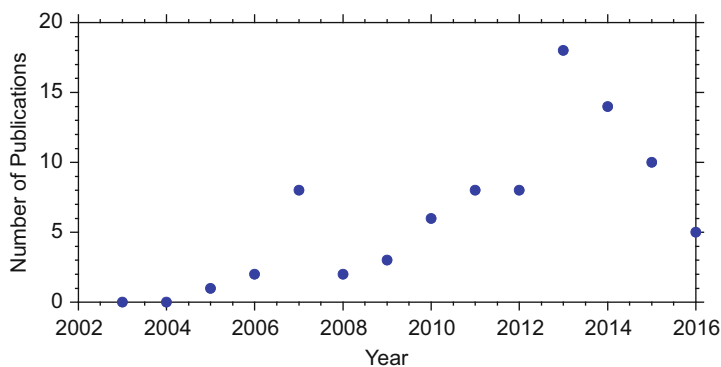


Fig. 9.3 Number of publications per year on the subject of “nanoparticle + X-ray + imaging” provided by the search program *Web of Science*

encompasses the core material of contrast agents, which can be gold nanoparticles or micelles. Fourth is the surface coating of contrast agents, which can be peptides or silica shells. The fifth and final area is the method of delivery, including injection and inhalation. Targeting and biodistribution analysis are also included in this subsection. All these five areas have been investigated in recent years. There are no known clinical trials using nanoparticles as imaging contrast agents to date.

9.3.1 *New Imaging Methods*

The first topic of this section covers new methods developed in the area of nanoparticle-enhanced X-ray imaging in recent years. Although other techniques may be relevant, the focus here is on techniques that support the use of nanomaterials as contrast agents in X-ray imaging. One common parameter that can be used to gauge the capability of these techniques is the unit weight percent contrast increase (UWPCI, in units of HU WP^{-1}) resulting from the introduction of nanomaterials. The units for contrast is HU, or Hounsfield Units. Whenever possible, the value of UWPCI is specified for each work, and all the values found in the publications cited are summarized at the end of this section in Fig. 9.15. If the detection method is based on fluorescence rather than absorption, then unit weight percent signal-to-noise ratio (S/N) (UWPSN) instead of unit WP contrast increase is given. However, due to infrequent references to S/N in reports, this figure of merit is seldom used.

Sun et al. [89] explored the use of gold nanoparticles for the purpose of performing computed tomography (CT). The nanoparticles employed ranged from 4 to 60 nm in diameter. The uptake and cell viability of gold nanoparticles by HeLa S3 cells were studied. Using 4, 20, 40, and 60 nm gold nanoparticles, X-ray attenuation was measured. 4 nm gold nanoparticles had the greatest uptake. The results showed that the equivalent attenuation was 600 HU for 0.1 mol/L gold loading or 300 HU WP^{-1} in terms of UWPCI. This magnitude of UWPCI was the average value for gold nanoparticle contrast agents.

Cui et al. [49] investigated the use of silica-coated gold nanorods for enhancing the contrast of X-ray imaging. Their results showed that silica-coated gold nanorods increased the contrast of CT at the rate of 15 HU for a 3 mg/mL loading, equivalent to 50 HU WP^{-1} . This value was at the low end of the spectrum of UWPCI for nanomaterials as contrast agents. CT results are shown in Fig. 9.4. Based on the contrast increase, the loading of nanomaterials at the tumor site was approximately 54 mg/mL. The authors reported a 10 mg/mL loading at the tumor site.

Cho et al. [90] investigated the potential of using gold nanoparticles to assist X-ray imaging by using X-ray fluorescence from gold irradiated with 110 kVp X-rays. This was the first fluorescence-based CT work using nanoparticles. A conventional X-ray source equipped with an X-ray hard aperture was used to excite 1 cm diameter gold solution targets filled with 1 and 2 WP gold. A CdTe photodiode detector was used to probe X-ray fluorescence. For 2 WP gold solutions, the fluorescence signal was around 600 counts on top of 2000 counts due to background

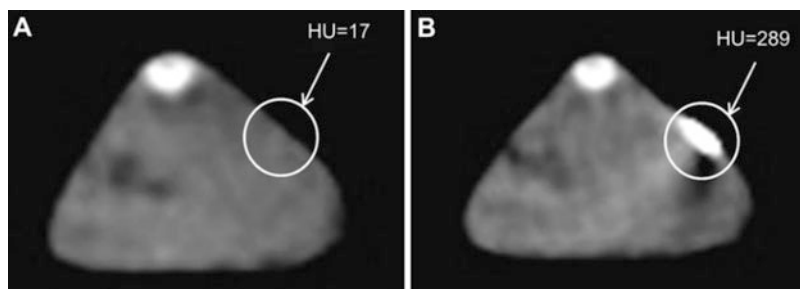


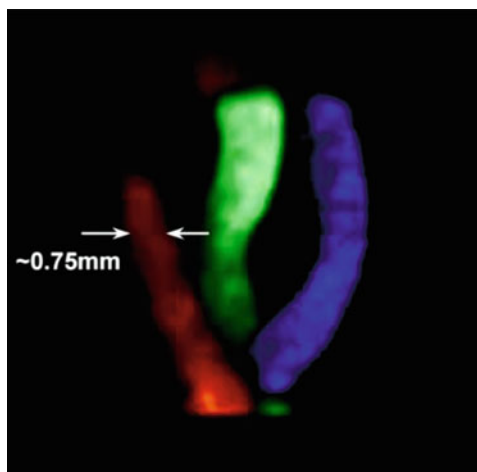
Fig. 9.4 Images of mice without (a) and with (b) silica-coated gold nanorods. (Reprinted from Cui et al. [49]. Copyright (2008) with permission from Elsevier.)

(scattering). Background removal gives higher contrast images. These results were simulated by Cho et al. [91], providing guidance for their subsequent imaging work. It is possible to use UWPSN to quantify the images of nanomaterials. However, unlike HU that is widely used in transmission imaging, most works in fluorescence imaging do not specify their S/N values, making it difficult to quantify figure of merit of fluorescence-based imaging methods using this parameter.

Cho et al. [92] again studied tumor imaging with the assistance of nanoparticles in the framework of X-ray fluorescence computed tomography (XFCT). The authors used a traditional X-ray tube with a conically shaped lead aperture or collimator. Three gold nanoparticle-loaded regions were embedded in a phantom made of poly (methyl methacrylate) (PMMA). CdTe X-ray detectors located behind the apertures were used to detect X-ray fluorescence at 90° from the incoming X-rays. For the 3 cm diameter phantom, the embedded 0.5 cm diameter gold-loaded samples were detected with a 0.5 WP gold loading, and the 2 WP gold-loaded region was clearly visible. Cho et al. [93] used fluorescent X-rays emitted from the L-shell of gold nanoparticles near 10 keV for imaging. A signal-to-noise ratio (S/N) of 8 was achieved with 2 WP of gold in the water phantom, giving rise to 4.0 UWPSN. A year later, Cho et al. [94] used a Monte Carlo method to theoretically study how to best detect tumors using XFCT. The authors found that the use of X-ray filters could increase S/N and obtained a S/N of 20 when 1 mm Pb filters were used in conjunction with 81–100 keV X-rays.

In a work by Meng et al. [95], sheetlike 15 keV X-ray beams from Advance Photon Sources (APS) were used to excite samples to induce X-ray fluorescence. The beam was as thin as a few microns and arrays of beams were used, either in the form of 15 beams (3×5 array) of 0.3 mm diameter or 35 beams of 0.1 mm diameter. The phantoms were comprised of Fe (25 mM), Zn (50 mM), and Br (25 mM) solutions which filled three plastic tubes of 0.75 mm diameter. Fluorescence was measured using a CCD detector with 250 eV energy resolution. The most visible sample was the tube filled with Br solution. Figure 9.5 shows the image of three tubes. Although no nanomaterials were used, it was expected that the imaging method could be readily extended to detecting nanomaterials as contrast agents.

Fig. 9.5 XFCT image of three tubes of 0.75 mm diameter using 35 beams of 0.1 mm diameter. Colors were added to differentiate the three tubes filled with three samples of Fe, Zn, and Br solutions. (Permission of SPIE and Meng [95].)



Wen et al. [96] discussed a method of using conventional X-ray sources to perform coherent X-ray imaging of several objects including vials of solution of water and oil. The X-rays were 17.48 keV from a molybdenum target. The authors observed the first harmonic of the Fourier transformed images, which could be used to derive the scattered images of the samples. Fine features on the order of 60–200 nm were observed, suggesting that it is possible to image nanomaterials in solution. They also observed scattering with some unusual images.

Bazalova et al. [97] theoretically studied fluorescence CT principles for X-ray imaging of gold targets in theoretical phantoms. X-ray dose, gold loading, target dimension, and location in the phantoms were all taken into consideration. The authors demonstrated that XFCT was superior because it does not depend on the surrounding tissues, whereas conventional CT does. A scanning beam configuration was also employed by Bazalova et al. [98], and the authors called the technique scanning beam digital X-rays. In another effort, Xing et al. [99] demonstrated the imaging of embedded gold, gadolinium, and barium targets in phantoms using XFCT. Their experimental setup was similar to Cho et al. [92], and the results suggested that gadolinium provided high contrast as well.

Shi et al. [100] reported the results of their study of CT imaging using gold nanoparticles entrapped in dendrimers in a mouse model. The size of gold nanoparticles was between 2 and 4 nm. The amine-terminated fifth-generation dendrimers were slightly larger, although no data on the exact size was available. A clear image was obtained, showing the injected gold nanoparticles in mice. The loading was 10 μL of 20 mM dendrimer-entrapped gold nanoparticles. No toxicity data was available. Their results showed an increase of 1000 HU with a 2 WP gold loading, resulting in a UWPCI of 500 HU WP^{-1} .

Hallahan et al. [101] synthesized multifunctional FePt nanoparticles for targeting and imaging of cancer. The particle size was 2.7 ± 1.0 nm, and the surface was further modified by adding polyethylene glycol (PEG) and then HVGGSSV peptide

ligands. This specific peptide targeted irradiated tumor microvascular cells. The mice were treated with 3 Gy of 300 kV X-rays from a linear accelerator, and the nanoparticles were administered 4 h after irradiation. The authors showed localization of the targeted nanoparticles in tumors using near-infrared (NIR) imaging in lung cancer-bearing mice and quantified the uptake. The control peptide SGVSGHVN-FePt nanoparticles did not show any localization. This work did not use X-ray imaging in the conventional sense.

Ren et al. [102] demonstrated that it was possible to use CT to probe silica-coated gold nanorods in xenograft mice. The initial gastric tumor size was 5 mm. The injection solution had a 3 mg/mL or a 0.3 WP gold loading. The average size of gold nanorods was 44 nm long with an aspect ratio of 2.9. The thickness of silica coating was 15 nm. The loading in the tumor was estimated to be 0.2 WP, and the imaging yielded a contrast of 56 HU, resulting in a UWPCI of 280 HU WP^{-1} . The X-ray images prior to and post gold nanorod injection showed a slight change. In contrast, the same amount of gold nanorods generated a better contrast when near-infrared light (NIR) was used. Physical enhancement, which is close to but lower than attenuation enhancement based on the discussion given in Chap. 2, would be 0.2–0.3 DEU for 0.2 WP uptake. Figure 9.6 shows the imaging results.

Rose-Petruck et al. [103] developed a new method to image gold nanoparticles in solutions. The authors first obtained an X-ray absorption image of the sample, followed by Fourier transformation of the image to the reciprocal space. Their X-ray microfocus source was 20 W and sample exposures were 3 min. Their uptake data showed less than 3 pgs of gold per cell for 10 or 50 nm gold nanoparticles, which was equivalent to a 6 ppm fraction of the sample volume or a 0.012 WP gold loading in the cell (1 ng). Figure 9.7 shows the transmission images and Fourier transform pattern. Based on the S/N shown in the figure, much lower loadings of

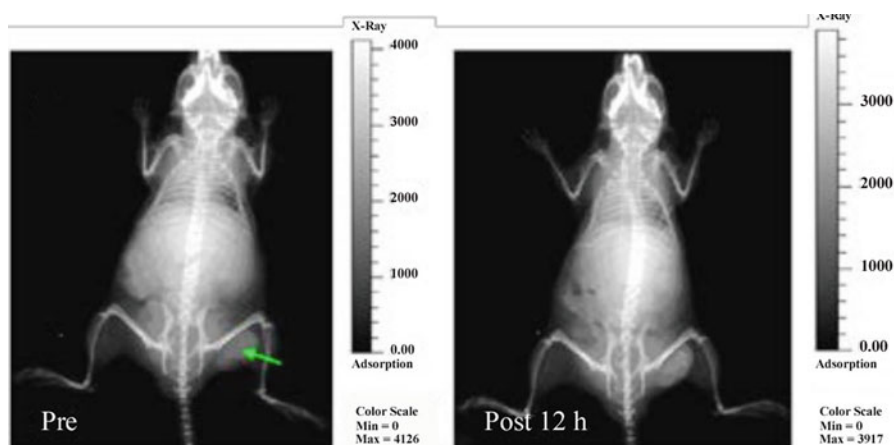


Fig. 9.6 CT imaging of a gastric tumor with silica-coated gold nanorods in mice. The loading was 0.2 WP in the tumor. The arrow shows the 5 mm tumor prior to (left) and after (right) injection of gold nanomaterials. (Reprint with permission from Ren et al. [102]. Copyright (2011) of Optical Society of American.)

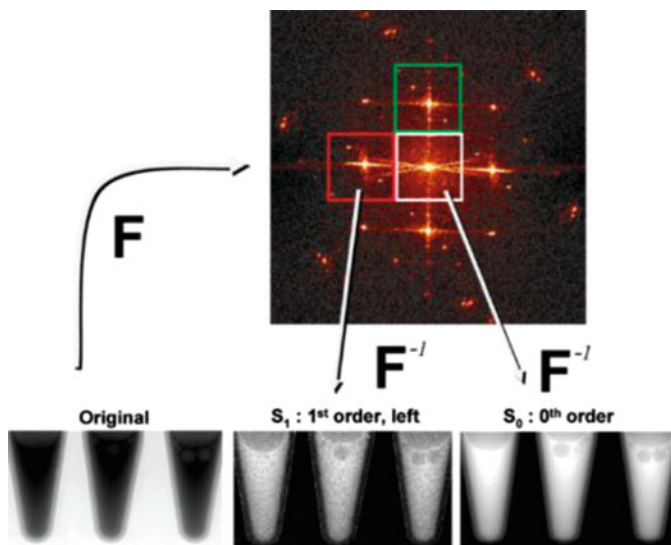


Fig. 9.7 Fourier transformation of transmission imaging for gold nanoparticles in solutions. The detection sensitivity was about 0.01 WP of gold in water. (Reprinted with permission from Rose-Petruck et al. [103]. Copyright (2011) American Chemical Society.)

gold in the sample can be detected. The authors proposed to use this method for cancer imaging.

Another method of X-ray fluorescent imaging was developed recently by Guo et al. [104], who discussed the results of X-ray imaging of tumor phantoms buried in large water phantoms with the assistance of nanoparticles. Figure 9.8 illustrates the principle. The idea was to use a needle X-ray beam to irradiate a sample while detecting X-ray fluorescence emitted from nanoparticles in the sample in the direction perpendicular to the needle X-ray beam path, a practice similar to the detection configurations used in several other reports. Apertures in front of the detectors were used to allow only X-rays emitted from certain points in the sample to enter the energy-dispersive detectors. This way, fluorescent X-ray photons emitted from the nanoparticles was measured with minimal interference from scattered X-rays.

Figure 9.9 shows the results of imaging a volume of interest embedded in a water cube. The loading of gold in the simulation was 1 WP and the shapes were cylindrical disks. Panel A shows the overall imaging result, which shows the location of the nanoparticle-loaded volume. Panels B and C show the side views of silver- and gold-loaded target volumes. Panel D shows the whole sample volume. Panels E and F shows the top views of the imaging. For 33 keV X-rays, Ag was more visible than Au.

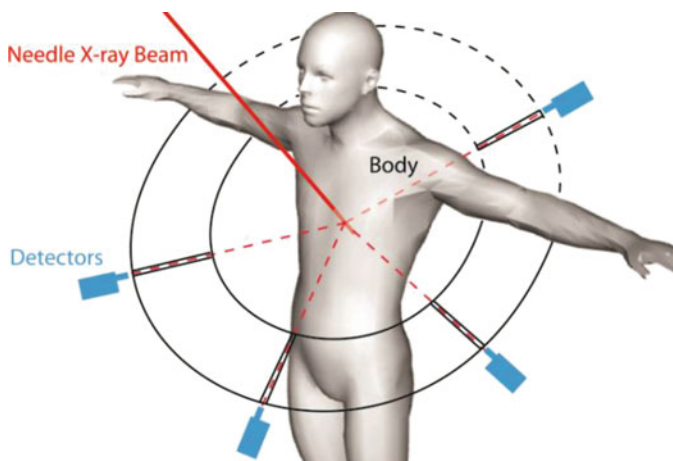


Fig. 9.8 Illustration of using X-ray fluorescence to detect nanoparticles in tumors in the human body. Multiple detectors were used to detect the nanoparticles at the targeted point in the body irradiated with an X-ray beam. The X-ray beam, the detectors, and the apertures were aligned before imaging [105]

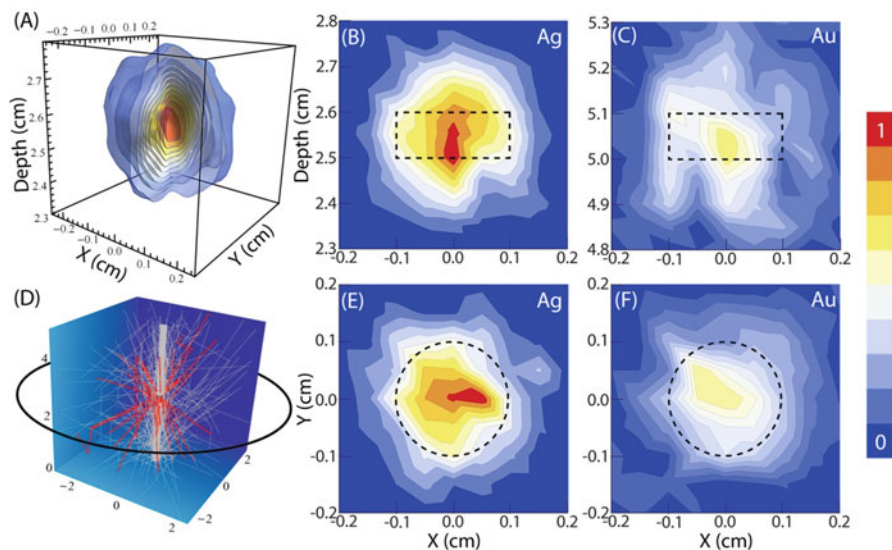


Fig. 9.9 Simulated results of detection of gold nanoparticles in tumor phantoms. A 10 cm water cube was used as the phantom. The results showed that it was possible to detect a 1 WP silver- and gold-loaded 2 mm diameter and 1 mm height disk-shaped tumor using the detection setup shown in Fig. 9.8

Table 9.4 List of animal types and nanomaterials used in imaging works

Objects	Nanomaterials	Refs.
Mice	AuNPs	Hainfeld et al. [5]
Rats	AuNPs	Pradhan et al. [29]
Juvenile swine	AuNPs	Boote et al. [106]

9.3.2 Imaging Objects

The second area is the object of imaging. Only a few kinds of objects have been used, which include mice, rats, and swine. Table 9.4 lists all of the objects reported in the literature. Nanomaterials used in these animal studies are also listed. All objects are small compared with the human body. Representative references are given.

9.3.3 Core of Contrast Agents

Nanomaterials as contrast agents have been developed quickly in the last decade. Table 9.5 lists the core materials of the nanomaterial contrast agents for X-ray imaging reported in the literature. The discussion in this subsection follows chronologically the groups who performed the work.

Hainfeld et al. [107] used gold nanoparticles as a contrast agent for X-ray imaging. Their results, which were also shown in their 2004 publication [5], clearly revealed mouse veins after injection of gold nanoparticle solutions into the tail veins. Figure 9.10 shows the images before injection (left panel) and 2 min after injection (right panel). The veins were clearly visible with the injection of gold nanoparticles. The diameter of the vein shown in the right panel was approximately 0.2 mm. Since 30 HU (or 7 HU) was the minimum contrast difference needed to differentiate two objects, and the image in the right panel shows a contrast much higher than the minimal needed for differentiation, the contrast change should be greater than 30 HU. The loading, as claimed by the authors in their 2004 publication, was higher than 0.2 WP. Combining these two pieces of information, UWPCI should be on the order of 150 HU WP^{-1} .

Hainfeld et al. [108] employed gold nanoparticles to image brain tumors in mice. The average size of gold nanoparticles was 11 nm and gold loading in the tumor was 1.5 WP. The results suggested that nanoparticles crossed the blood-brain barrier and were taken up by the tumor more effectively than healthy brain tissues, resulting in a ratio of 19:1 nanoparticles in tumor to healthy tissue. The X-rays were 100 kVp with a 1.7 mm Al filter. The authors found that the toxicity LD_{50} for gold nanoparticles alone was 5 g/kg or 0.05 WP, which is low compared to the loadings used in many reports. Although unspecified, this loading should be the value for the whole volume of the animal, as the tumor loading of gold was much higher than this value. It was also unclear as to whether this LD_{50} was with respect to healthy mice or cancer-bearing mice. The authors used a loading of 4 g/kg or 0.04 WP injection dose of gold nanoparticles for imaging. The contrast change was 1050 HU at 15 h after injection

Table 9.5 List of nanomaterials used in X-ray nanochemistry imaging. Composition, size, uptake and X-ray energy are given. Contrast change or increase is listed and UWPCI is calculated based on contrast change and uptake. The results are arranged chronologically according to the corresponding authors. Multiple papers from the same group are grouped together

Composition	Size (nm)	Uptake amount (WP)	X-ray energy	Fluo	Contrast increase (HU)	UWPCI (HU/WP)	Ref.
Au	1.9	0.3	22 kVp	-	-	-	Hainfeld et al. [107]
Au	11	1.5	45 kVp	-	1050	875	Hainfeld et al. [108]
Au/Gd	2.4	1	40 kV	-	1287	1287	Roux et al. [109]
Au	4-60	2	120 kVp	-	600	300	Sun et al. [89]
C	-	Pure	30 kV	-	-	-	Wen et al. [96]
Au (theory)	-	0.1-1.0	60-140 keV	-	-	-	Yusa et al. [110]
Au	20	0.038	80, 140 kVp	-	2.2-13	130	Boote et al. [106]
Au	1.9	1.0-2.0	110 kVp	Yes	-	-	Cho et al. [90]
Theory	-	<2	110 kVp	Yes	-	-	Cho et al. [91]
Au	1.9	0.5-2.0	105	Yes	-	-	Cho et al. [111]
Au	-	<2	62 kVp	Yes	-	-	Cho et al. [93]
Au	Theory	-	105 kVp	Yes	-	-	Cho et al. [94]
Au	12-29	-	80 kVp	-	130	-	Jon et al. [112]
Fe, Zn, Br	Solutions	-	15 keV	Yes	-	-	Meng et al. [95]
Au	2-4	0.15	80 kV	-	>7	>50	Shi et al. [100]
AuNP@SiO ₂	88	-	110 kVp	-	20	300	Mulder et al. [113]
Au@SiO ₂	18/46	-	10-40 Kv	-	300	-	Cui et al. [49]

	Theory			110 kVp	Yes				
Au				110 kVp	Yes				Manohar et al. [114]
SiO ₂ -covered AuNRs	15/44	0.2		130 (kVp)	-	56	280		Ren et al. [102]
Au	10-50	6 ppm		95.6 kV	Special				Rose-Petruck et al. [103]
Gd oxide	1.1	5-6 ppm		>50.2 keV	-				Roux et al. [115]
TiO ₂	2-3	1.5		50, 125 kVp	-	26.6	17.7		Kuncic et al. [116]
Au (saline solutions)	-	2		150 kVp	Yes				Bazalova et al. [99]
Au	15	0.05		20-100 kV					Kunzel et al. [117]
Au	1.9	14.1		120 kVp	-	3000	114		Tu et al. [118]
Bi ³⁺ /SWCNTs		0.1		110 kVp		36	360		Wilson et al. [119]
Au		0.05-0.5		45 kVp	-	60-225	1200-450		Cole et al. [120]
Pt	10 nm	5-30 ppb		1.25 MeV	-	0.27	Optical density		Deyhimighighi et al. [121]
Au/SiO ₂	17/60/12	3.6		50 kVp	-	1100	306		Zhao et al. [122]
Au		1		100 kVp	Yes				Guo et al. [105]
Au	30/90			45 kV	-	220			Kannan et al. [123]
Au	10, 50	0.002		80-100 kV	-				Rose-Petruck et al. [124]
Au/FeOx NPs	100	0.3 (0.0003-0.3)		55 kVp		110	366		Casey McQuade et al. [125]
LF3:Tb/Si ₂ O/Dye	40	24.9		<45 kV	-	3000	121		Yang et al. [126]
Gd/Yb/SiO ₂	280/500			120 kV	-	2144	1230		Yang et al. [127]
Au	3.9-41				-	60			Chang et al. [76]
Au/Fe ₃ O ₄	50 nm	0.8		50 kVp		700	875		Mei et al. [62]
Au	7, 9, 19, 38	1				900	900		Bulte et al. [128]
Bi	3.6	1.72		80 kV	-	1193	690		Li et al. [71]
Au nanorods	10 × 50	2		60 kVp	-	300	150		Xu et al. [129]



Fig. 9.10 Image of mice without nanoparticles (left panel) and injected with 1.9 nm gold nanoparticle solutions (right panel). A vein only a fraction of mm in diameter was visible in the right panel (marked by the arrow). (From Hainfeld et al. [5]. doi: <https://doi.org/10.1088/0031-9155/49/18/N03>. © Institute of Physics and Engineering in Medicine. Reproduced by permission of IOP Publishing. All rights reserved.)

and the half-life was 24 h. UWPCI was 875 HU WP^{-1} for a 1.2 WP loading (in tumor) given by the authors.

Roux et al. [109] developed a chelate surfactant layer on gold nanoparticles for combined X-ray and MRI imaging of animals that can potentially be used in clinical applications. The ligands included DTPA, DTPADA, and DTDTPA. The average size of the gold nanoparticles was 2.4 nm. The X-rays were from synchrotrons and both CT and microbeam configurations were used. Fifty-one beams of $25 \mu\text{m}$ diameter X-ray beams, whose energy were as high as 100 keV, from the European Synchrotron Research Facility (ESRF) were used. Rats injected with gold nanoparticles irradiated with X-rays survived almost twice as long as those that were not treated with gold nanoparticles, suggesting that gold nanoparticles irradiated with X-rays inhibit tumor growth.

Boote et al. [106] performed CT imaging of a phantom and juvenile swine using gold nanoparticles as a contrast agent. The average size of gold nanoparticles was 50 nm. The uptake was found to be $0.38\text{--}0.68 \text{ mg/g}$ in the liver and spleen, which corresponds to gold loadings of $0.038\text{--}0.068 \text{ WP}$. Images obtained by the authors with the gold contrast agent showed an average increase of contrast of 7 HU, which was lower than the normally required minimal 30 HU to separate two objects. The average UWPCI was 180 HU WP^{-1} , similar to other results obtained with mice models. Given the size of swine being an order of magnitude larger than mice, the results were encouraging.

Jon et al. [112] used a specially prepared gold nanoparticle as both a contrast agent and therapy enhancer. The authors coated the gold nanoparticles with a prostate-specific membrane antigen RNA aptamer, which targeted prostate cancer cells that expressed the antigen proteins. The results showed a $4\times$ increase in CT imaging contrast for the targeted results compared to a non-targeted control imaging measurement.

Kannan et al. [130] showed that gold nanorods were an effective X-ray image enhancer. The nanorods had an average diameter of around 30 nm and a length of 90 nm, giving rise to an aspect ratio of 3. The uptake was rapid, and an increase in

contrast of 90 HU was observed after one injection and 200 HU after the second injection. No unit mass contrast increase was available. Zhao and Ma et al. [122] demonstrated the use of folic acid conjugated silica-coated gold nanorods for CT imaging. The dimensions of the nanorods were 60 nm long and 17 nm in diameter. The thickness of the silica coating was 12 nm. At 36 mg/mL concentration, which was 3.6 WP, the contrast increase was 1100 HU, corresponding to a 306 HU WP⁻¹ UWPCI.

Roeder et al. [120] developed bisphosphate-functionalized gold nanoparticles as an X-ray contrast agent. The ligand had an amine group that can bind to gold surface and a phosphonate group that binds to calcium ions on hydroxyapatite crystal surface. The gold nanoparticles were 12 nm in size. Up to 225 HU increase was detected using a three-dimensional CT imaging method, although approximately 20 WP of gold was found in the targeted region. UWPCI obtained in this work was only 11 HU WP⁻¹, which was approximately an order of magnitude less than the lowest obtained by others. A similar work by the group is mentioned later in this section when surfactants are discussed.

Yang et al. [126] produced LaF₃:Tb nanoparticles covered with silica and tethered with organic dye molecules. A LaF₃:Tb core was used to absorb X-rays for CT imaging purposes as well as for scintillation so that the emitted photons transferred their energy to the dye molecules through FRET. Although not explicitly expressed, the average size of the core was 40 nm, and the authors claimed the silica layer thickness ranged from 3 to 45 nm. The contrast increase was 3000 HU per 0.7 M of LaF₃:Tb. UWPCI was 121 HU WP⁻¹, calculated based on the contrast increase and the molecular mass of 355 g/mol, which resulted in a 24.9 WP loading. Figure 9.11 shows the results.

Yang and Lin et al. [127] studied a multimodal imaging approach to image nanomaterials in vivo. This time the authors employed Gd and Yb nanomaterials. Similar to their work mentioned above, the contrast increase reached 3000 HU but

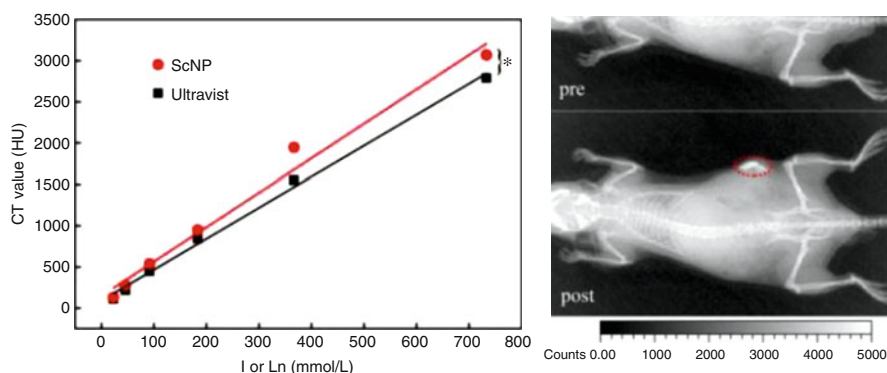


Fig. 9.11 Image contrast (left panel) and images of animals (right panel) using LaF₃:b nanoparticles to enhance X-ray imaging. (Adapted in part from Yang et al. [126] with permission of the Royal Society of Chemistry.)

with only 25 mg/mL loading. This was equivalent to 1200 HU WP^{-1} , which was one of the highest UWPCI reported in the literature.

Tu and Lo et al. [118] studied gold nanoparticles as a contrast agent in CT planning for radiotherapy. The size of gold nanoparticles was 1.9 nm. The loading of gold nanoparticles in media in their experiments ranged from 28 to 141 mg gold per mL. The increase of imaging contrast was 322 HU for 28 mg/mL and 1608 HU for 141 mg/mL. These increases translated to 114 HU WP^{-1} UWPCI for gold in tissue. They also calibrated the gold nanoparticles against a standard of Conray 60, an iodine-based contrast agent. The authors suggested to use 22.5 mg/mL gold in clinical cases, which was over 2 WP (in tumor) and could cause more than twofold radiation enhancement if physical enhancement was considered.

Wilson et al. [119] discussed the work of using a new type of bismuth nanomaterial, i.e., evaporated bismuth trapped in or embedded in single-walled carbon nanotubes, for CT imaging. The X-ray energy was 110 kVp. Single-walled carbon nanotubes with bismuth showed an increase of 36 HU over imaging without bismuth, which was greater than the 30 HU difference required for distinguishing adjacent tissues. Bi^{3+} loading was 1 g/kg or 0.1 WP. The technique thus generated a 360 HU WP^{-1} UWPCI using their bismuth nanostructures.

Tsourkas et al. [38] used micelles-containing gold nanoparticles for imaging (and treatment) of tumors in mice. The micelle size was between 25 and 150 nm and gold nanoparticles in the micelles were 1.9 nm in diameter. The CT images showed gold contrast agent in HT1080 flank tumors 24–48 h after injection of nanoparticles. Nearly 6% of the injected dose of gold nanoparticle micelles was found in the tumor 48 h after nanoparticle administration, which corresponded to 0.57 mg/mL or 0.057 WP. The authors mentioned that the detection limit of using gold as contrast agent was 0.5 mg/mL, which was 0.05 WP gold in water. According to results acquired here, the contrast increase for adding gold was between 120 and 800 HU WP^{-1} , which means that 0.05 WP would generate a contrast increase between 7 and 40 HU. Tsourkas et al. [125] improved the imaging and therapy by incorporating magnetic nanoparticles into the micelles so that CT imaging could be performed in practical radiotherapeutic settings. The magnetic nanoparticles, or superparamagnetic iron oxide nanoparticles, were used to enable magnetic resonance imaging (MRI). Gold nanoparticles were used to provide radiosensitization.

Wang and Mei et al. [62] synthesized iron oxide nanoparticle-functionalized gold nanocages for simultaneous CT and MRI imaging. Moreover, T1- and T2-weighted MRI imaging were obtained. UWPCI was on the order of 500 HU WP^{-1} . In another work, Tian and Pan et al. [131] employed Au@Pt nanodendrites synthesized for the purpose of imaging and treatment of tumors. The gold core had a diameter of 8 nm and the platinum nanobranches, as the authors called them, on the surface of the gold cores were approximately 10 nm long, making the whole nanodendrites nearly 30 nm in diameter. The nanodendrites were then PEGylated. CT imaging showed nearly 1800 HU increase at 10 mg/mL loading, giving rise to an 1800 HU WP^{-1} UWPCI. The nanodendrites were also used for tumor treatment, and the best results were obtained when both near-infrared and X-ray irradiation were present.

Yang and Li et al. [71] used 3.6 nm bismuth nanoparticles coated with LyP-1 peptide ligands to increase contrast in tumor imaging. Their calibrated unit concentration contrast increase was 13.8 HU mM^{-1} , which was equivalent to 690 HU WP^{-1} . Zhao and Xu et al. [129] developed gold nanorod-based nanoparticles for CT imaging. A silica shell was coated onto the nanorod core, and ethanolamine-modified poly(glycidyl methacrylate) ligands were conjugated to the surface of the silica shell. Glioma tumor-bearing mice, after injection of the nanomaterial, were imaged and up to 300 HU contrast increase was measured with nearly 20 mg/mL incubation concentration. No uptake data was available.

Several review articles on contrast agents have been published in recent years. The applications of these agents are not limited to X-rays. Most of the reviews covered more materials than what is discussed here, so readers interested in contrast agents for modalities other than X-rays can read these reviews. The chemistry involving synthesis and functionalization of the nanoparticle-based contrast agents share a common knowledge base with X-ray nanochemistry.

Among these reviews, Cormode et al. [132] summarized the results of using gold nanostructures for diagnosis and therapy. Cormode et al. [88] reviewed contrast agents developed from micelle and liposomes. Anton et al. [133] reviewed inorganic nanoparticles as contrast agents. Cole et al. [134] summarized the results of using gold nanoparticles as contrast agents for X-ray imaging. There have also been systematic efforts to improve contrast agents, such as employing ytterbium nanoparticles. For example, Liu et al. [135] reviewed the use of ytterbium nanoparticles for X-ray imaging. Li et al. [136] reviewed the use of several gold nanostructures including nanoparticles and nanorods for CT imaging and imaging guided therapy.

9.3.4 Surfactants of Contrast Agents and Impact on Targeting, Delivery and Biodistribution

Surfactants are an important component of nanomaterial-assisted X-ray imaging. Although the contrast often originates from the nanomaterial core, its surface can influence uptake, targeting, and other properties of contrast agents, such as delivery and biodistribution. Many groups have worked on formulating nanomaterials for medical applications. These efforts have also helped advance X-ray nanochemistry. The current focus of X-ray nanochemistry is to learn about the fundamental processes, such as to enhance the effectiveness of X-ray irradiation through defining a number of chemical, biological, and nanochemical reactions, and these reactions are influenced by the surfactants as well. It should soon be clear that delivery and targeting of the nanomaterials will be needed not only for imaging but also for more advanced X-ray nanochemical applications, such as triggered release, because targeting and delivery will be important for practical applications once the fundamental enhancement mechanisms of triggering are understood and developed.

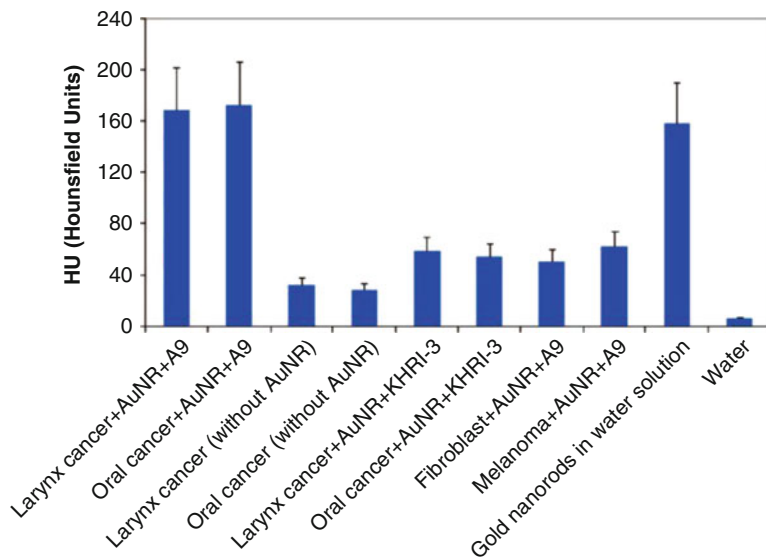


Fig. 9.12 Effect of targeting of gold nanorods (AuNR). The first two bars are about five times the third and fourth, demonstrating the effect of targeting. (Reprinted (adapted) with permission from Popovtzer et al. [139]. Copyright (2008). American Chemical Society.)

Many chemicals can help improve selective binding of nanomaterials to targets. For example, cell-penetrating peptides (CPP) on the surface of nanomaterials can facilitate the delivery of nanomaterials into the cell. There are many reviews on this subject and readers are encouraged to read them if interested. For example, Shen et al. [137] reviewed the work on CPPs. Sée et al. [138] reviewed the literature on delivering gold nanoparticles into mammalian cells.

A large number of groups have worked on targeting, and many demonstrations are available to show the effectiveness of targeting in terms of increasing the imaging contrast of and damage to tumors. For example, Kopelman et al. [139] showed a proof of concept of targeting to improve CT contrast. A fivefold improvement was recorded when gold nanorods (AuNR) were used. Figure 9.12 shows the results. Many other cellular surface components such as hypoxia-inducible factor (HIF-1) can be targeted.

Roeder et al. [140] discussed the use of bisphosphate-functionalized gold nanoparticles as a contrast agent for detection of breast microcalcification. This type of nanoparticles selectively concentrated at the reacting or tumor sites and increased the contrast to facilitate detection of these sites because phosphate functional groups targeted and reacted with hydroxyapatite (HA) in the breast. The authors found that the contrast increased by 300 HU with a 25 mg/mL or 2.5 WP HA loading at the tumor site. Gold loading was not specified. The results obtained by Cole et al. are shown in Fig. 9.13. Targeting therefore further improved the performance of high contrast nanomaterials, and minimized the total amount of nanomaterials used in imaging.

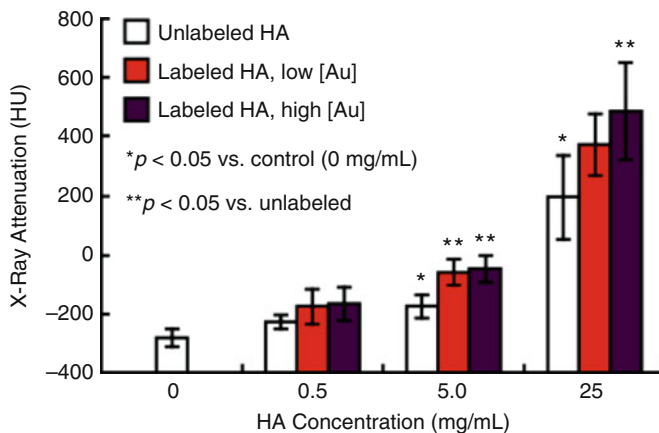


Fig. 9.13 Bis-phosphate functionalized gold nanoparticle contrast agent reported by Roeder et al. [140]. HA loadings are shown, although gold loading was not quantitatively determined and shown. (Reprinted from Cole et al. [140]. Copyright (2014) with permission from Elsevier.)

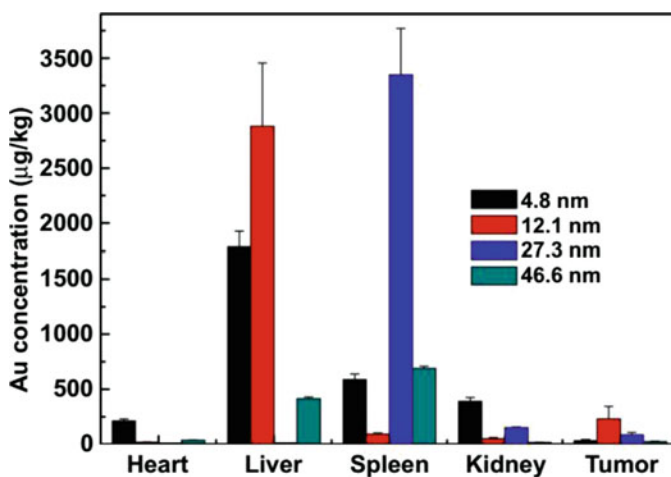


Fig. 9.14 Biodistribution results after delivery of gold nanoparticles into animals. Four sizes of gold nanoparticles were used, and most of the nanoparticles were found in the liver and spleen. (Reprinted from Zhang et al. [141]. Copyright (2012), with permission from Elsevier.)

Results on biodistribution have been provided by many groups. The data are critical to the determination of the cause for the enhancement as well, although not all the published reports contained this important piece of data. Biodistribution information is usually obtained through elemental analysis of different organs using mass spectrometry. A typical result is shown in Fig. 9.14, which was obtained by Zhang et al. [141].

9.3.5 Summary of Imaging

Imaging, when combined with other more direct methods of measuring the uptake such as ICP-MS, can also be used to evaluate or predict physical enhancement based on the difference between mass energy absorption coefficients μ_{en}/ρ and mass attenuation coefficients μ/ρ as discussed in Sect. 2.2. This is because imaging can be used to obtain mass attenuation coefficients μ/ρ , and since mass attenuation coefficients μ/ρ has a fixed relationship with mass energy absorption coefficients μ_{en}/ρ , which determine physical enhancement, it is therefore possible to predict physical enhancement using imaging contrast. In addition, as shown above, imaging can be used to provide information on biodistribution, both qualitatively and quantitatively.

As indicated above, nanomaterial-assisted X-ray imaging has been mainly used in small animal models and rarely in large-size animals or human phantoms. Further, toxicity issue has to be addressed before human imaging is possible. The work done so far has established the baseline for loadings of nanomaterials as well as X-ray energy and other parameters such as targeting and delivery. These studies have paved the way for imaging larger objects.

Figure 9.15 summarizes most of the results mentioned in this section. Loading in the units of WP is used in the horizontal axis and UWPCI in the units of HU WP^{-1} is

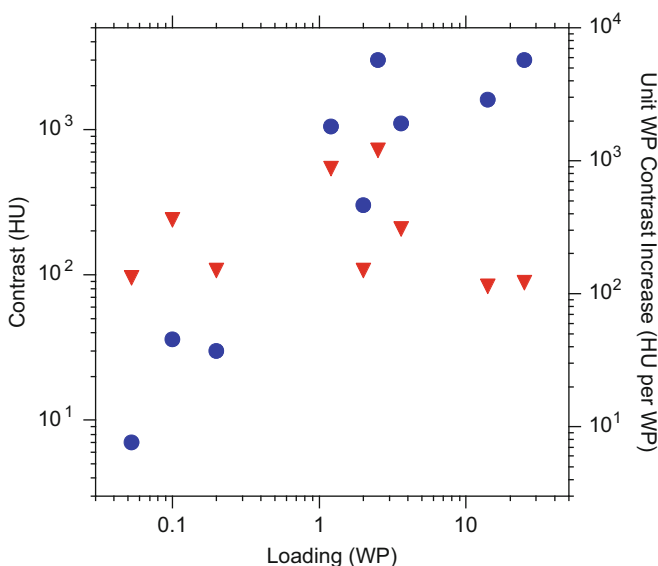


Fig. 9.15 Summary of the results of nanoparticle-enhanced X-ray imaging. Contrast results are given (blue circles). The values of unit WP contrast increase (UWPCI) in HU WP^{-1} (red triangles) from adding nanomaterials are also given, which are greater than 100 HU WP^{-1} for all the results reported in the literature

used for the right vertical axis (red triangles). Contrast change in units of HU is shown in the left vertical axis (blue circles). As it is shown here, all the works shown in this section, with the exception from one study, generated UWPCI between 120 and 800 HU WP⁻¹. Using 30 HU as the minimum contrast difference between adjacent tissues, the minimum loadings for these new imaging contrast agents are between 0.0375 and 0.25 WP, which are below the LD₅₀ toxicity level for most nanoparticles. However, since most results shown here are acquired using small animal models, these criteria will have to be revised upward in clinical trials and treatment of patients if the imaging objects are much larger than the tested objects described here. Loadings would have to be orders of magnitude higher because of the much greater thickness of human body unless sectional images are taken. It is very likely that 1 WP nanomaterials are needed for imaging large objects. At this level, many nanomaterials are toxic. If there is no guarantee that nanomaterials only target tumors or only large amounts of nanomaterials accumulate at tumors, then either more sensitive imaging methods such as X-ray fluorescence-based approaches have to be used, or only small objects are imaged.

When high loadings (>1 WP) of nanomaterials are needed for imaging, then most likely the same nanomaterials can be used to effectively enhance the efficacy of X-ray treatment. If only physical enhancement is involved, then about a 1.0 DEU enhancement can be reached. On the other hand, if efficient X-ray-triggered drugs are developed and used, the dose requirement for the treatment may be lowered to 0.1 Gy or even 0.01 Gy, which is far less than even the acute dose of 1 Gy for the human body. In this section, no dose information is given. For CT of human bodies, the dose is usually kept below 0.1 Gy or 10 rem (head CT) or even below 0.01 Gy or lower (chest). It would be convenient to use the same nanomaterials and similar doses to both image and treat tumors with X-rays in human bodies.

In the next section, results of theoretical studies of enhancement of energy deposition are reviewed.

9.4 Theoretical Work on Cancer and Animal Treatment

The theory used here is based on physical enhancement described in Chap. 2, not full quantum simulations of molecular or biological events. Many of the theoretical works have already been presented in Chap. 2, so here only those that are closely related to medical applications but not fully described in Chap. 2 are summarized. Even though no quantum or molecular dynamics simulations are involved, the theoretical results shown both here and in Chap. 2 can still help explain experimental *in vivo* and *in vitro* results in the form of predicting the magnitude of physical enhancement. While biological systems are complex and often the measured enhancement values are heavily influenced by biological processes or pathways, at least it is still possible to conduct these theoretical works to help discern whether the observed enhancements can be interpreted by the increased absorption of X-rays

from the added nanomaterials. If the magnitude of the theoretically predicted physical enhancement is far different from the experimentally measured enhancement values, then chemical or biological enhancement or other processes could dominate. Such revelation may promote researchers to work toward uncovering the true causes of enhancement.

Table 9.6 lists the groups that have reported the results of theoretical prediction of the enhancement of using nanoparticles on cancer treatment. Many nonmedical studies are discussed in Chap. 2. The desired enhancement calculations for medical applications address situations closely related to the *in vitro* and *in vivo* experiments. As discussed in Chap. 2, the magnitude of physical enhancement, which is the only enhancement that can be accurately simulated theoretically to date, is approximately 1.4 DEU WP^{-1} of gold in water under 33 keV X-ray irradiation. Table 9.6 includes calculations that showed much greater enhancement factors, as high as $10,000 \text{ DEU WP}^{-1}$ of gold in water. The causes for such a large disparity of enhancements reported in the literature are explained in Sect. 2.3.3.3 and Fig. 2.19.

Cho [142] employed a BEAMnrc/DOSXYZnrc code and simulated the enhancement by gold in phantoms under X-ray irradiation. The results are discussed in Chap. 2. The main conclusion was that there was enhanced energy deposition in water to which gold was added. The magnitude of enhancement was 1.0 DEU for 0.7 WP gold in water, a value that agreed with many studies reported in the literature.

McMahon et al. [143] calculated enhancement of energy deposition by gold contrast agents under 150 kVp and 15 MV X-ray irradiation. A loading of 10 mg/mL or 1 WP was used in their calculations. The authors proposed a “figure of merit,” which was the ratio of total dose in the tumor to the highest dose in nearby healthy tissues. Their results are shown in Fig. 9.16, which indicate approximately an enhancement of 1 DEU WP^{-1} for 150 kVp X-rays either with (dashed line) or without (solid line) Al foil filter. X-rays reached the enhancement site had to traverse through a 50 mm thick tissue, which was a *de facto* filter that made X-rays harder (more energetic) even without the use of filters. The predicted enhancement values were close to those predicted by other calculations shown in Chap. 2. The enhancement was negligible for 15 MV X-rays (dotted line). The results on high-energy MV X-rays were also close to those obtained by others. These results suggested again that if significant unit WP enhancement was observed using MV X-rays, then the enhancement should be caused by chemical or biological enhancement.

Yusa et al. [110] theoretically studied the role of colloidal gold as a contrast agent. The authors found that with 1 WP gold in tissues, the contrast increase was 70% of the contrast obtained with bone in tissues of the same dimensions irradiated with 88 keV monochromatic X-rays. Assuming the bone model is cancellous, then the UWPCI is approximately 490 HU WP^{-1} . The results, however, could not be directly used to infer energy deposition enhancement because the calculated 70% increase was an attenuation increase, not the energy deposition increase. The two values are not close to each other at 88 keV based on the discussion given in Chap. 2.

Gokeri et al. [144] theoretically investigated irradiation of a gold-loaded tumor region in a realistic head phantom irradiated with an array of X-ray microbeams. Their method used an array of parallel microbeams of X-rays and a gold contrast

Table 9.6 List of works in theoretical studies of physical enhancement in biological systems. The results are arranged chronologically, from the earliest to the most recent. Composition and size of nanomaterials are given, as well, X-ray energy, the package used in the simulation and targets are given

Composition	Size (nm)	Cell/target	X-ray energy	Package	Ref.
Au	Atoms	Phantoms	140 kVp, 6 MV	BEAMnr/DOSXYZnrc	Cho [142]
Au	Atoms	Phantoms	150 kVp, 15 MV	Geant4	McMahon et al. [143]
Au	Atoms	Contrast agent	60–140 keV	EGS5	Yusa et al. [110]
Au	Atoms	Phantoms	30–600 keV	MCNPX	Gokeri et al. [144]
Au	1.9, 5, 30, 100	Water	20–157 keV, 6 MV	MCNP-5	Pignol et al. [145]
Au	2–50	MDA-MB-231	20–150 keV, 160 keV	Geant4/Geant4-DNA/LEM	McMahon et al. [51]
Au	2	MDA-MB-231	6 and 15 MV	Geant4/C4DNA/LEM	McMahon et al. [70]
Z = 53–81	Atoms	Phantoms	50–600 keV	PENELOPE	Martinez-Rovira et al. [146]
Au	1.9	Slab models	80–120 kVp	Homemade based on Cole (ref)	Ngwa et al. [147]
Au	30	PC-3	300 kVp	MCNP-5/PENELOPE	Pignol et al. [148]
Au	Atoms	Tumor capillary vessels	150 kV	Geant4	Annato et al. [149]
Au	30, 50, 100	Phantoms	50–120 keV, 1.3–18 MV	MCNPX	Mesbahi et al. [150]
Au	50	Bladder cancer cells	200 keV	Geant4	Jeynes et al. [151]
Au	2, 15, 50, 100, 200	Water	60–150 kVp	PENELOPE/Geant4/ENSnr	Li et al. [152]
Terpyridine-Pt complex	Atoms	F98 and B16	160 kVp/6 MV	Geant4	Pradhan et al. [29]
Ag, Au	5–250	Liquid	40 keV	Homemade	Wardlow et al. [153]
Au	100	Generic spherical cells	60 kVp	PARTRAC	Xie et al. [154]
Au	3–50	HeLa	keV, MeV	Geant4	Chang et al. [76]
FeOx, Au	20, 50	U87	6 MV	Geant4-GATE.7.0	Retif et al. [61]
Au	2	MDA-MB-231	160 kVp, 6 MV, 15 MV	Geant4-G4DNA	Antilli et al. [155]
Au	2, 15, 20 50	MDA-MB-231, F-98	51, 150 keVp, 6 MV	LEM	Schuemann et al. [156]

The packages are discussed in Sect. 2.3.3

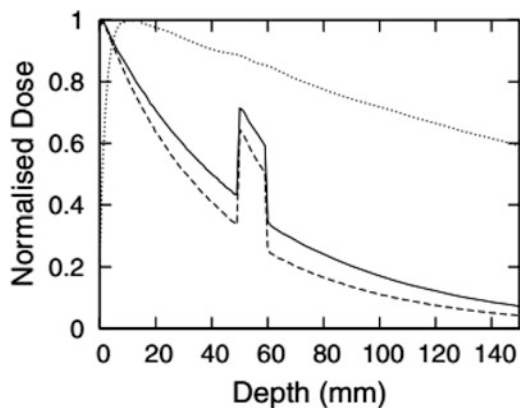


Fig. 9.16 Calculated enhancement for 150 kVp and 15 MV X-rays. Nearly 1.0 DEU was obtained when 1 WP gold nanoparticles were irradiated with 150 keV X-rays (solid and dashed lines). Enhancement was negligible for 15 MV X-rays (dotted line). (From McMahon et al. [143]. doi: <https://doi.org/10.1088/0031-9155/53/20/005>. © Institute of Physics and Engineering in Medicine. Reproduced by permission of IOP Publishing. All rights reserved.)

agent for therapy. Although no nanomaterials were used, similar therapeutic effects exist regardless of the form of gold, whether it was in the form of atoms or nanoparticles. The form of materials would affect the delivery or targeting of the material. In the work by Gokeri et al., up to 20 beams of 0.68 mm diameter were employed to irradiate a head phantom. 7 mg/g or 0.7 WP gold in tumor was loaded in the tumor, and an approximately 40% increase in dose enhancement or a 0.4 DEU enhancement was observed in in-beam dose. The average X-ray energy was 107 keV with the spectrum of X-ray covering 30–600 keV. The calculated enhancement of 0.57 DEU WP⁻¹ for the spectrum was close to the experimentally measured enhancement using a mice model, suggesting that the observed enhancement could be caused by physical enhancement.

Pignol et al. [145] explored the potential of using gold nanoparticles in clinical scenarios. The codes the authors used were MCNP-5 with cross-section data from ENDF/B-VII and PENELOPE 2008.1. The size of the nanoparticles ranged from 1.9 to 100 nm. The results included detailed contributions from different types of electrons such as photoelectrons and Auger electrons. The calculations also considered energy absorbed internally by gold nanoparticles. Figure 9.17 shows the trajectories of electrons emitted from gold nanoparticles. The results showed that for 6 MV radiation, more than 100 WP of gold in cells was needed to generate a measureable enhancement, which was not clinically possible or achievable. For 300 kVp, only a 0.5 WP gold loading in water was needed to generate a measureable enhancement, which is possible in clinical settings. These results agree with those shown in Chap. 2.

Ngwa et al. [147] discussed a method of using gold nanoparticles to improve radiosurgery for neovascular age-related degeneration. Their modeling configuration is shown in Fig. 2.20 in Chap. 2. The authors reported an enhancement of 1.5 DEU

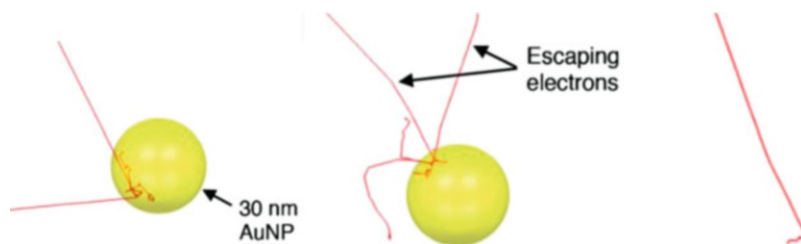


Fig. 9.17 Calculated electrons tracks in water from those emitted from a 30 nm gold nanoparticle irradiated by 6 MV X-rays (left and middle panels) and I-125 source (right panel, maximum 35 keV X-rays). One noticeable difference is that the track shown in the right panel is over 10 μm long (the 30 nm nanoparticle is invisible), whereas the tracks shown in the left and middle panels are only tens of nanometer long. (From Pignol et al. [145]. <https://doi.org/10.1088/0031-9155/56/15/001>. © Institute of Physics and Engineering in Medicine. Reproduced by permission of IOP Publishing. All rights reserved.)

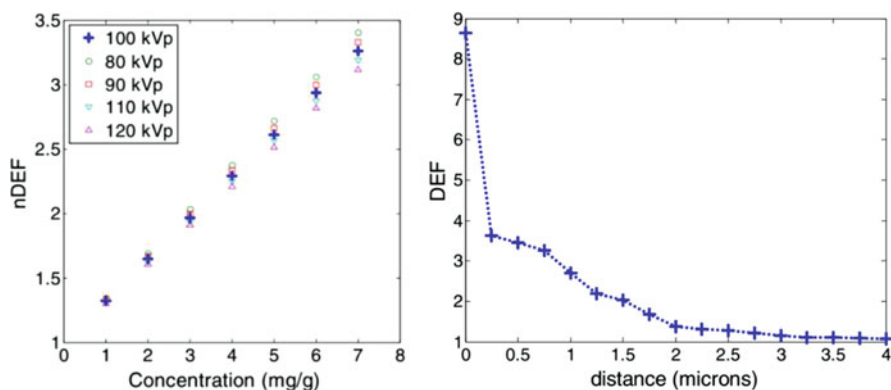


Fig. 9.18 Nuclear dose enhancement factors (nDEF) at different concentrations of gold calculated for gold nanoparticles irradiated with X-rays at energies between 80 and 120 kVp (left panel). The right panel shows the spatial profile of nDEF. (From Ngwa et al. [147]. <https://doi.org/10.1088/0031-9155/57/20/6371>. © Institute of Physics and Engineering in Medicine. Reproduced by permission of IOP Publishing. All rights reserved.)

per 0.5 WP gold in water for several X-ray energies between 80 and 120 kVp. This was equivalent to 3.0 DEU WP⁻¹ unit weight percentage enhancement, which was higher than the typical 1.0 WP⁻¹ enhancement based on type 1 physical enhancement or 1.4 DEU WP⁻¹ physical enhancement. The increase was possibly due to type 2 physical enhancement, as the authors labeled the dose enhancement as nuclear dose enhancement factor (nDEF). Figure 9.18 shows the results of nDEF and dose enhancement factors near a 500 nm thick slab using 100 kVp X-rays, which clearly show type 2 physical enhancement.

In one of several publications, Amato et al. [149] estimated enhancement from gold in capillary phantoms under X-ray irradiation. They employed large amounts of gold, including 10, 20, 50, 100, and 200 mg/g in the phantom, which corresponded

to 1–20 WP gold loadings in tissue. They modeled several paths of gold diffusion through the capillary vessel as well as the depth effect. The X-ray energy was 150 kVp. The authors calculated unit WP enhancement for gold in phantom, and the results showed 0.65–1.0 DEU WP⁻¹. This range of magnitude of enhancement agreed reasonably well with the type 1 physical enhancement of nearly 1 WP⁻¹ for 40 keV X-rays shown in Chap. 2.

Mesbahi et al. [150] theoretically modeled dose enhancement from gold nanoparticles under ionizing radiation of 50–120 keV to MeV photons. They obtained 0.4–2.7 DEU for monochromatic kilovoltage X-rays. The optimal energy was found to be 90 keV. For 0.7 WP, the enhancement was 1.0 DEU for 90 keV X-rays, corresponding to unit WP enhancement of 1.4 DEU WP⁻¹. This value is identical to the values obtained in Chap. 2 as well as those shown in this section. In contrast, the predicted enhancement was only 0.03 DEU for MeV X-rays, which also agrees with other results.

Li et al. [152] used three Monte Carlo packages, PENELOPE-2011, GEANT4, and EGSnrc, to simulate dose enhancement by gold nanoparticles. Four sizes of gold nanoparticles under X-rays at four energies between 60 and 150 kVp were used. Twenty water shells whose thicknesses are between 10 nm and 1 μ m around the gold nanoparticle were used to evaluate the enhancement. All three packages predicted local enhancement near the surface of gold nanoparticles, as suggested in Chap. 2. The enhancement values predicted in this work were higher than those shown in Fig. 2.35. For a 100 nm diameter gold nanoparticle, over 1000 DEU enhancement was predicted within the first 10 nm water shell using PENELOPE. This high enhancement value was caused by the irradiation configuration of X-rays, illuminating only a small cross-section of water matching the size of gold nanoparticles, as explained in Fig. 2.19. Such artificial reduction of the denominator in enhancement calculation increased the magnitude of enhancement because enhancement is the ratio of energy deposition by electrons released from gold to from water as shown in Eq. 2.1. A significant reduction in the amount of energy deposited in water by electrons produced from X-rays interacting with water resulted in a significant reduction to the denominator.

Jeynes et al. [151] theoretically estimated the influence of secondary electrons emitted from gold nanoparticles in cells under both X-ray and proton irradiation. X-ray energy was up to 200 keV and proton energy was up to 250 MeV. Geant4.10.p01 together with CLHEP2.1.3.1 and ROOT 5.28.00 were used. RT112 bladder cancer cell line was used to obtain the experimental results. Significant increase of secondary electron emission was found with X-ray irradiation of gold nanoparticles, whereas only 10–20% increase was found with protons.

Xie and Li et al. [154] employed a PARTRAC code to simulate nuclear DNA damage and enhancement factor with 100 nm diameter gold nanoparticles positioning in a spherical cell and surrounding, but without entering, the spherical nucleus in the middle of the cell. 60–200 kVp X-rays were used in the simulation. The overall DNA strand break enhancement factor, however, was less than 20% (0.2 DEU) for 100 nm gold nanoparticles and 60 kVp X-rays. Higher enhancement occurred when the gold nanoparticles were on the nucleus surface than in the

cytoplasm. Pradhan et al. [29] compared enhancement by 1 and 7 mg/g Pt loadings in tumor phantoms under irradiation of 160 kVp and 6 MV X-rays. For 7 mg/g loading or 0.7 WP Pt in tumor, the enhancements were 0.81 DEU and 0.14 DEU for 160 kVp and 6 MV, respectively, calculated using a Monte Carlo method (Geant4). The unit WP enhancements were therefore 1.15 DEU WP^{-1} at 160 kVp and 0.2 DEU WP^{-1} at 6 MV. These values generally agreed with the results shown in Chap. 2.

Moshirian et al. [157] theoretically studied homogeneous and inhomogeneous distribution of gold in tumors deep in tissues. The authors found that 55 keV X-ray energy was optimal for maximal dose enhancement in the tumor. The maximum enhancements in various settings were much greater than approximately 1 DEU WP^{-1} . For example, the highest enhancement was 17.5 DEU in the inhomogeneous loading of 0.7 WP gold in water phantoms. These results demonstrate the utility of using type 2 physical enhancement to damage nearby targets.

Zygmanski et al. [158] reviewed the modeling of dose enhancement calculations in clinical X-ray irradiation settings. The authors provided a general discussion of the enhancement and compared the results of dose enhancement ratio (DER) obtained using two theoretical packages, CEPXS and GEANT4, and found the two results agreed with each other. For a 100 nm gold slab under 100 keV X-ray irradiation, an experimental condition reachable with metal implants, DER was as high as 30 DEU. DER at the surface of the gold slab was 110 DEU for 20 keV X-rays, which suggested that the enhancement was largely type 2 physical enhancement.

Retif et al. [61] described a new theoretical method that helped rank the effectiveness of organometallic nanoparticles in enhancing radiation effects, which were not limited to DNA damage originated from radiation induced energy deposition. In addition, the authors considered irregular distributions of nanoparticles in cells, similar to what Moshirian et al. observed. Although the authors claimed that the method was not to estimate the enhancement itself, they also asserted that the outcome agreed with the results of *in vitro* measurements. Their results suggested that the ranking of the nanoparticles should be 20 nm iron nanoparticles (best), 20 nm gold nanoparticles (middle), and 50 nm gold nanoparticles (worst).

Thomson et al. [159] investigated theoretically the influence of multiple cellular structures on enhanced energy deposition in nuclei. The geometric arrangement was similar to what was known as the lattice effect described by Guo et al. [160]. No nanoparticles were used. 20–370 keV X-rays were considered. The results and method are applicable to the cases where nanoparticles are embedded in the cells.

Schuemann and Ye et al. [156] theoretically studied enhancement of energy deposition in two types of cell by four sizes of gold nanoparticles coating the surface of the cells. The enhancement was caused by local effect model (LEM) and was close to type 2 physical enhancement defined in Chap. 2. Only a single cell was considered in this study, so the configuration was set up to study type 2 physical enhancement. Three energies of X-rays at 51 keV, 150 kVp, and 6 MV were used. The sizes of gold nanoparticles were 2, 15, 20, and 50 nm. The gold nanoparticles were all outside the cell. The results showed less than 1.0 DEU for 2 WP gold around

the cells for both 51 keV and 150 kVp X-rays and negligible enhancement for 6 MV X-rays. These results are in agreement with those obtained by others as shown in Chap. 2.

Attili et al. [155] theoretically simulated the enhancement of energy deposition by electrons in the nuclei of MDA-MB-231 cells. The authors also used LEM to describe their scenario, which was similar to type 2 physical enhancement described in Chap. 2. Gold nanoparticles were 2 nm in dia., and a Monte Carlo method using Geant4 version 10.1 toolkit was employed to simulate the energy deposition. X-rays were 160 keV, and 6 and 15 MV. The results showed that ionization probabilities per Gy for these 2 nm gold nanoparticles in water at these energies were 4.35×10^{-7} , 2.35×10^{-7} , and 2.25×10^{-7} , respectively. The authors did not specify whether these ionization events were ionization of core electrons. The first value was similar to what is given in Chap. 2. However, the last two values were high, which were within a factor of two of that at 160 kVp. Given the fact that X-ray absorption by gold at 6 MV was nearly three orders of magnitude less than at 160 kVp, the ionization for these small nanoparticles at 6 and 15 MV must be caused by charged particles generated from Compton scattering or pair production when X-rays interacted with water. Under such conditions chemical enhancement described in Chap. 3 should dominate because water absorption of X-rays dominated. If this is correct, then physical enhancement at these high MV X-ray energies should be much less than that by X-rays at keV energies, as reported in a large number of studies. The authors then compared the simulated survival fraction data with the experimentally measured results and found a good agreement at all these three energies.

The results shown in this section confirm that the magnitude of originally conceived physical enhancement in the form of the sum of average types 1 and 2 physical enhancement can only produce an approximately 1.4 DEU WP^{-1} . Potential medical applications would follow this guideline if physical enhancement is the source of enhancement. When much higher physical enhancement values are needed, then it is necessary to use peak type 2 physical enhancement described in Chap. 2, which can reach 10–50 DEU or even higher but requires large nanoparticles or aggregates of nanoparticles. However, such enhancement only exists in a region close to the surface of nanoparticles.

9.5 Treatment of Cancer (In Vitro) Cell Lines with Nanomaterials and X-Rays

9.5.1 Survey of In Vitro Work

Many efforts have been devoted to studying the enhancement of damage to cancer cells. Although cellular work is not as impactful or direct as animal models or even human clinical trials, cellular work does provide the necessary foundation and guidance for animal and clinical work. Logically there have to be some

understanding about the chemical systems such as nanomaterials even before the cell work, thereby fundamental chemical and physical works are needed before the cell work. The approach of going directly to animal may leave many issues unresolved, but at the same time, such an approach with positive results may inspire basic work. The significance of the cell work is that it bridges fundamental studies and animal and clinical work.

Chapter 8 covers cell work using healthy cells. In this chapter the target is cancer cell lines. The fast-growing nature of cancer cells should make them more susceptible to enhanced radiation effects, which is shown in Table 9.1. However, when compared with Table 8.4, the difference is not obvious.

Most of the discussion on enhancement effects cites the “traditional” enhancement or physical enhancement of the effectiveness of X-ray irradiation by nanoparticles under X-ray irradiation. This type of enhancement leads to release of electrons, followed by increased energy deposition in cells, which then converts to generation of additional reactive oxygen species. On the other hand, work has begun to create next generations of chemical and nanochemical systems following X-ray nanochemistry principles such as using triggered release of targeted delivery of highly potent drugs for ultimate enhancement of cell killing. In vitro work help test these promising possibilities. The triggered release results are given in Sect. 9.8.

Table 9.7 shows the groups that used cell work to examine the effect of nanomaterials. Another way to look at these results is that they are the applications of X-ray nanochemistry in damaging tumor cells by X-rays assisted with nanomaterials. X-ray-triggered release of drugs is not shown here. Table 9.7 also lists parameters important to performing cell work. The information includes cell lines, assay types, uptake/loading and nanoparticle compositions, X-ray dose and energy, enhancement, and the groups that performed the study. These parameters are described in the text as well.

Most work used purchased gold nanoparticles to test the damaging power of nanomaterials to cells under X-ray irradiation. More advanced nanomaterials are being synthesized to improve targeting tumor cells and damage because the unit WP enhancement from gold or other elements is usually fixed. Primitive nanoparticles only provided limited benefits and will not be commercially competitive, and future cancer treatment will have to use more advanced nanomaterials or mechanisms to assist cancer treatment. Nonetheless, the work published to date has helped establish a foundation for future endeavors.

The cited reasons in the literature for damage to cancer cells have generally been physical enhancement, which then causes the subsequently increased production of reactive oxygen species (ROS) in tumor cells. To date little effort had been devoted to demonstrating the existence of other damaging mechanisms in cells although those alternative mechanisms were suggested in several reports. For instance, biological enhancement is described in Chap. 4. There is also the possibility of chemical enhancement shown in Chap. 3. These possible mechanisms will have to be investigated in the future with improved synthesis of nanomaterials and more advanced instruments and methodologies.

Table 9.7 In vitro studies of enhancement of radiation damage of cancerous cells by nanoparticles under X-ray irradiation. The results are arranged alphabetically for the corresponding authors

Cell line	Assay	Uptake (WP)/ (#NPs)	X-ray Energy/dose (Gy)	NMs/surface	Enh (DEU)	Ref.
Colon cancer cells (HT-29)	MTS	>5	9 MV/8	50 nm AuNPs	0.90	Arab-Batrani et al. [39]
DU-145, MDA-231-MB	Clonogenic, γ -H2AX	–	160 kVp/2	1.9 nm AuNPs	–0.19–0.97	Butterworth et al. [45]
MCF-7 breast cancer	MTT	0.3/(1.21 \times 10 ⁵)	200 kVp, 1.3 MeV/10	10 nm AuNPs/cysteamine, Glu		Chen et al. [65]
MCF-7	Clonogenic	–	Cs-137/4	2.0–2.5 nm AuNPs/SUMO2/3	0.49, 7.88	Chen et al. [44]
HepG2	Clonogenic, γ -H2AX	0.00173	50 kVp/1–6	16 nm AuNPs/tirapazamine-conjugated PEG	0.25	Chen and Li et al. [37]
PC3	MTT	–	120 kVp/2	4 nm Cu&Co doped ZnS/PEG w/wo TBrRh123	0.03–1.4	Chen et al. [161]
HeLa, EMT-6	MTT, clonogenic	/10 ⁹	73 keV ^a /10	FeOxNPs	0.33–0.6	Chen and Margaritondo et al. [162]
HeLa, NIH3T3	MTT	3.6	–/8	500 Se NPs/PEG	0.5	Chen et al. [69]
PC3				Ce doped LaF ₃		Chen et al. [163]
HeLa	γ -H2AX, clonogenic	0.7	105 keV, 6 MV/	14–74 nm AuNPs/citrate	0.66, 0.17	Chithrani et al. [35]
MCF-7, SKOV-3	Cell viability assay	–	No X-ray irradiation experiment	10.4 nm AuNPs/lipoic PAA with cisplatin	–	Cook et al. [48]
A549	–	–	250 kVp/3 Gy	1.4 nm AuNPs/pHLIP	<10%	Cooper et al. [67]
MDA-MB-231	γ -H2AX	0.7	20–70 keV/1.5	1.9 nm AuNPs	0.95	Currell et al. [164]
A549	Clonogenic, γ -H2AX, 53BP1 foci	–	6 MV/8	Bi ³⁺ on 5 nm Gd ₂ O ₃ NP@SiO ₂ /DOTAGA	1.0	Detappe & Berbeco et al. [165]
U87	γ -H2AX, clonogenic	Optical	⁶⁰ Co	3 nm GdNPs	0.14–1.83	Falk et al. [166]

RG2 glioma	Mobility	TEM	125 keV	1.9 nm AuNPs	Geso et al. [58]
Panc 1 cells	MTS	–	6 MeV/6	12 nm Au NPs/ PEG and verteporfin	Goldys et al. [167]
Glioma C6	CM-DCF fluorescence	1 (attenuation of X-rays)	4 MeV/3	<5 nm SiNPs	Gonzalez & Kotler et al. [19]
HeLa	MTT, clonogenic	–	120–250 kVp, ⁶⁰ Co/2 Gy	AuNPs 47 nm/FA/4-ATP	Hashemi et al. [73]
CT26 colorectal	Clonogenic	0.1/(1 × 10 ⁶)	6 MV/2	4.7 nm AuNP/PEG	Hwu et al. [22]
EMT-6 and CT26	MTT, clonogenic, γ -H2AX	N/A	6.5, 8, 73 keV, 6 MeV/10	AuNP	Hwu et al. [28]
MDA-231 breast cancer	Clonogenic	–	160 kV, 6, 15 MeV/6	1.9 nm AuNPs	Jain et al. [50]
A549 lung cancer	MTT, clonogenic	–	6 MV/6	Cisplatin nanoliposomal	Jiang et al. [15]
Du-145	Methylene blue	–	160 kVp/0–25	60 nm C-Ag/PEG	Juzenas et al. [24]
HeLa, PC3	MTT	–	200 kV (average 60–70 keV)/1,5–6	8–9 nm Eu or Gd doped ZnO	Kharrazi and Amani et al. [170]
Du-145	Colony formation assay	2.7 × 10 ³ (Fe)	6 MV/2–8	20 nm Fe ₃ O ₄ / amino-group dextran	Khoei et al. [171]
CT26 colorectal	MTT	3–17/	7.1 keV/5, 20	10.6 nm FeONP/alginic acid	Choi et al. [21]
HTB-72 skin melanoma	Clonogenic	–	150 kVp, 450 kVp/8	1.9 nm (water-soluble organic shell), 50 nm Au NPs	Kim et al. [40]
9 L gliosarcoma	Clonogenic	–	10 MV/8	Rare earth (0.05–0.5%)	Konstantinov et al. [172]
Caco-2, MCF-7, 3 T3	DCF	–	120 kV/1–3	9–20 nm (γ -Fe ₂ O ₃) _{1-x} (Fe ₃ O ₄) _x (SPIONS)/malate or citrate	Krysch et al. [46]
HeLa	Clonogenic, MTS	Confocal imaging	220 kVp	2–3 nm AuNP/PEG	Kumar et al. [173]
MCF-7, T47D, MDA-MB-231	Clonogenic	30/(1.6 × 10 ⁶)	300 kVp/8	30 nm AuNPs/CPP-PEG	Latimer [52]

(continued)

Table 9.7 (continued)

Cell line	Assay	Uptake (WP)/ (#NPs)	X-ray Energy/dose (Gy)	NMs/surface	Enh (DEU)	Ref.
HeLa	Colony formation essay	–	^{137}Cs (662 keV)/ 1–8	4.8, 12.1, 27.3, 46.6 nm Au NPs/PEG	0.41	Liang et al. [141]
HT1080 fibrosarcoma	Clonogenic	TEM	200 keV, 1 and 6 MeV/8 or 2×4	MBTXR3 (50 nm HfONP/ biocompatible)	0.12 (at 10% SF)	Maggiorella et al. [10]
F98	Alexa annexin V/dead cell apoptosis kit	–	90 keV/0–20	3 nm GdNPs (AGuIX®)	0.045	Martinez-Rovira et al. [172]
MDA-MB-231 breast cancer	–	0.88/(1.3 × 10 ⁸)	6, 15 MeV/5	2 nm AuNPs	0.18–0.24	McMahon et al. [70]
HeLa	WST-1/CFU	–	100 kV/5 Gy	TiO ₂ , ZnS:Ag, CeF ₃ , CdTe QDs	1.0	Misawa et al. [173]
HeLa	γ-H2AX	–	28 keV/1.0	50 nm AuNPs/methyl polymer	0.7–1.3	Ngwa et al. [174]
HCT116 colorectal	γ-H2AX	3.3	80 kV/10	3 nm AuNPs/tiopronin	1.0	Paquette et al. [34]
HeLa	MTT	0.1	6 MV/8	3 nm FePtNPs/cysteamine	<0.1	Quan and Jiang et al. [175]
HeLa	MVP	–	5–60 keV (max intensity at 10 keV)	La in micelle (Hyp-GdEuCl ₂ micellar particles)	No cell damage experiment	Refrégiers et al. [178]
DU-145 prostate cancer	MTT, CG	0.023/(6.7 × 10 ⁴)	200 kVp/2	7 nm AuNPs/Glu	0.5–1.4	Roa et al. [64]
DU-145	MTT, CG	0.024 (7 × 10 ⁴)	1176 keV/2 and 4	7 nm AuNPs/Glu	0.2–0.35	Roa et al. [66]
A549	Clonogenic	–	6 MV/2	SiC (20 nm)/SiO ₂ x (20 nm thick) nanowire/porphyrin	2.53	Salviati et al. [177]
MIAPaCa-2	Colony formation essay, γ-H2AX	–	150 kVp with 1 mm Al filter/0–5	50–100 nm TiO ₂ NPs/PAA	0.40 (at 10% survival)	Sasaki et al. [178]

H460	Clonogenic	–	6 MV/8	CdSe/ZnS/PEG	0.2	Sheng et al. [33]
K562	Nuclear diffusion factor	None	40 kV/3	13 nm AuNPs microdisks	<0.4	Su et al. [41]
MDA-MB-231	Clonogenic	–	225 kVp, 6 MV/6	100 nm hollow Au (inner 50 nm)/PEG	0.5, 0.1	Sun, Mao and Hao et al. [181]
T98G, Du145, MDA-MB-231	Clonogenic	0.07–1.5/ (2.2×10^8)	/8	1.9 nm AuNPs	0.14–0.92	Taggart et al. [26]
9L gliosarcoma cells	Clonogenic	–	125 kVp, 10 MV/1–8	50–70 nm Bi ₂ O ₃ NPs	0.48, 0.25	Tehei et al. [12]
HT1080 fibrosarcoma	Clonogenic, γ -H2AX	–	150 kVp/6	Micelles of 1.9 nm AuNPs/PEG	0.7	Tsourkas et al. [38]
PC-3	Methylene blue	–	160, 320 kVp/2	12 nm Y2O3 NPs/TAT peptide or psoralen-functionalized TAT	0.92, 1.44	Vo-Dinh et al. [57]
U251	CCK-8 assay (cell viability)	–	6 MV/4	15.38 nm Ag NPs/PVP	0.5	Wen and Gu et al. [60]
HepG2 liver cancer	MTT	–	⁶⁰ Co/5	Se aggregates/DOX	0.2	Xu and Zhang et al. [9]
A549, KB	XTT	6/	100 kV/10	4 nm AuNPs/Glu, FA	2.6–15 ^b	Yan et al. [16]
4 T1	Clonogenic	5 μ g/mL	/0–8	3.6 nm Bi NPs/PEG, Lyp-1	0.26	Yang and li et al. [71]
4 T1	MTT, clonogenic, γ -H2AX	–	/2–8	100 nm Au (20 nm) @FeS/PEG	0.37	Yang, Wu and Yang et al. [11]
MCF-7	Clonogenic	0.00075–0.0315	6 MV/2.25	2 nm Au NPs/glutathione(GS) or PEG	–0.16, 0.44, 0.27–0.50	Zheng et al. [180]
K562	–	–	662 keV/20–100	14–16 nm AuNPs	–	Zhang et al. [181]

NPs, nanoparticles, NMs nanomaterials, AuNPs gold nanoparticles, CG clonogenic, Glu glucose, PEG polyethylene glycol, SF surviving fraction, FeONP iron oxide nanoparticles, DOX doxorubicin, FA folic acid, pHLLP pH-sensitive low-insertion peptide, 4-ATP 4-aminothiophenol, DOTA tetraazacyclododecane tetraacetic acid

^aReported by the authors

^bCalculated enhancement based on the reported data

From the presentations given in this section, it will become clear that uptake is critical to understanding the origin of enhancement. Uptake information, however, is not available in many studies, and even with uptake data, the measured enhancements could not often be satisfactorily explained by the added nanomaterials through only physical enhancement. As stated before, incubation concentration is not the same as uptake concentration, as cells often regulate the uptake of nanoparticles depending on the size, shape, and surfactants of nanomaterials.

9.5.2 Enhancement of Damage to Tumor Cells Assisted by Nanomaterials under X-Ray Irradiation

The published results are reviewed chronologically, following the same protocol used in other chapters in the book. Publications from the same research group are discussed together.

Publications of studying cancer cell damage assisted by nanomaterials under X-ray irradiation began to appear in the literature in 2007. Misawa et al. [175] investigated HeLa cell damage under X-ray irradiation using several nanomaterials to enhance the effectiveness of X-ray irradiation. The nanomaterials included TiO₂ nanoparticles, ZnS doped with Ag particles, CdTe quantum dots, and CeF₃ particles. X-ray energy range was between 20 and 170 keV and X-ray dose was up to 5 Gy. No quantitative uptake data was available although images obtained in this work do suggested efficient uptake of CdSe quantum dots. The enhancement was significant as well—the results showed that survival fraction dropped down to 10% with only 2–3 Gy of 100 kVp X-rays, and LD₅₀ was around 1 Gy for quantum dot-treated HeLa cells, which suggested a greater than 1.0 DEU enhancement for these nanoparticles.

Roa and Xing et al. [64] used gold nanoparticles in prostate cancer cells to demonstrate the utility of gold nanoparticles in cancer therapy. The authors showed that glucose-coated gold nanoparticles improved the uptake over other nanoparticles such as neutral gold nanoparticles. The size of their nanoparticles was ca. 7 nm in diameter. The authors used DU-145 prostate cancer cell line. The radiation was 200 kVp X-rays and dose was 2 Gy. The uptake data showed 6.73×10^4 gold nanoparticles per cell, which was equivalent to 0.023 WP of gold in water. This would only give rise to a 2–3% increase in radiation damage if physical enhancement dominated. Radiation alone inhibited 16% of the tumor cell growth, whereas inhibition increased by 30% and 45% when gold nanoparticles were added, suggesting a 1.4 DEU enhancement. This experimental measured enhancement was much higher than the value predicted by physical enhancement shown in Chap. 2. The authors did not predict the enhancement themselves. However, the authors did note that tumor killing did not completely correlate with the uptake concentrations of nanoparticles. The observed results might be explained by biological enhancement because the size of nanoparticles was 7 nm, making it possible for

these nanoparticles to enter the nuclei, although chemical enhancement could not be ruled out either.

Roa and Xing et al. [66] studied Du-145 incubated with glucose-coated 7 nm gold nanoparticles and irradiated with γ -rays emitted from ^{137}Cs . The uptake was determined to be 7.0×10^4 nanoparticles per cell, which was only 0.024 WP, similar to what mentioned above. The observed enhancements using MTT assay at 2 and 4 h after irradiation were 0.22 and 0.35 DEU. Hence the enhancement per unit WP was 9 and 16 DEU WP^{-1} , much higher than the average 1.0 DEU WP^{-1} offered by physical enhancement for keV X-rays. This implied that type 2 physical enhancement or other categories of enhancement such as chemical or biological enhancement might play an important role.

Chen and Xing et al. [65] studied the enhancement of radiation damage to breast cancer cell line MCF-7 by 10 nm gold nanoparticles coated with several different surfactants. Among the ligands, cysteamine was found to generate maximal uptake, reaching 1.2×10^5 gold nanoparticles or 0.03 WP of gold in a cell. However, glucose-covered gold nanoparticles did not have the highest uptake (3.0×10^4) but caused the most damage to the cells. The X-ray energy used in the work included 200 kVp X-rays as well as γ -rays from ^{131}Cs and ^{60}Co sources. The total dose was 10 Gy for each irradiation and the assay was MTT. 200 kVp was the most effective X-ray energy for generating enhancement. These results suggested that a different enhancement mechanism from physical enhancement should be in control. Figure 9.19 shows the uptake and cell viability results.

Hwu et al. [22] used 4.7 nm gold nanoparticles for the purpose of enhancement of radiation damage to mice tumor cells CT26. They observed approximately 1×10^6 gold nanoparticles per cell, which corresponded to 0.1 WP of gold in those cells. Synchrotron X-rays between 8 and 15 keV with an average of 12 keV were used and an approximately 0.13 DEU enhancement was observed, which gave rise to a 1.1 DEU WP^{-1} unit WP enhancement. Hwu et al. [28] investigated enhancement by PEGylated gold nanoparticles under the irradiation of several X-ray sources,

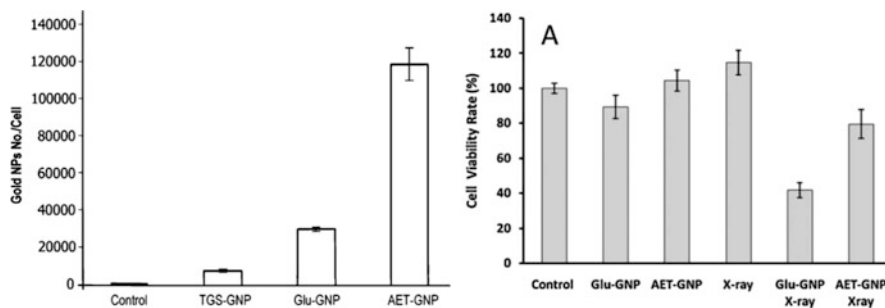


Fig. 9.19 Uptake (left panel) and enhancement results (right panel) using MCF-7 breast cancer cell line and 200 kVp X-rays with 10 nm gold nanoparticles. Damage by Glu-GNP was the highest even though uptake of AET-GNP was the highest, proving uptake was not the only parameter that controlled the outcome. (Reprinted with permission from Chen and Xing et al. [65]. Copyright (2008) by John Wiley and Sons.)

including a Cu K α X-ray source, a commercial biological radiator with an average X-ray energy of 73 keV and a 3 MV X-ray source. Compared to X-ray irradiation alone, survival rates were lowered by up to 45% for cells incubated with gold nanoparticles and irradiated with X-rays.

Sheng et al. [33] showed the results of their study of quantum dots conjugated with photofrin under 6 MV X-ray irradiation. H460 cells were used in the test. The authors suggested that energy transfer efficiency approaches 100% from the excited quantum dots to a high coverage of photofrin molecules on the surface. Increased cell damage was observed with both radiation and nanomaterials treatment.

Geso et al. [58] employed microbeams from synchrotron X-rays to irradiate gold nanoparticles and endothelial cells deposited on a flat surface. The average X-ray energy was 125 keV. 1.9 nm gold nanoparticles and rat glioma RG2 cells were used. The microbeam irradiation was beneficial for the healthy cells near the tumor cells to recover, similar to “wound healing,” a process that is not well understood. The authors confirmed that healthy cells tend to spill to the irradiated strips very quickly and found that tumor cells also tended to help neighboring dying cells, but at a much slower rate than the healthy cells. This finding suggested that at the tissue level, microbeam approach might be more beneficial than at the cellular level.

Zhang et al. [183] investigated interactions of gold nanoparticles with K562 cells under irradiation of 662 keV X-rays. The dose range was 2–10 kR or 20–100 Gy. Surface plasmon resonance profiles were measured to determine the impact of X-ray radiation on the nanoparticles. The authors argued that radiation produced species such as electrons and radicals changed the plasmonic response. Cytotoxicity was measured with different incubation concentrations, although no direct X-ray irradiation of gold nanoparticles in K562 cells were carried out.

Since 2009, as described in Sect. 9.6.3, Nanobiotix Inc. has been working on a nanoparticle-based drug that can absorb X-rays and destruct tumor. The company used at least two cancer cell lines, HC116 and HT1080. A patent issued to Levy et al. [184] had a priority date of June 5, 2008. The nanomaterials were known to be crystalline HfO₂ nanocrystals. X-rays were 200 kVp with a 0.2 mm Cu filter. For cells, 4 Gy of radiation was used. Similar studies were carried out by Maggiorella et al. [10] in which the two types of cells were irradiated with 0.38 MeV, 1.25 MeV, and 6 MV X-rays for 8 or 2 \times 4 Gy. The estimated enhancement was 0.12 DEU based on clonogenic assay results.

Butterworth et al. [45] studied dose enhancement using nine cell lines and several endpoints including DNA damage. Their dose enhancement factor was the ratio of 2 Gy to the dose required to produce the same surviving fraction in the presence of gold nanoparticles as that of 2 Gy radiation alone. This was one of the two ways to calculate enhancement using the surviving curve shown in Fig. 9.1. The X-rays were 160 kVp. The incubation concentrations were between 10 and 100 μ g/mL of 1.9 nm gold nanoparticles. They observed cell dependent dose enhancement factors. Except for Agg-1552B and T98G, higher incubation concentrations (not the uptake) did not yield higher magnitude of enhancement. Not all the cells experienced enhancement. This study demonstrated the need for scrutiny of enhancement mechanisms as well as the experimental protocol. The results are listed in Table 9.8, which shows the

Table 9.8 Dose enhancement results obtained by Butterworth et al.

Cell	DEF (10 µg/mL)	DEF (100 µg/mL)
AGG-1552B	1.16	1.97
Astro	1.04	0.96
DU-145	0.98	0.81
L132	0.86	0.87
MCF-7	1.41	1.09
MDA-231-MB	1.67	1.11
PC-3	1.07	1.02
T98G	1.30	1.91

Adapted from Butterworth et al. [45]

enhancement is from anti-enhancement (-0.19 DEU) to an enhancement of 0.97 DEU. The values listed in the table are DEFs, which is the relative enhancement.

Chen and Margaritondo et al. [162] studied cell survival after irradiating HeLa and EMT-6 cells incubated with iron oxide nanoparticles decorated with dextran molecules. The uptake of nanoparticles was studied, both qualitatively with TEM imaging and quantitatively with ICP-MS. The enhancement, however, was less than 0.1 DEU. Kong et al. [185] used gold nanoparticles to enhance the efficacy of radiotherapy of ovarian cancer cells. The authors used both X-ray and γ -rays and glucose-coated as well as naked gold nanoparticles. Ten sizes of gold nanoparticles between 12 and 17 nm were used, and 13 nm gold nanoparticles were found to produce the highest uptake, and $160,000$ nanoparticles were found per cell, corresponding to a 0.4 WP loading of gold in the cell. LD_{50} for the cell was 5 Gy, but the authors used up to 25 Gy in their work. Glucose-coated gold nanoparticles were found to generate better uptake than the naked nanoparticles. An enhancement between 0.2 and 0.4 DEU was measured, suggesting that the cause for the enhancement could come from physical enhancement by 0.4 WP gold.

Chithrani et al. [35] used gold nanoparticles of different sizes, ranging from 14 to 74 nm in diameter, in their radiation dose enhancement study. The gold nanoparticles were synthesized with a citrate reduction method, and no further treatment was performed to the nanoparticles. Uptake of gold nanoparticles into cells was measured, and incubation of 8 h was found adequate. The highest uptake was achieved for 50 nm gold nanoparticles, and 6000 gold nanoparticles per cell were detected. This loading corresponded to a 7 mg/g or 0.7 WP of gold in the cell if the cell mass is 1 ng. HeLa cells were used and γ -H2AX assay was used to detect cellular DNA damage. Figure 9.20 shows the results of uptake (left panel) and survival (right panel). Using the doses at 0.1 surviving fraction, the enhancement is estimated to be 0.5 DEU. Chithrani et al. [186] improved the uptake of 14 nm gold nanoparticles by conjugating peptides to the surface of the nanoparticles. The uptake was improved from 1000 nanoparticles to 2500 nanoparticles per cell. Increased damage to DNA was observed with the peptide-conjugated 14 nm gold nanoparticles.

The results of nuclear DNA damage obtained by Chithrani et al. in terms of double-strand breaks by gold nanoparticles incubated with HeLa cells are shown in Fig. 9.21. Based on two assays of γ H2AX and 53BP1, the enhancement of DSBs

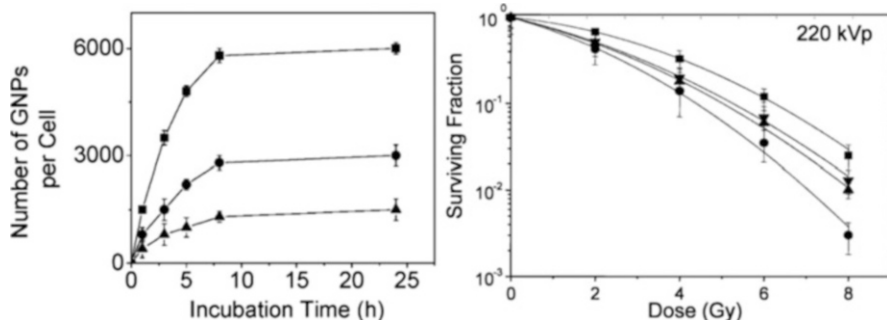
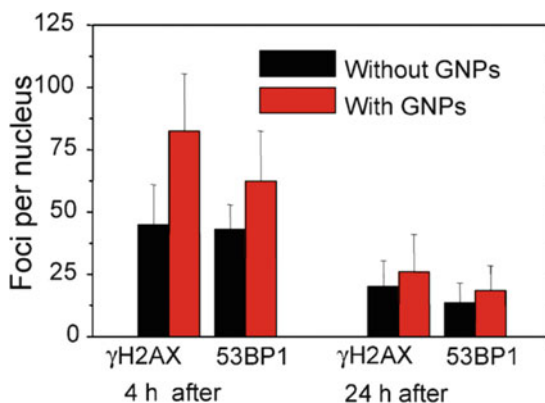


Fig. 9.20 Results of three size gold nanoparticles for enhancement. 14 (triangle), 50 (round), and 74 (square) nm gold nanoparticles were used. The left panel shows the uptake data and the right panel shows the survival data. An enhancement of 0.5 DEU is deduced from the surviving data using doses at 10% fraction. (Reprinted with permission from Chithrani et al. [35]. Copyright (2010) by Radiation Research. All rights reserved.)

Fig. 9.21 DNA damage by gold nanoparticles and X-ray radiation. More damage occurred to DNA when the cells were irradiated 4 h after incubation than 24 h. (Reprinted with permission from Chithrani et al. [35]. Copyright (2010) by Radiation Research. All rights reserved.)



was between 0.1 and 1.0 DEU. The results suggested a maximum enhancement of about 1.0 DEU was reached when irradiation was given 4 h after incubation. It is interesting to note that DNA damage was reduced to half in the control sample 24 h after incubation, as shown in Fig. 9.21.

Jain et al. [50] used linear accelerators (LINAC) at 6 and 16 MeV and 160 keV X-rays to irradiate MDA-MB-231 and two other cell lines for enhancement. The cells were exposed to up to 6 Gy of radiation. LD₅₀ dose was about 4 Gy and 1.9 nm gold nanoparticles were used. No uptake results were shown. At 4 Gy dose, the surviving fraction (SF) was about 40%. With gold nanoparticles, the enhancement to the damage was 0.05–0.45 DEU for 160 kV and negligible at 6 MeV. The results are given in Fig. 9.22.

Chen et al. [44] reported the damage to MCF-7 cells by gold nanoparticles under X-ray irradiation. Their intended damage mechanism was through blocking the DNA repair pathways. The gold nanoparticles were 2.0–2.5 nm and were conjugated with surface ligands bound to the DNA repair proteins. With 4 Gy of radiation and incubation concentration of 0.1 μ M, the damage was increased by approximately 30%.

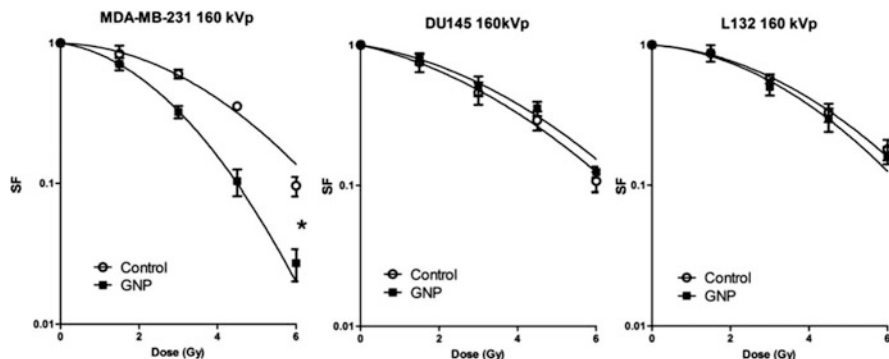


Fig. 9.22 Damage to three cell lines using 1.9 nm gold nanoparticles under irradiation of 160 keV X-rays. Enhancement is observed only with MDA-MB-231 cells. (Reprinted from Jain et al. [50]. Copyright (2011) with permission from Elsevier.)

Jiang et al. [15] conducted a study of A549 human lung cancer cell damage using cisplatin embedded nanoliposomes under irradiation of up to 6 Gy of 6 MV X-rays. The survival fraction was 2–3% at 6 Gy and LD_{50} was 1.5 Gy. Upon adding the formulated drug, LD_{50} decreased to 1 Gy, producing an enhancement of 0.5 DEU. In their in vivo data, the authors used 6 Gy and formulated nanodrugs and observed delayed growth of tumors. The in vivo results will be shown in the next section.

Yan et al. [16] found that dual ligand-coated gold nanoparticles increased the uptake of nanoparticles by cells. The two ligands on the gold nanoparticles were glucose (Glu) and folic acid (FA). The average size of the gold nanoparticles was 4–5 nm in diameter, although there were much smaller gold nanoparticles in the mixture. The increase of uptake due to the coverage of FA on the nanoparticles was 3.9- to 12.7-fold. The experiments were done using cell lines KB and A549. The highest uptake was 6×10^{-11} g in a 10^{-9} g cell, which was equivalent to 6 WP gold in water. X-rays were from a cabinet source operated at 100 kV, 3 mA and at 1.46 Gy/min dose rate. The cells were exposed to 10 Gy of radiation. If only physical enhancement existed, then an enhancement of 6–8 DEU was expected. The authors found that A749 cell line responded poorly to treatment with gold nanoparticles, whereas KB responded favorably. Viability of A549 cells was barely reduced after irradiation with 10 Gy of radiation. Viability of KB did not decrease with only X-ray irradiation. With 6 WP gold, cell viability was only reduced to 80% for A549 and 20% for KB. The results clearly showed the disparity of cells vulnerability toward X-ray radiation or reactive oxygen species generated from X-ray irradiation.

McMahon et al. [70] studied the nanoscale energy deposition within cells using 2 nm gold nanoparticles and 6 and 15 megavoltage X-rays. Breast cancer cell line MDA-MB-231 was used. 1.3×10^8 gold nanoparticles were found in each cell, corresponding to a loading of 0.88 WP. No toxicity data was available. The enhancement was 0.18 DEU for 15 MeV X-rays and 0.24 DEU for 6 MeV X-rays. These give a unit WP enhancement of 0.25 DEU WP^{-1} for these high-energy X-rays. The authors also measured the X-ray and electron energy spectra beneath a 5 cm water sample for 6 MeV X-rays. They then used the electron energy spectra to

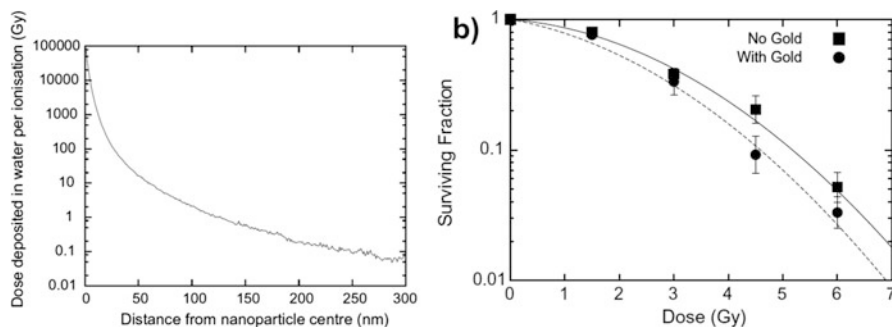


Fig. 9.23 Radiation enhancement by 2 nm gold nanoparticles under 15 MeV X-ray irradiation. The results show a small enhancement of 0.18 DEU, which agreed with the theoretically predicted physical enhancement for X-rays at this energy. (Reprinted from McMahon et al. [70]. Copyright (2011) with permission from Elsevier.)

calculate energy deposition in water around 2 nm gold nanoparticles. For irradiation with 1 Gy of 6 MeV X-rays, only 2.3×10^{-7} gold nanoparticles were directly ionized. This meant there were about 150 ionized gold nanoparticles per cell with 5 Gy of radiation using the uptake data obtained by the authors. The authors also calculated energy deposition profiles for the gold nanoparticle and found that the magnitude of energy deposition decreases exponentially as a function of distance from the nanoparticle. The decay constant was approximately 5.4 nm based on their calculation results, which was similar but greater than the one obtained by Guo et al. [187]. The left panel of Fig. 9.23 shows the local effect of energy deposition, and the right panel shows the clonogenic results. There was a reasonably good agreement between the theoretically predicted physical enhancement and measured enhancements, as shown in the right panel of Fig. 9.23. As pointed out in Chap. 4 and other places in the book, physical enhancement may not generate the measured enhancement when large amounts of small catalytically active gold nanoparticles are used. It will be interesting to see in the future whether the agreement observed here is coincidence.

Xu and Zhang et al. [9] investigated a doxorubicin trapping diselenide polymer aggregate under γ -ray irradiation. They used HepG2 cell (human liver cancer) line in their work. The authors studied the drug release under X-ray irradiation. The results are discussed in Sect. 9.7 as well. After 5 Gy of irradiation, nearly 20% reduction in cell viability was observed. The authors quantified hydroxyl radical generation and observed an increase of hydroxyl radical production upon adding the di-Se block copolymer aggregates into the samples under X-ray irradiation.

Vo-Dinh et al. [57] designed a nanosystem that absorbed X-rays and converted the absorbed X-ray energy into fluorescence that helped generate singlet oxygen. The nanoscintillator was Y_2O_3 , which emitted UVA light after absorption of X-rays. Fluorescent molecule psoralen was tethered to the surface of Y_2O_3 nanoparticles. Psoralen absorbed UVA emitted from Y_2O_3 and generated singlet oxygen, a known process. Prostate cancer line PC-3 was used in the study. The incubation concentration was up to 100 ppm of Y_2O_3 , although no data of uptake was available. The dose

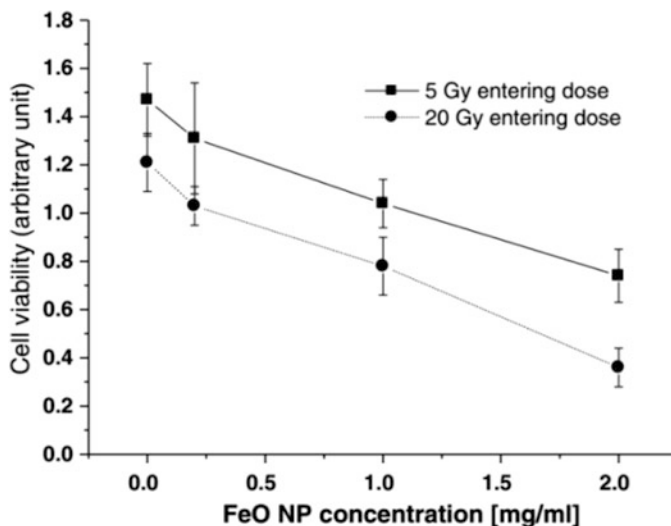


Fig. 9.24 Cell viability after irradiation with 7.1 keV X-rays in the presence of 13 nm iron oxide nanoparticles. Two doses were used, and the trends were similar. (Used with permission from Choi et al. [21] under CC BY 2.0 license.)

was 2 Gy for 160 keV and 320 keV X-rays. The survival was lowered by approximately 10–30% at a 100 ppm incubation concentration.

Choi et al. [21] studied damage to cells and tumors using FeO_x nanoparticles under synchrotron X-ray irradiation. The authors used X-rays at 7.1 keV to irradiate nanoparticles in CT26 tumor cells. The size of nanoparticles was 13 nm. The authors called the method photo-activated therapy (PAT). The incubation concentrations were between 0.2 and 2 mg/mL. The uptake was between 30 and 169 μg Fe in 10^6 cells. If the average of cell mass is 1 ng, then the loading of Fe per cell was 3–17 WP. The cell viability data showed decreased viability at increased FeO_x incubation concentrations, and a similar trend was observed between two doses of 5 and 20 Gy. Based on the data, a 17 WP loading of Fe in a cell increased the reduction of the viability by 50% when irradiated with 5 Gy of radiation. No data showed the effect of radiation only. Figure 9.24 shows the results of cell viability at two doses.

Liang et al. [141] studied cell viability after irradiating the cells with X-rays in the presence of gold nanoparticles. Four different sizes of PEGylated gold nanoparticles were used, including 4.8, 12.1, 27.3, and 46.6 nm. Two different incubation concentrations were used with HeLa cells. Up to 8 Gy of X-ray irradiation was used. 4.8 nm nanoparticles were found to pose mild cytotoxicity after 48 h at 0.1 mM or higher gold concentrations. 12.1 nm gold nanoparticles were found to be the most effective in destructing HeLa cells under X-rays. Survival fraction decreased to 10% at 4 Gy with 12.1 nm gold nanoparticles (0.1 mM gold), which was 50% less than that incurred with 6 Gy irradiation without gold nanoparticles. The authors also performed in vivo tests, whose results are shown in the next section.

Gonzalez and Kotler et al. [19] studied MeV irradiation of <5 nm silicon nanoparticles incubated with glioma C6 cells. Dynamic light scattering

measurements showed 2–3 nm diameter, and transmission electron microscopy showed a much larger size distribution of 3–90 nm. Photoluminescence of the particles was at 420 nm. Using fluorescence assays, authors studied the production of hydroxyl radicals, superoxide radicals, and singlet oxygen and found their yields were enhanced by 9 to 22 times. Uptake was measured in a relative manner, which showed higher uptake at longer incubation times. For 6-h incubation, attenuation of 4 MeV X-rays was doubled by the cells with the nanoparticles. Under the same condition, six times more reactive oxygen species were generated with silicon nanoparticles than without the nanoparticles. It is speculated by the authors that the observed 6 DEU enhancement was caused by biological processes triggered by increased amounts of reactive oxygen species. The 100% increase in absorption only supported an up to 2 DEU physical enhancement. The observed 6 DEU enhancement therefore must be caused by other mechanisms. A likely reason is silicon nanoparticles interacting with DNA repair proteins and blocking their functions, as mentioned in Chap. 4.

Ngwa et al. [174] employed low-dose-rate X-rays to interact with gold nanoparticles in HeLa cells. The incubation concentration was 0.02 WP. The nanoparticles were 50 nm in diameter and covered with methyl polymer. The dose was provided from a I-125 (emitting X-rays at 3.6 keV and 30.5–35.3 keV) source and activity was 2.6 mCi, which corresponded to a dose rate of 2.1–4.5 cGy/h. The total dose was up to 1 Gy. The enhancement was between 0.7 and 1.3 DEU. No uptake data was available, making it impossible to determine whether the measured enhancement matched the theoretically predicted physical enhancement at this specified X-ray energy.

Cook et al. [48] demonstrated an interesting system in which cisplatin was conjugated to the surface of gold nanoparticles. The formulation was used for chemoradiation therapy, and the authors suggested that Auger electrons emitted from gold played a vital role. The authors observed enhanced cell destruction of both MCF-7 and SKOV-3 cancer cells using the formulation under X-ray irradiation. Figure 9.25 shows the formulation and the survivability data. No attempts were made to determine the enhancement values.

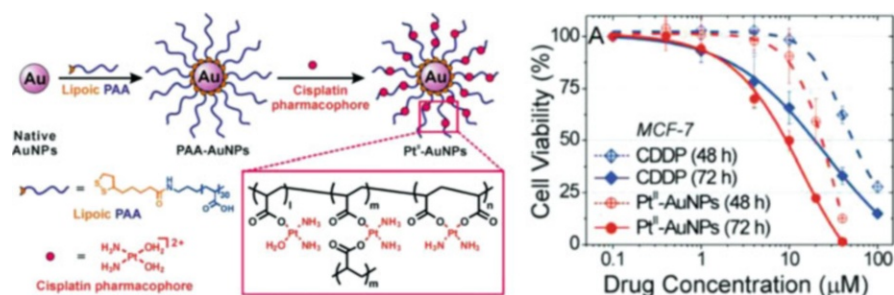


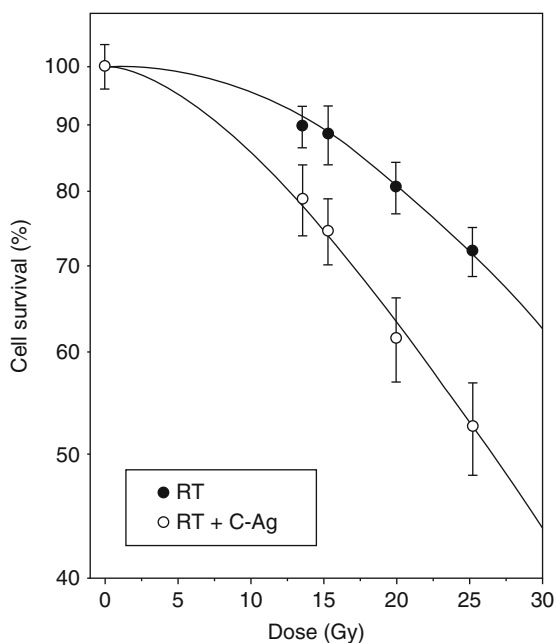
Fig. 9.25 Results of cell viability after treatment with formulated cisplatin using gold nanoparticles (AuNPs) covered with poly acrylic acid (PAA) ligands irradiated with X-ray radiation. (Adapted in part from Cook et al. [48] with permission of the Royal Society of Chemistry.)

Kumar et al. [171] reported a third-generation gold nanoparticles covered with several ligands for optimal radiation therapy. The authors chose HeLa cell line in their study. The uptake was visualized with attached fluorophores, but without direct quantification in terms of weight percentage. The average size of the gold nanoparticles was 2.5 nm. The X-ray energy was 220 kVp and the dose rate was 5.45 Gy/min. 0.5 mg/mL and 2.0 mg/mL incubation concentrations were used. The authors employed a clonogenic assay to determine the enhancement, and an enhancement up to 2.8 DEU was measured.

Juzenas et al. [24] discussed a new nanomaterial with a silver shell and a carbon core for cancer therapy. The authors used cancer cells including prostate cancer cells Du145 and irradiated the cells with 160 kVp X-rays. The X-ray source was a Faxitron source, running in CW mode at 160 kV/6.3 mA. The dose rate was 1 Gy/min. The size of the nanomaterial ranged from less than 10 nm to greater than 100 nm, with an average size of 60 nm. The authors called the nanomaterial C-Ag-PEG. The cell survival test was performed 24 h after irradiation. Only incubation concentrations were given and no uptake data was available. If the doses at 70% cell survival fractions were used to determine the enhancement, then adding C-Ag-PEG nanomaterial created a 0.6 DEU enhancement. Figure 9.26 displays the results of cell damage.

Latimer [52] investigated enhanced radiotherapy using 30 nm gold nanoparticles conjugated to polyethylene glycol (PEG) and then cell-penetrating peptides (CPP). The author used three cell lines including MDA-231-MB and obtained the uptake and cell survival data. The results showed enhanced uptake for 30 nm nanoparticles,

Fig. 9.26 Enhancement from silver-coated carbon nanoparticles under X-ray irradiation. (From Juzenas et al. [24]. doi: <https://doi.org/10.1088/0957-4484/24/32/325103>. © Institute of Physics and Engineering in Medicine. Reproduced by permission of IOP Publishing. All rights reserved.)



which agreed with the literature data shown in this chapter. The uptake amplification factor ranged from nearly 2 times to more than 11 times. The highest uptake occurred to T47D cells, which had more than 1.6×10^6 30 nm gold nanoparticles per cell and corresponded to over 40 WP of gold in the cell. This amount of gold was supposed to generate 40 DEU physical enhancement of damage for 40 keV X-rays. The experimental results showed 0.1 DEU WP^{-1} for PEG-AuNPs and 0.3 DEU WP^{-1} for CPP-PEG-AuNPs in T46D cells, which were lower than the predicted enhancement for 300 keV X-rays. It was unclear as to what caused the discrepancy, although scavenging can be a reason. For MCF-7 cells, the uptake was 1.9×10^5 of 30 nm gold nanoparticles per cell or 5 WP of gold in the cell. The measured enhancements are 0.9 DEU WP^{-1} for PEG-AuNP and 1.1 WP^{-1} for CPP-PEG-AuNPs. These results were higher than those predicted by theory for 300 keV X-rays. The results suggested that parameters such as cell types other than the amount of nanoparticles and their surface may play important roles in determining the enhancement of cellular destruction by nanoparticles under X-ray irradiation.

Chen et al. [163] reported the use of Ce^{3+} -doped lanthanum(III) fluoride nanoparticles as an X-ray-driven photodynamic therapeutic agent. The authors used several assays to measure the damage, including oxidative stress, mitochondrial damage, and DNA fragmentation on prostate cancer cells (PC3) after exposed to 90 kVp X-rays.

Konstantinov et al. [170] claimed that they observed a 0.33 DEU enhancement to cancer cells with 50–500 $\mu\text{g}/\text{mL}$ loading of tantalum pentoxide nanoparticles. The X-ray energy was 10 MeV. If physical enhancement were considered, then for a 0.005–0.05 WP loading, the enhancement would be less than 1%. However, the specified loading was the incubation concentration, not uptake, meaning cells might have much high concentrations of nanomaterials in them. The authors also speculated that photoelectric and/or pair production processes may contribute to the observed enhancement. Without the uptake data, however, one could not determine the origin of enhancement.

Khoei et al. [169] showed the results of their cancer cell damage study with iron oxide nanoparticles irradiated with 6 MeV X-rays. The cell line was Du-145 prostate carcinoma cell line. The authors obtained a 0.2 DEU enhancement in the range of 2–8 Gy of irradiation. The nanoparticle incubation concentration was 0.1 WP. No uptake information was available. Their cell survival fraction was 80% at 2 Gy and 10% at 4 Gy. This result shows that LD_{50} can be different even for the same cell line but in different experiments.

Tsourkas et al. [38] used HT1080 human fibrosarcoma cells to test the effectiveness of dicoblock copolymer PEG-PCL formulated micelles filled with 1.9 nm gold nanoparticles. The size of the assemblies ranged from 28 to 142 nm measured by DLS, and a similar size range was detected using TEM. The authors also performed animal tests (shown in Sect. 9.5). The authors did not examine the form of micelles at the end of the experiments, whether gold nanoparticles were still in the micelles or released from the micelles. Survival fraction was at 10% after 5 Gy of irradiation. The enhancement was 0.32 DEU (using 50% survival fraction with and without gold). No uptake data was available.

Superparamagnetic iron oxide nanoparticles were synthesized and used by Kryschi et al. [46] to destruct cancer cells. The size of the nanomaterial was on the order of 10 nm. Two coatings were used, which were malate and citrate. Three cell lines were used, which were Caco-2, MCF-7, and 3 T3. 1 or 3 Gy X-ray irradiation was administered, and fluorescence assay was used to measure the cellular reactive oxygen species. The results were complex as nonlinear dose dependency was observed in the 1–3 Gy dose range.

Chen et al. [161] synthesized a new afterglow nanoparticle upon X-ray irradiation. The nanoparticles were Cu and Co co-doped ZnS and had an average size of 4 nm. The afterglow emitted at 550 nm. The lifetime of the afterglow was 8 sec ($1/e$). They authors then conjugated photosensitizer tetrabromorhodamine-123 to the surface. The ligand was known for its photodynamic therapy (PDT) properties. PC3 cells were used to gauge the PDT capability of the whole complex. Enhancement could not be determined due to lack of X-ray-only results.

Hashemi et al. [73] used gold nanoparticles coated with folate ligands in their enhancement study of radiotherapy of HeLa cells. The average size of gold nanoparticles was 47 nm. ^{60}Co and an X-ray source operated between 120 and 250 kVp were used. The dose range was between 1.18 and 3.43 Gy. The authors noticed a nearly eighthfold increase in uptake for foliate-conjugated gold nanoparticles compared to as-synthesized PEGylated nanoparticles. The uptake of these gold nanoparticles into HeLa cells was measured, and at the 24-h incubation time, more than 3×10^4 gold nanoparticles were in each cell, giving rise to a 3.4 WP gold loading in the HeLa cell using 1.0 ng cell weight. If physical enhancement dominates, then the enhancement should be around 3.4 DEU for 33 keV X-rays, less so for 120 keV, and only a fraction of it for ^{60}Co . According to the authors, the enhancement was higher for folate-conjugated gold nanoparticles. The enhancement was 0.6 DEU for 120 kVp X-rays using 60% survival fraction. The nanomaterials may pose anti-enhancement in addition to physical enhancement for the 47 nm gold folate-coated gold nanoparticles because the measured enhancements were lower than the predicted physical enhancement.

Su et al. [188] employed bismuth nanoparticles conjugated to iron oxide magnetic nanoparticles with folic acid surfactants to target circulating tumor cells (HeLa) in the blood. The tumor-bound nanoparticles were collected with permanent magnets. 40 kVp X-rays were used. Dose and dose-rate information was not provided. MTT and comet assays were used to detect cell viability and DNA damage. Enhanced damage in the presence of bismuth nanoparticles was observed.

Ma and Su et al. [79] investigated the use of gold nanoparticles for enhancing the effect of radiation damage to human glioblastoma cells under X-ray irradiation. 13.5 nm diameter gold nanoparticles coated with several different surfactants were synthesized to improve uptake of nanoparticles. The authors observed more DNA damage with positively charged surfactants on gold nanoparticles, although no quantitative results were given with respect to the uptake and damage. Ma and Su et al. [41] developed a unique nanosystem to study the effect of nanostructures on damage to cells under X-ray irradiation. They created microdisks using multiple layers of gold nanoparticles (13 nm diameter) on glass slides. Several cell lines

including K562 cells attached to the microdisks were irradiated with 40 kV X-rays. The enhancement ranged between zero and approximately 0.4 DEU. Due to irregularity of the microdisks, gold loadings next to cells were difficult to quantify. However, a clear advantage of this approach was the cleanness of the pathway to identify the origin of enhancement because unless nanoparticles diffuse away from the microdisk, enhancement, albeit small, should all come from only physical enhancement.

In their latest work, Su et al. [86] reported enhanced cancer treatment with cell-penetrating peptide (CPP)-modified gold nanoparticles. The gold nanoparticles were 10 nm in diameter with large standard deviations. Two cell lines, HeLa and human fibroblasts, were used. Production of reactive oxygen species was measured, and CPP-conjugated gold nanoparticles were found to enhance the yield by more than twofold. Nuclear DNA damage was measured with and without X-ray irradiation, but no significant differences were found. The overall results suggested some effectiveness of using CPP-conjugated gold nanoparticles.

Sun, Mao, and Hao et al. [179] reported the use of hollow gold nanoparticles as radiosensitizers. The hollow gold nanoparticles had a 50 nm inner and 100 nm outer diameter. The particles were covered with PEG ligands. MDA-MB-231 breast cancer cell line was used in the study, and the endpoint of cell viability in terms of its metabolic activity was measured with MTT assay. The authors found little toxicity for up to 0.35 mM gold in solution. Less than 4 Gy of radiation was used at 225 kVp and 3.9 Gy/min dose rate. High-energy X-rays at 6 MV and 14 Gy/min was also used. The enhancement for keV and MV X-rays were 0.5 and 0.1 DEU, respectively. It was difficult to compare the measured enhancements with expected enhancements because no uptake data was available.

Salviati et al. [179] used porphyrin conjugated to silicon carbide/silica (SiC/SiO_x) nanowires in X-ray excited photodynamic therapy. They used click reactions to link porphyrins to the surface of the nanowires. 6 MeV X-rays (γ -rays) were used, which relied mainly on pair production and Compton scattering processes to generate secondary electrons to excite porphyrins and produce singlet oxygen. Low doses (0.4–2 Gy) of X-rays and lung adenocarcinoma cells were used. The enhancement was a 75% reduction in cell population when treated with porphyrin conjugates compared to the control without porphyrin. The authors also compared the results of using nanomaterials and X-rays with those without using them. Enhancement due to the combination of the nanomaterials and X-rays was subtle but measurable.

Cooper and Reshetnyak et al. [67] reported using 1.4 nm gold nanoparticles tethered to pH-sensitive low-insertion peptide (pHLIP) to treat lung carcinoma A549 cells under X-rays. They found enhanced damage to the cell treated with gold nanoparticles. The X-rays were 250 kVp. The uptake data was not available, and enhancement was 0.1–0.2 DEU when samples were exposed to a low dose of 1.5 Gy of X-rays.

Réfrégiers et al. [176] reported a study of HeLa cell damage using lanthanide trapped in micelles to produce singlet oxygen for X-ray-induced radiophotodynamic therapy (RPDT). The lanthanide (Gd and Eu in their study) in the form of ions were chelated to C12 ligands to form the micelles. The authors showed fluorescence from

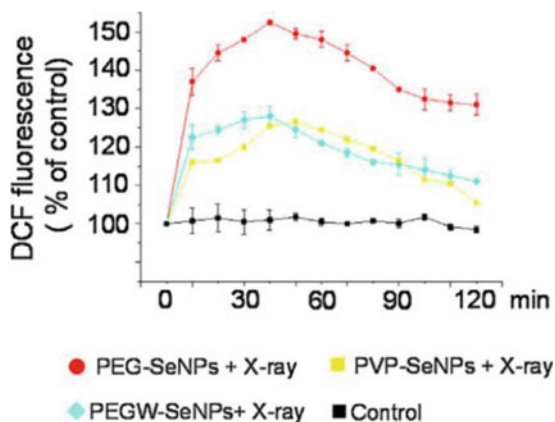
lanthanides when micelles were in HeLa cells and measured the production of singlet oxygen. No enhancement data was available.

Detappe and Berbeco et al. [187] studied the response of pancreatic cancer cells to the treatment of gadolinium-based nanoparticles under 220 kVp and 6 MeV X-ray irradiation. The nanoparticles were called AGuIX®, which were used in many imaging studies. The authors found that 6 MeV X-rays provided the best trade-off between penetration depth and enhancement. At 10 cm depth, the measured enhancement was 0.3 DEU, which was promising.

Chen et al. [69] studied selenium particles for enhancement under X-ray irradiation. The authors used both commercial and homemade selenium nanoparticles covered with polyethylene glycol (PEG) ligands and found that commercially made particles disintegrated under X-ray irradiation. The particle sizes were large, on the order a few hundred nanometers. HeLa cells were used, and MTT assay was used to determine the cell viability. X-ray information was not found, although the dose was specified to be 8 Gy, which was relatively high for HeLa cells. The highest enhancement was obtained using the commercial selenium particles. The authors attributed the damage to fragmentation of selenium particles, which according to the authors led to the generation of reactive oxygen species and oxidative stress detected by the authors using dichlorofluorescein (DCF) assay. The results are shown in Fig. 9.27. Enhancement was estimated to be 0.5 DEU. Uptake was determined with ICP-MS.

Falk et al. [166] studied the effect of gadolinium (Gd) nanoparticles under γ -rays (^{60}Co) on treating U87 cells. The diameter of the Gd nanoparticles was 3 nm, and the molecular weight was 8.5 kDa, corresponding to a density of approximately 1.0 g/cm^3 , which was identical to water. Incubation was conducted and uptake was studied with optical detection of the nanoparticles conjugated with cy5.5 dye molecules. Gd nanoparticles were found in cytoplasm of U87 cells although no Gd nanoparticles were found in the nuclei. No quantitative data on uptake of the nanomaterials was available. The assay was γ -H2AX to detect nuclear DNA damage as well as clonogenic assay to detect cell reproduction ability. After 1 and

Fig. 9.27 Reactive oxygen species generated by the introduction of selenium particles under X-ray irradiation. (Reprinted from Chen et al. [69]. Copyright (2016) with permission from Elsevier.)



4 Gy of irradiation, the authors measured moderate enhancements due to the addition of Gd nanoparticles. DNA damage was found to be dependent on the incubation time. Based on the data, enhancement values were 1.83 DEU at 1 Gy (at 0.55 survival) and 0.14 DEU at 4 Gy (at 0.37 survival). It was more likely that higher doses of radiation were needed in practice, and the enhancement values under those conditions could be even smaller because survival fractions would be lower. On the other hand, the density of the Gd nanoparticles was close to water, suggesting that the observed enhancement could be further increased if higher density Gd nanomaterials are used without causing significantly higher toxicity.

Taggart et al. [26] investigated the effect of 1.9 nm gold nanoparticles. Three cancer cell lines, MDA-MB-231, DU-145, and T98G, were used. Four cell assays of detecting reactive oxygen species level, mitochondrial oxidation, mitochondrial polarization, and cell survival were used. The uptake was between 1×10^7 and 2.2×10^8 nanoparticles per cell, corresponding to 0.07–1.5 WP of gold in these cells (assuming 1 ng cell mass). The lowest uptake occurred to DU-145 and highest for T98G. After 24 h of incubation, the uptake for Du-145, MDA-MB-231, and T98G was 1.0×10^8 , 1.5×10^8 , and 2.2×10^8 , respectively. 2, 4, and 8 Gy of radiation doses were administered, and enhancements were between 0.92 DEU at 2 Gy for T98G and 0.14 DEU at 8 Gy for MDA-MB-231 using clonogenic assay. Based on these results and the results of reactive oxygen species scavenging reactions, the authors suggested that the use of these nanoparticles caused oxidative stress and eventual damage to mitochondria, which led to cell death. The measured enhancements were within the range of predicted physical enhancement values for the loadings of gold in the cells.

Quan and Jiang et al. [175] studied the sensitivity of HeLa cells to FePt nanoparticles under X-ray irradiation. The authors claimed that the nanoparticles possessed a chemoradiotherapeutic effect. The size of nanoparticles was close to 3 nm and had different compositions, ranging from $\text{Fe}_{26}\text{Pt}_{74}$ to $\text{Fe}_{77}\text{Pt}_{23}$. It turned out that these nanoparticles were toxic to the cell. At 10 $\mu\text{g}/\text{mL}$ incubation concentration, cell viability was reduced to half. With X-ray irradiation and nanomaterials, viability was further reduced over the sum of radiation and nanomaterials acting separately, albeit insignificantly. At 8 Gy, the viability was 32% with X-ray and nanomaterials, which corresponded to an enhancement of less than 0.1 DEU. Cellular uptake of Pt was measured and was only 0.1–0.2 $\mu\text{g}/100 \mu\text{g}$ or 0.1 WP. Physical enhancement should be around 0.1–0.2 DEU at this Pt loading, which agrees with the experimental value.

Sasaki et al. [178] synthesized titanium peroxide nanoparticles (shown in Chap. 6) and used them to generate hydroxyl radicals. The peroxide nanoparticles apparently were found to be much more efficient, by at least 20-fold, in generating hydroxyl radicals under X-ray irradiation than TiO_2 nanoparticles. However, in the presence of glutathione, hydroxyl radical production yield was severely reduced. DNA damage detected by $\gamma\text{-H2AX}$ assay was enhanced by more than 100%. X-ray irradiation alone (5 Gy) used in the animal work did not reduce tumor size at all. When X-ray irradiation was combined with the nanoparticles, a 2.4 DEU enhancement was measured, using the tumor sizes given by the authors.

Wen and Gu et al. [60] used silver nanoparticles to enhance the effect of cell destruction under X-ray irradiation. U251 cells and 6 MV X-rays were used. 3-Methyladenine (3-MA) autophagy inhibitor and antioxidant N-acetyl cysteine (NAC) were used to determine the role of reactive oxygen species. It was found that silver nanoparticles were toxic, and the enhancement was about 0.5 DEU based on caspase-3 assay without NAC and became nearly zero with NAC. When 3-MA was used, enhancement was close to 2 DEU without NAC and was still 1.0 DEU with NAC. The results could be useful to other in vitro and in vivo work.

Martinez-Rovira et al. [172] discussed the use of gadolinium nanoparticles under X-rays to treat glioma cells. Fourier Transform Infrared (FTIR) spectroscopy was used to measure the response or enhancement. The gadolinium nanoparticles were purchased, which consisted of gadolinium compound-decorated nanoparticles. The size was 3 nm. Average X-ray energy was 90 keV and dose rate was 1.1 Gy/min. The responses were analyzed and identified as changes to DNA backbone phosphate groups. Metabolic activity measurements showed the effect of the nanoparticles, which was the most prominent after greater than 5 Gy of irradiation. The measured LD₅₀ dose for F98 cells was greater than 20 Gy, which was higher than most of the LD₅₀ values reported in the literature.

Currell et al. [163] used 1.9 nm gold nanoparticles on MDA-MB-231 cells and performed both DNA damage and theoretical simulations of the damage. Imaging of the nanoparticles suggested that detectable nanoparticles largely remained outside the nuclei. However, the results did not completely exclude the possibility of the nanoparticles entering the nuclei because the detection method was through surface plasmon resonance using two-photon excitation, and no calibration was given. Results of simulations using the local effect model (LEM) mentioned in Chap. 2 suggested that these nanoparticles outside the nuclei in the amount of 0.7 WP could be responsible for the damage of DNA measured in the work. The results suggested a strong energy dependency of nuclear DNA damage under monochromatic X-ray irradiation, with the peak of damage occurring at 55 keV (experimentally) or 40 keV (simulation). According to the measurements, there was little or no enhancement for X-rays below 20 keV or above 70 keV, agreeing with the claim made in Chap. 2, [stating that enhancement peaks around 50 keV](#).

Tehei et al. [12] reported the study of using bismuth oxide nanoparticles to assist radiotherapy. 9 L gliosarcoma cell line was used, and X-ray energies were 125 kVp and 10 MV. Incubation concentration was 50 µg/mL although no uptake data was available. A moderate enhancement of 0.48 and 0.25 DEU were observed at these two energies. In another report, bismuth nanoparticles (3.6 nm) were synthesized and used to explore their enhancement potential to radiotherapy by Yang and Li et al. [71]. The nanoparticles were PEGylated and targeting peptide LyP-1 ligands were conjugated to the surface. 4T1 cells were used in the study. Approximately 5 µg/mL was found in the cell for LyP-1 covered nanoparticles, which was only 5 ppm. PEGylated nanoparticles had only 40% of the uptake of the LyP-1 covered nanoparticles. However, both uptake values were low and there should be no measurable physical enhancement. The authors showed an approximately 2 DEU enhancement, which was unexplainable using physical enhancement mechanisms shown in Chap. 2.

Zheng et al. [180] reported that ligands on 2 nm gold nanoparticles were critical to determination of their sensitizing properties. If the ligand was PEG, then the nanoparticles were basically radioprotectors, i.e., scavenging radicals in the MCF-7 cell. If the ligand was zwitterionic glutathione, then the nanoparticles functioned as sensitizers. The authors also studied the uptake and found that glutathione-coated gold nanoparticles were 20 times better than PEG-coated gold nanoparticles in terms of being able to enter the cell. The authors also pointed out that uptake did not affect the enhancement or scavenging properties of these nanoparticles. This outcome is in agreement with the conclusions shown in Chaps. 2 and 3, stating that very small nanoparticles are unlikely to produce physical enhancement, and if any enhancement is found, it is more likely to be chemical enhancement, which depends on the surface structure.

Kharrazi and Amani et al. [168] reported the synthesis of lanthanide-doped ZnO-based nanoparticles and application of this nanomaterial in treating HeLa and PC3 cancer cells. Therefore, this was at least a case of type 3 physical enhancement described in Chap. 2. The average size of the nanoparticles was between 4 and 10 nm. The authors also conjugated rhodamine B molecules to the surface of nanoparticles. Mild toxicity was observed with ZnO nanoparticles and rare earth-doped ZnO nanoparticles. When combined with X-ray or γ -ray irradiation, decreased cell viability was observed. It is interesting to note that the viability was about 10% with a single 6 Gy X-ray irradiation. The viability was near 40% when under three fractions of 2 Gy X-ray irradiation, suggesting that fractionation irradiation was less lethal than a single dose. The authors observed that a 2 Gy X-ray irradiation of 20 $\mu\text{g}/\text{mL}$ loading of Eu-doped ZnO nanomaterials was equivalent to a three-fractionation of 2 Gy X-ray irradiation, both reducing the viability to 30%. If enhancement is calculated based on the accumulated dose, which is clearly inaccurate, then a 2.0 DEU enhancement is observed here.

Paquette et al. [34] studied the effect of tiopronin-coated gold nanoparticles on the destruction of HCT116 cells. The ligand was chosen to maintain the nanoparticles soluble and stable at high gold nanoparticle concentrations. The average X-ray energy was 26 keV. LD_{50} dose was only 1.5 Gy, indicating HCT116 cells were radiosensitive to 26 keV X-rays. The nanoparticles were around 3 nm. γ -H2AX assay was used to measure the enhancement to DNA damage. Uptake measurements revealed up to a 3.3 WP gold loading in cell using 1 ng cellular weight. Nearly 1.0 DEU was measured using the DNA damage assay, which corresponded to a unit WP enhancement of 0.3 DEU WP^{-1} . The results suggest that these nanoparticles are scavenging as well as generating enhancement.

Chen and Li et al. [37] explored the effect of tirapazamine-conjugated gold nanoparticles on liver cancer cell HepG2 under X-ray irradiation. Tirapazamine was known to produce hydroxyl radicals in the presence of a very low level of oxygen. The gold nanoparticles were 16 nm. LD_{50} was only 1 Gy for the cell line, and enhancement was on the order of 0.2 DEU for hydroxyl radical production in water and 0.3 DEU for surviving fraction reduction.

Kim et al. [40] compared two sizes of gold nanoparticles for therapeutic purpose. The authors employed 1.9 and 50 nm gold nanoparticles and 150 and 450 kVp

X-rays. The cell line was HTB-72 skin melanoma. Incubation concentration was around 0.01 WP. Although no quantitative uptake data was available, TEM images were available to show that uptake of 50 nm gold nanoparticles was much higher than 1.9 nm gold nanoparticles. Enhancements was 0.3 and 2.7 DEU for 1.9 and 50 nm gold nanoparticles at 2 Gy of 150 kVp X-rays. Greater enhancements were observed at higher doses, reaching 6.8 DEU at 7 Gy. This trend was counterintuitive because usually the enhancement decreases as the dose of irradiation increases.

Goldys et al. [167] explored the use of verteporfin-conjugated 12 nm gold nanoparticles in X-ray-mediated photodynamic therapy. Verteporfin was a porphyrin derivative. Light excitation at 690 nm of the nanomaterial in Panc 1 cells apparently reduced the cellular viability by more than 50%, demonstrating that singlet oxygen generation ability of verteporfin was not reduced by gold nanoparticles. However, the effect of 6 Gy of X-ray excitation was minimal, showing only a 0.05 DEU enhancement.

Arab-Bafrani et al. [39] studied the treatment of colon cancer cells with 50 nm gold nanoparticles and 9 MeV radiation. Cell viability or survival fraction was evaluated using MTS assay. 6×10^4 gold nanoparticle uptake was measured with atomic absorption (AA) spectroscopy. This level of uptake corresponded to over 5 WP of gold in cells, which was supposed to generate at least a 5 DEU enhancement if only physical enhancement, was considered. Using LD₅₀ for HT29 cells without and with gold nanoparticles, an enhancement of approximately 1.0 DEU was obtained. This result again suggests that gold nanoparticles without special treatment would scavenge, reducing the enhancement caused by these nanoparticles.

Yang, Wu, and Yang et al. [11] developed a similar approach employed by Li et al. [188]. The latter used WS₂ nanodots instead of Au@FeS nanomaterials. In Yang's work, gold nanoparticle core-FeS shell nanostructures coated with PEG ligands were synthesized and used in the mouse model. The gold core was approximately 20 nm, and after FeS shell wrapping, the overall size of the nanoparticles was approximately 100 nm. Laser light at 808 nm was used to heat the samples, and up to 70 °C was measured using irradiance of 1 W cm⁻². 4T1 cell line was used in the in vitro experiments and a 4 Gy X-ray dose was used, which caused a 20% reduction in surviving fraction. These results suggested that LD₅₀ was 12 Gy for 4T1 cells, which was higher than normal cells. The nanomaterial caused only a 0.1 DEU enhancement. The largest enhancement occurred when laser and X-ray irradiation of the nanomaterials were combined.

Geso et al. [25] tested titanium dioxide nanoparticles as radiosensitizers. The size of the nanoparticles was about 30 nm and the surface was modified with amine or PEG, and 80 kV and 6 MV X-rays were used. Up to 8 Gy of X-ray dose was used. HaCaT and DU-145 cells were used in the study. Results from MTS assay suggested LD₅₀ for both cell lines were the same, which was about 6–8 Gy. Clonogenic results, however, suggested the LD₅₀ was 2–4 Gy for both cells. The results suggested that not only enhancement measurements depended on assays; LD₅₀ also depended on the assay as well. The particles were found to be not toxic to the cells. The enhancements at two energies were similar, ranging from 0.56 to 0.77 DEU for 80 kV X-rays and 0.37 to 0.67 DEU for 6 MV X-rays at 4 mM titanium dioxide

nanoparticle incubation concentration. Reactive oxygen species generation was considered to be the cause for the enhancement. If the ionization of nanoparticles was caused by the electrons produced from X-rays interacting with water, then the closeness of the two enhancement magnitudes at two energies can be explained.

Detappe and Berbeco et al. [165] engineered a hybrid nanomaterial that had a Gd_2O_3 core and SiO_2 shell covered with DOTAGA ligands whose terminal groups trap Bi^{3+} ions. The final size was less than 5 nm in diameter measured with DLS. The nanomaterial was called SiBiGdNP. The radiation was 6 MV X-ray. Clonogenic assay was used to measure the survival fraction of A549 cells. Without the nanomaterials, LD_{50} was 6 Gy. With the nanomaterials LD_{50} was 3 Gy, giving rise to a 1.0 DEU enhancement. No uptake data was available.

9.5.3 Summary

All these results shown in this section, despite variations and fluctuations from report to report, reveal three general trends. First, there is usually an enhancement to the destruction of cancerous cells under X-ray irradiation when gold nanoparticles are added. All the reported studies show some enhancement. The second trend is that the measured enhancements are similar, of the order of 0.5–1.0 DEU. This may be caused by how the experiments are performed or by something more profound. The third trend is that based on the uptake and enhancement data, which are summarized in Fig. 9.28, a small number of reports show the value of the measured enhancement being close to the theoretically predicted physical enhancement. However, this agreement happens to occur only when the predicted physical enhancements are close to 0.5 DEU, essentially the same as the average enhancement for most

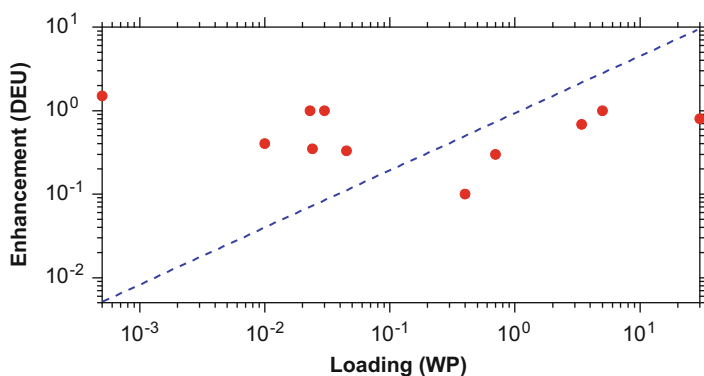


Fig. 9.28 Experimentally measured enhancements (round dots) for actual loadings of gold or other nanoparticles in the cell. Also shown is the predicted physical enhancement at the corresponding uptake or gold loading (dashed line). The enhancement uses dose enhancement units (DEU); the loading has the unit of weight percentage of gold (WP) in the cell

measurements. This implies that this agreement is possibly just a coincidence than a true cause-effect agreement.

Unfortunately, there are almost no mechanistic studies to conclusively explain the origin of enhancement. It is difficult to isolate enhancement mechanisms unless experiments are extremely well controlled because cellular responses are complex. One example of a better-controlled experiment is to use γ -H2AX assay to measure nuclear DNA damage by large nanoparticles. If the size of gold nanoparticle is larger than 30 nm, and if the end point is nuclear DNA damage, then it is most likely the enhancement is physical enhancement because gold nanoparticles are located outside the nuclei and hence cannot cause chemical or biological enhancement—these gold nanoparticles can only remotely deposit energy in the nuclei to damage nuclear DNA. These studies show that carefully designed nanomaterials and irradiation experiments are needed to isolate individual enhancements and determine enhancement mechanisms.

Figure 9.28 summarize the experimentally measured enhancements cited in this section, and it is evident that most of them have enhancement magnitude around 0.5 DEU or between 0.1 and 1.0 DEU, even though uptake are as low as 10^{-3} WP and as high as 40 WP. As a reference, the predicted physical enhancement as a function of gold loading is also shown in Fig. 9.28 (dashed line). The two trends are clearly uncorrelated, which suggests that the measured enhancement does not depend on physical enhancement. It seems the cells have an internal regulating mechanism. Several articles and Chap. 4 discuss the possibility and various forms of biological enhancement. Future work is needed to uncover the true causes for the measured enhancements.

9.6 Treatment of Tumor (In Vivo) Tissues with Nanomaterials and X-Rays

This section contains two parts. The first addresses in vivo work. The second part discusses preclinical or clinical trials.

9.6.1 Survey of In Vivo Work

The works published in the area of using X-ray nanochemistry to treat animals are listed in Table 9.9. The first publication in this area was done by Heinfeld et al. [5]. Unlike the study of other experimental drugs, this first work used an animal model, although to this date it is still unknown whether the effect measured in this work was solely caused by the predicted physical enhancement.

Hainfeld et al. [5] used Balb/C mice (average weight 35 g) infected with mammary carcinoma cells as their animal model to determine the effect of gold

Table 9.9 List of in vivo studies of enhancement of radiation damage by nanoparticles to tumors in animals. The results are ordered chronologically according to the corresponding authors and clustered for the each corresponding author when multiple papers are published by the same group. Enhancement (Enh) values are calculated by the author of this book if not given in the published reports

Animal type	Uptake amount (WP)	Composition	Size (nm)	Ligand name	X-ray energy/dose (Gy)	Enh (DEU)	Ref.
Mice	0.23/1.8	Au	1.9		30	0.59/5.5 ^a	Hainfeld et al. [5]
Mice		Au			250 kVp		Hainfeld et al. [191]
Mice	1.5	Au	11	– (from nanopores)	100 kVp/30	2.00	Hainfeld et al. [108]
Mice	–	–	–	HVGGSSV	/3Gy ^b	–	Jaboin et al. [190]
Mice	7.4	Au	13	Citrate	6 MeV/50	0.50	Chen et al. [191]
Mice		Au	4.7	PEG	6 MV		Hwu et al. [22]
Mice	6 mg	Au	30 nm	PEG	6 MV/25	0.40	Popovtzer et al. [139] and [192]
Mice	–	PtFe		GIRLRG	/3		Hallahan et al. [31]
Mice/Lung		Nab-paclitaxel	–	HVGGSSV	300 kV/3		Hallahan et al. [82]
Mice	–	Cisplatin@liposome	100	–	6 MV/6–28	0.50	Jiang et al. [15]
Rats		Gd ₂ O ₃ @SiO ₂	1.1 core, 0.5 shell	DTPADA	50–350 keV (mean 90 keV)/		Roux et al. [115]
Mice		Au	15–20	PEG diacrylate			Hwu et al. [196]
Mice	0.004 (Fe/tumor)	FeOx	13–15	Alginate acid	7.1 keV/10–40		Choi et al. [21]
Mice	Measured 24 days after	Au	4.8–46.6	PEG-SH	137–Cs/5	–0.28–3.73	Liang et al. [141]
Mice	0.7	Au	50	(Commercial product, unknown)	6,18 MV/20	0.10	Anijdan et al. [197]

Mice	0.7–3.0	Au (nanorods)			PEG/cetuximab	140kVp/10	0.05–0.33	Krishnan et al. [198]
Mice	0.043	Au	2		PEG,RGD, AF647	220 kVp/10	3	Berbeco et al. [199]
Mice		Lu, Au, NaYF ₄ ; Yb/Er/Tm/Gd			PEG5000			Bu et al. [200]
Rat	0.7	Terpyridine-Pt complex	Molecules		–	160 kVp, 6 MV/15		Pradhan et al. [29]
Mice	0.055 ± 0.017	Au NP SuperPara FeOx@PEG-PLC micelle	2.2 Au, 14 FeO, 100 by DLS		–	150 kVp/6		Tsourkas et al. [125]
Mice	0.00066, 0.00038	Au	18		BSA	160kVp/3 + 2	0.10	Tu et al. [198]
Mice	–	SrAl ₂ O ₄ :Eu (SAO)@SiO ₂	400		Merocyanine 540 loaded in shell	50 kV/0.5	181.09	Xie et al. [199]
Mice	0.00095	Au	<2		Glutathione	662 keV (137-Cs)/5	1.65	Xie et al. [200]
Mice	2.5	Gd/Yb/Ln/SiO ₂	280 width/500 length		ZnPc, folic acid			Yang et al. [127]
Mice		Au	3–50		SH-PEG-COOH	keV, MeV	3.55	Chang et al. [76]
Mice/U14		Au	60		PEG	6 MV	0.07	Chen et al. [42]
Mice		Au, SiO ₂	20–200 nm		PEG, CTAB, DNA, RNA	80.7 keV	1.00	Li et al. [136]
Mice	–	Au@MnO ₂	50		PEG	160 keV/6	3.98	Yang et al. [204]
Mice	0.0001	Au/Fe ₃ O ₄	70		PEG, folic acid	50 kVp		Mei et al. [62]
Mice		Perfluorohexane@liposome	100		–	6 MV/0–10		Hu et al. [23]
Mice	1	Au	1500–3000			200 kVp/8	0.40	Das et al. [20]
Mice	–	SrAl ₂ O ₄ :Eu@SiO ₂	73.5 ± 26.9		–	50 kVp/5	2.26/4.02	Xie et al. [32]

(continued)

Table 9.9 (continued)

Animal type	Uptake amount (WP)	Composition	Size (nm)	Ligand name	X-ray energy/dose (Gy)	Enh (DEU)	Ref.
Mice	0.00074, 0.00222	Au rod@mSiO ₂	57.70 × φ14.44	PEG, RGD	6 MV/10	0.80, 3.44	Fu et al. [202]
Mice	3.3	Au	3	Tiopronin	26 keV	2.00	Paquette et al. [34]
Mice		Au in MnS in ZnS	30–40	PEG	/4, 6	2.60 (4 Gy), 1.25 (6 Gy)	Yang et al. [203]
Mice	0.00013 (Au), 0.00115 (Se)	Au-Se	120	RGD and ACP	6 MV/40 (fractional)	0.15 (IV) 0.37 (IT)	Chen et al. [13]
Mice		WS ₂ in polyaniline shell	6.1	Hyaluronic acid and chlorin e6	/6	0.20	Li et al. [188]
Mice		BSA/MnO ₂ /HI/DSP	150	PEG	/6	1.79	Liu et al. [204]
Mice	–	GdW ₁₀ (polyoxometalate) @chitosan	30	siRNA HIF-1α	–/10	2.47	Zhao et al. [36]

^aReported by the authors of the publications^bDose to activate tumor targeting

nanoparticles on radiotherapy. Following a week of tumor growth, animals were treated with 1.9 nm gold nanoparticles and then irradiation of 250 kVp X-rays. The dose was a single dose of 30 Gy. Based on the values given in the paper, gold loading in the tumor after gold nanoparticle administration was $(4.9/100) \times 1.35 \text{ g/kg} = 6.6 \text{ mg/g}$ or 0.7 WP. The peripheral had $(10/100) \times 1.35 \text{ g/kg} = 20 \text{ mg/g}$ or 2 WP. Blood had a gold loading of $(10/100) \times 1.35 \text{ g/kg} = 20 \text{ mg/g}$ or 2 WP. The estimated enhancement using 33 keV X-rays, which should produce highest physical enhancement allowed, was 1.0 DEU at the tumor and 2.8 DEU in the peripheral and blood. For 250 kVp, the predicted enhancement was close to 0.5 DEU, which was close to the measured enhancement of 0.4 DEU calculated by the author of the book using exponential growth models, although the authors reported an enhancement of 5.5 DEU. The results are shown in Fig. 2.21.

Hainfeld et al. [191] showed their results of gold nanoparticle treatment of cancer-bearing mice. The experimental setup was similar to what was described in their 2004 publication, i.e., 3 g kg^{-1} gold loading and irradiated with 250 keV for 30 Gy. In another similar study, Smilowitz et al. [208] studied the enhancement of radiation therapy by gold nanoparticles under X-ray radiation. They used murine squamous cell carcinoma. The authors found that 68 keV X-rays were more effective than 157 keV X-rays. This energy dependency result implied that gold absorption of X-rays played an important role. The authors also found that gold nanoparticles worked better with 42 Gy dose than 30 Gy. This suggested that enhancement obtained using the surviving curve was a valid assessment because enhancement calculated thereby was usually higher at lower doses. Hainfeld et al. [108] used 11 nm gold nanoparticles for intravenously injection for both imaging and treatment of brain tumors. The loading was 1.5 WP and the enhancement was approximately 2.0 DEU. The results are shown in Fig. 9.29. This enhancement was close to the theoretically predicted physical enhancement caused by the gold loading for 100 kVp X-rays. The chance for the nanoparticles to enter nuclei was small because of the relatively large size of gold nanoparticles of 11 nm, which reduced the probability of having chemical or biological enhancement. The half-life of the 11-nm gold nanoparticles was 24 h, which was much longer than the 42 min half-life for 1.9 nm gold nanoparticle mentioned earlier.

Chen et al. [209] studied scintillation from nanoparticles that helped increase the production of singlet oxygen. Porphyrins were the molecules of their choice. Various lanthanides were tested as well. Specifically, $\text{LaF}_3: \text{Ce}^{3+}$ nanoparticles were studied. As discussed in Chap. 2, scintillation belongs to type 3 physical enhancement, which is related to photons released from the added nanoparticles. Even though it was possible to measure the absolute quantum yield of the added scintillation nanomaterials as shown by Guo et al. [210], the parameter was not commonly measured in applications of these nanomaterials. Instead, measuring the yield of singlet oxygen was commonly performed. If there were no other nonlinear processes involved, then the two measurements should yield the same result.

Hallahan et al. [31] reported a method of using Pt compounds under 3 Gy X-ray irradiation to study radiation treatment of GL261 brain tumor xenografts as well as mice treated with other cancer cells including breast cancer cells MDA-231 and lung

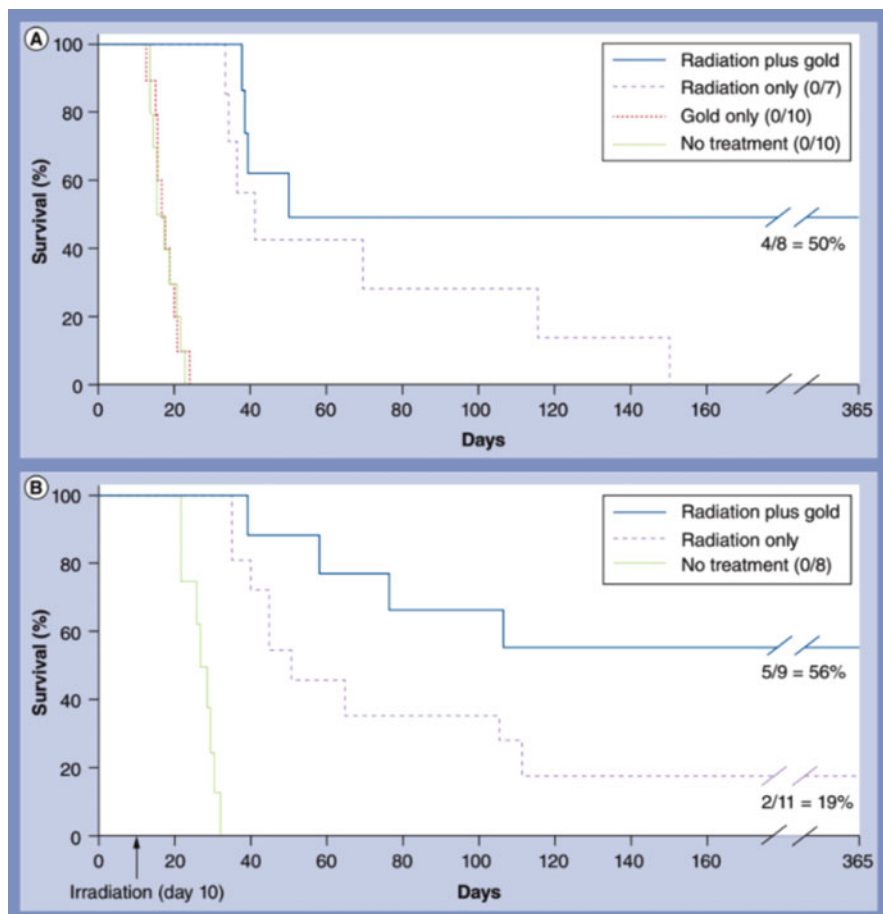


Fig. 9.29 Survival of mice treated with gold nanoparticles under X-ray irradiation. (Used with permission from Hainfeld et al. [107] under CC BY 3.0 license.)

cancer cells H460. The authors conjugated peptides to the surface of PtFe particles and investigated biological effects. In terms of accumulating in breast cancer tumors, GIRLRG peptide appeared to be an effective ligand when coated on the surface of PtFe particles. Hallahan et al. [82] again used peptides conjugated to nab-paclitaxel nanoparticles to bind to the radiation-inducible receptor in irradiated tumors. In this study, the authors used a mice model for lung cancer treatment. X-rays were used to activate the receptor to which peptide bound nanoparticles targeted. Optical imaging was used to confirm targeting of the nanoparticles. Hallahan et al. [101] reported on radiation-guided delivery of FePt nanoparticles coated with peptide for cancer treatment. The average size of FePt nanoparticles was 2.7 ± 1.0 nm. Accumulation of the nanoparticles at tumor sites after irradiation was observed, indicating the nanoparticles indeed targeting the radiation treated tumors.

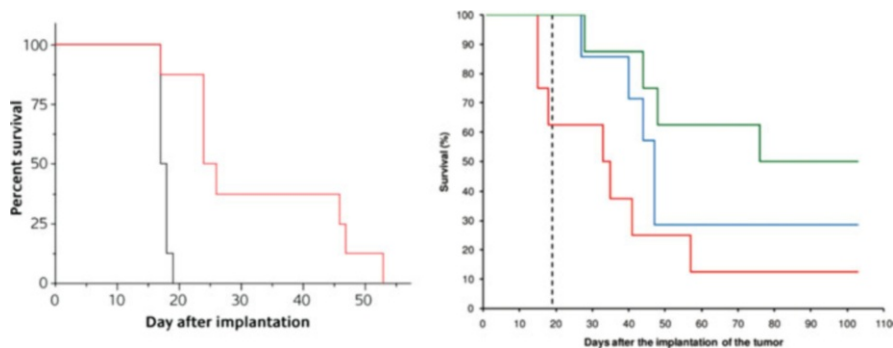


Fig. 9.30 Results of nanoparticle-enhanced therapy on treating 9L gliosarcoma-bearing rats. Percentage survival results using gold nanoparticles (left panel) are shown. Effect of rare earth-doped titania on the enhancement of radiation is shown in the right panel. (Left panel: Roux et al. [208]. Open access made possible by Gold Bulletin. Right panel: Adapted with permission from Roux et al. [115]. Copyright (2014) American Chemical Society.)

Chen and Wu et al. [191] employed cancer-bearing mice to investigate the effect of 13-nm gold nanoparticles under 6-MeV electron irradiation. Gold nanoparticles under irradiation showed a 25–50% improvement for a gold loading of 74 $\mu\text{g}/\text{mg}$ in tumor tissues using the survival fraction measurements performed over a 100-day study. This translated to a 0.25–0.5 DEU enhancement for or 7 WP gold in tumor loading. 7 WP gold nanoparticles in water is supposed to produce only 0.2 DEU enhancement because electron interaction cross-sections with gold is only three times that with water, which suggests that the observed enhancement could be caused by physical enhancement.

Roux et al. [208] developed chelate surfactants on gold nanoparticles for combined X-ray and MRI imaging of animals and potentially for clinical applications as well. Further, they evaluated the therapeutic impact of their nanoparticles. The average size of gold nanoparticles was 2.4 nm. X-rays were from synchrotrons and a microbeam configuration was used. Although no direct and quantitative data was available showing the uptake and enhancement, the authors used fisher rats and doubled the survival time for the treated animals. The authors showed evidence of using gold nanoparticles as both a contrast agent to detect and a therapeutic agent to treat 9L gliosarcoma tumors in mice. The results are shown in Fig. 9.30 (left panel). Roux et al. [115] used microbeam radiation to irradiate Gd-based nanoparticles for therapeutic purpose. Gd nanoparticles were used as a contrast agent for MRI. The authors found that with sufficient amounts of Gd in the tumor, cancer-bearing mice could stay alive longer after Gd nanoparticle-treated mice were irradiated with X-rays. 9L gliosarcoma-bearing rats were used, and the treatment results are shown in Fig. 9.30 (right panel). The skin entrance dose was set at 400 Gy, which was significantly higher than normal animal work.

Hunting et al. [209] used MRI to visualize nanoparticles for enhanced radiotherapy of cancer-bearing mice. Their 5 nm average-size gold nanoparticles, covered with gadolinium capturing ligands of dithiolated diethylenetriaminepentaacetic,

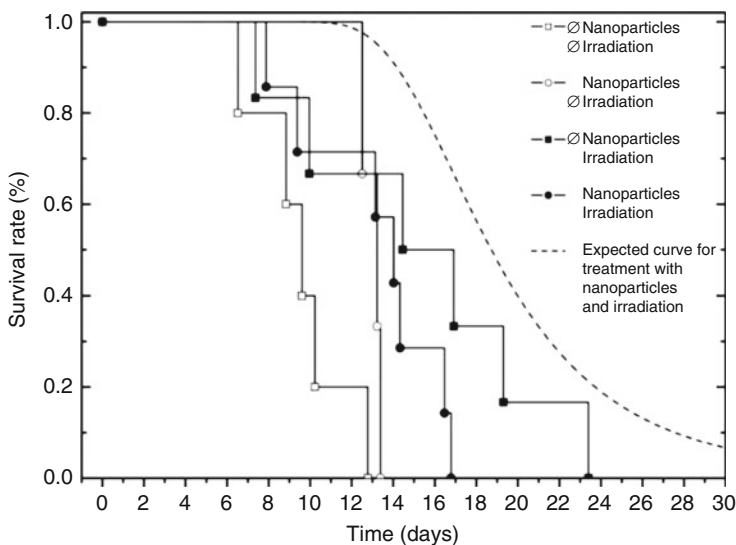


Fig. 9.31 Survival of mice treated with gold nanoparticles under X-ray irradiation. Experimental results are compared with the theoretical predictions (dashed line). (Adapted from Hunting et al. [209], reprinted by permission of Taylor & Francis Ltd. <http://www.informaworld.com>)

were injected into the mice in the tail veins. The radiation dose was 10 Gy at 150 kVp. The MRI results showed 10 μg gold nanoparticles in 30 μL or 30 μg of tumors, giving rise to a 33 WP gold loading in tumor. If the average physical enhancement existed, then a 33 DEU maximum physical enhancement was expected. Figure 9.31 shows the results, which indicate that the measured enhancement is lower than the expected enhancement. Nonetheless, there was enhancement by gold nanoparticles when irradiated with X-rays.

Jiang et al. [15] conducted treatment of tumor in mice with cisplatin-packed nanoliposomes. Single dose of up to 28 Gy was administrated to both A549 cells and Lewis lung carcinoma. The authors counted the jejunal crypts after sacrificing the mice. Tumor growth delay (TGD) (in vivo) and cell survival curve (CSC) (in vitro) were obtained and used to estimate the efficacy of the combination of radiation and drugs. Irradiation was carried out 72 h after drug administration, at which time the drugs were distributed to the tumor sites. Jejunal crypt survival curves were determined using the linear-quadratic model (L-Q). Nanoliposomes were nontoxic, but their drug-containing versions showed inhibition of A549 cell growth/colony formation. Tumor growth was delayed with X-ray irradiation and with drug bearing nanoliposomes, and tumor growth delays were more pronounced than jejunal crypt cells in mice. The cell survival fraction was 2–3% at 6 Gy. The best result was obtained with a 72-h delay between the injection of nanodrugs and irradiation. Tumor growth was delayed up to 26 days upon treatment with nanodrugs and radiation.

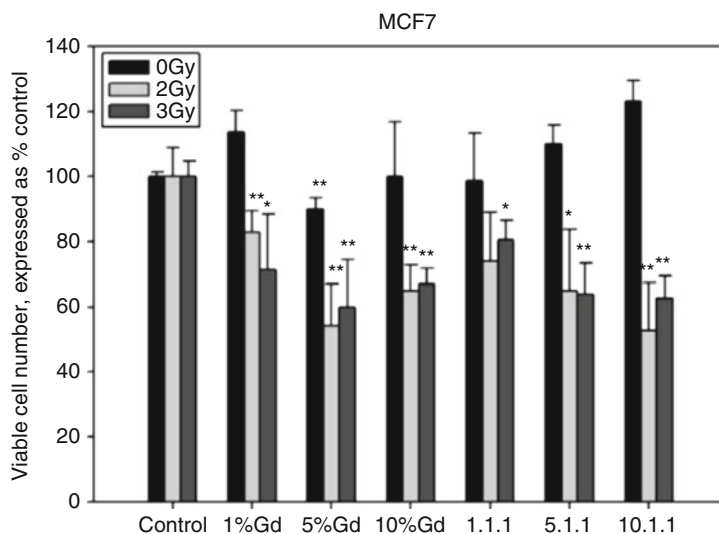


Fig. 9.32 Effect of rare earth-doped titania on the enhancement of the effect of radiation. (Reprinted from Townley et al. [210]. Copyright (2012) with permission from Elsevier.)

Townley et al. [210] reported using X-rays to activate lanthanide (Gd and other elements)-doped titania nanoparticles for cell killing. The authors stated that the average size was 60 nm with multiple grains of 3–10 nm. They also coated the nanoparticles with a layer of silica and estimated the thickness to be around 1–2 nm. The dose of irradiation was 3 Gy from X-rays with an 80–90 keV average energy. Cell proliferation was reduced by 75% after treatment. The authors attributed the enhancement to increased production of reactive oxygen species in the presence of these nanomaterials. Figure 9.32 shows the results of enhancement measurements.

In addition, Townley et al. [211] studied rare earth element-doped TiO₂ nanoparticles for radiation therapy. They also coated a 1–2 nm layer of silica on the outside of the nanoparticles. They irradiated animals using X-rays emitted from an X-ray tube operated at 200 kVp. Emission from rare earth elements under X-ray irradiation was used for excitation to produce reactive oxygen species. The results confirmed that X-ray irradiation of the said nanomaterials reduced the tumor size by half.

Choi et al. [21] discussed their work of using synchrotron X-rays at 7.1 keV to irradiate FeO_x nanoparticles in a mouse tumor model. This was a unique study because the X-ray energy was low and X-rays were resonantly absorbed by the nanoparticles, similar to what was done by Townley et al. mentioned above. The authors called the method photo-activated therapy (PAT). They treated CT26 tumors and CT26 tumor-infected mice. Tumor regression assay was used to estimate enhancement. A similar set of in vitro results are presented in Sect. 9.5.3. The size of the nanoparticles was 13 nm. Cytotoxicity of FeO_x nanoparticles was observed at 0.2 WP, which was the incubation concentration. After uptake, the concentration in

the cell was 30 μg or about 0.3 WP (30 μg in a cell weighing 1 ng). FeO_x nanoparticles alone already significantly delayed the growth of the tumor. The loading of FeO_x nanoparticles was verified to be 40 ppm (40 $\mu\text{g}/\text{g}$) in tissue. This loading was low compared with the gold loading in gold nanoparticle sensitized X-ray treatment of cancer-bearing animal models. The total X-ray dose was 40 Gy, delivered over 10 days. Their results are shown in Fig. 9.33. The combination of X-rays and FeO_x nanoparticles had the best effect. Radiation alone also showed significant improvement, almost as good as the combined radiation and nanoparticle

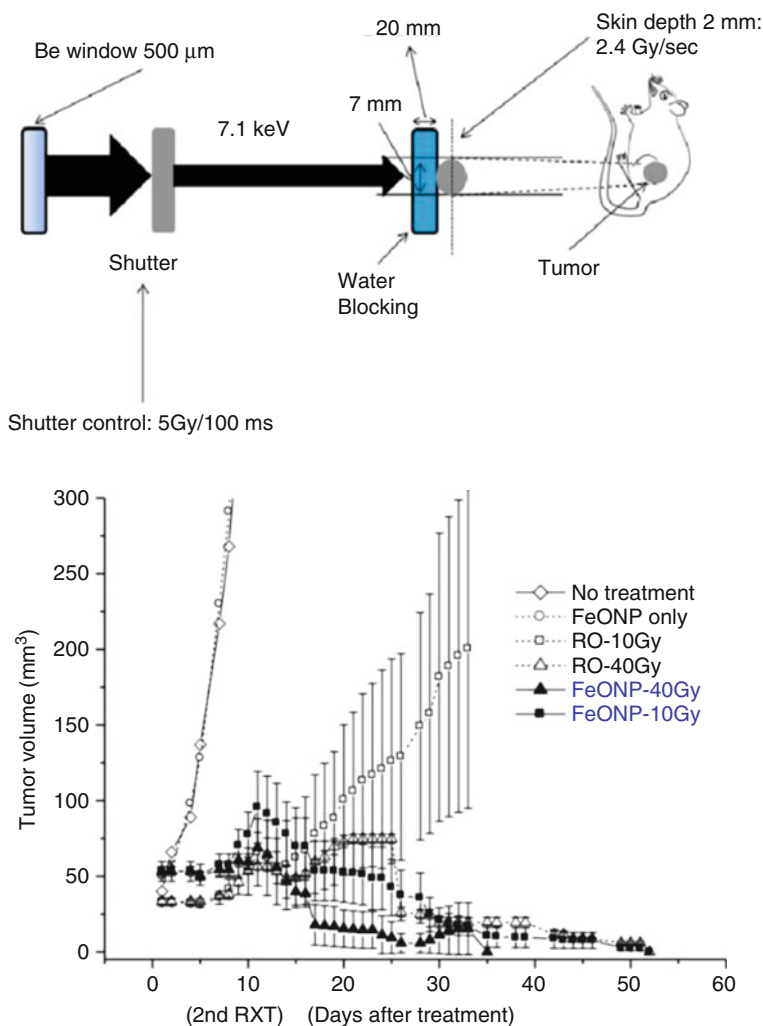


Fig. 9.33 Resonant interactions of X-rays and iron oxide nanoparticles in mouse tumors for radiotherapy. 10 and 40 Gy doses were used. The top panel shows the experimental setup, and the bottom panel shows the results. (Adapted from Choi et al. [21]. Used with permission under CC BY 2.0 license.)

effect. The results indicated 100% mice survived after 40 Gy treatment with FeO_x nanoparticles. On the other hand, only 20% survived after a 10 Gy irradiation. The authors also performed enhancement studies with high-energy X-rays emitted from accelerators, but no enhancement was detected.

Liang et al. [141] reported the results of their study on the effect of the size of gold nanoparticles on treating cancerous cells and mice. They used PEGylated gold nanoparticles for radiation therapy. γ -rays, U14 mice model, and 5 Gy of radiation were used in their work. The sizes of the gold nanoparticles were 4.8, 12.1, 27.3, and 46.6 nm. The results showed that 4.8 nm gold nanoparticles had the highest toxicity. The mice were monitored up to 28 days. Tumor size was used for determination of enhancement of treatment efficacy. They observed size dependency and found that 12 and 27 nm gold nanoparticles were better than 4.8 and 46 nm for slowing down the growth of cancer cells.

Anijdan et al. [194] used MV X-rays to irradiate tumor-bearing mice administered with gold nanoparticles. 6 and 18 MV X-rays were used at a dose of 20 Gy. 50 nm gold nanoparticles were used. The accumulation of gold in tumor was reported to be 7 mg/g, similar to what Hainfeld et al. [5]. The enhancement based on survival probability was on the order of 0.1 DEU.

Krishnan et al. [195] published their patent application of using targeted gold nanorods (AuNR) for treatment of cancerous cells and animals. The animal model results using tumor volume as a gauge of enhancement showed the best outcome with inhibitor cetuximab conjugated C225-AuNR under X-ray irradiation. The results of using PEGylated AuNR (PEG-AuNR) under X-ray irradiation were similar to that of irradiation alone. Results from cellular work were also presented in the application.

Tsourkas et al. [38] used a tumor-bearing animal model to study the effectiveness of 1.9 nm gold nanoparticles in micelles made of amphiphilic diblock copolymer poly(ethylene glycol)-*b*-poly(ϵ -caprolactone) PEG-*b*-PCL. The size of the assemblies ranged from 28 to 142 nm measured by DLS, and similar sizes were measured with TEM. The dose used by the authors was 6 Gy at 150 kVp. Treatment of HT1080 flank tumors using X-rays and the gold nanoformula showed a 0.7 DEU enhancement with 0.57 mg/mL or 0.057 WP gold loading in tumors measured with ICP-PES. This level of gold loading was supposed to produce only a few percent of physical enhancement, which was 10% of the measured enhancement. The loading of gold in the tumor and X-ray dose was lower than what others used in other animal models. Figure 9.34 shows the results by Tsourkas et al.

Tu et al. [198] performed both *in vitro* and *in vivo* measurements on glioblastoma tumors. The cellular apoptosis data suggested some enhancement when BSA-coated 18 nm gold nanoparticles were irradiated with X-rays. The *in vivo* data was mildly encouraging, showing that X-rays plus gold nanoparticles were slightly more effective than X-rays alone.

Guo and Xie et al. [200] studied the radiotherapeutic effect of ultrasmall gold nanoparticles, each containing only 29–43 gold atoms. The nanoparticles were covered with glutathionate ligands. The nanoparticles were injected into mice, and the loading in the tumor was of the order of 8–10 μ g/g, which was too low to create

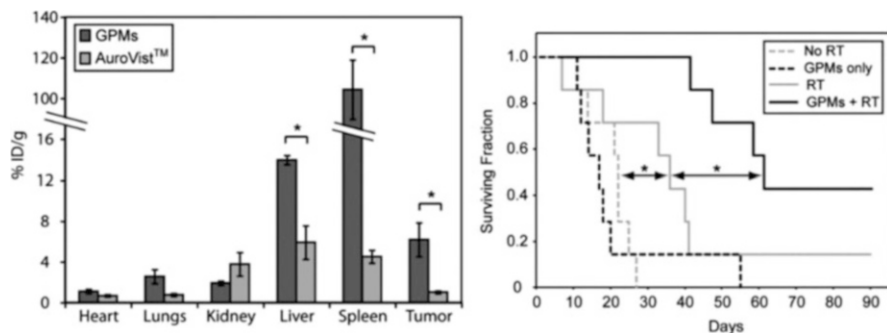


Fig. 9.34 Enhancement in terms of survival fraction increase after treatment with nanoliposomal 1.9 nm gold nanoparticles and radiation. The left panel shows the biodistribution and the right panel shows the surviving fraction results. (Reprinted in part with permission from Tsourkas et al. [38]. Copyright (2015) American Chemical Society.)

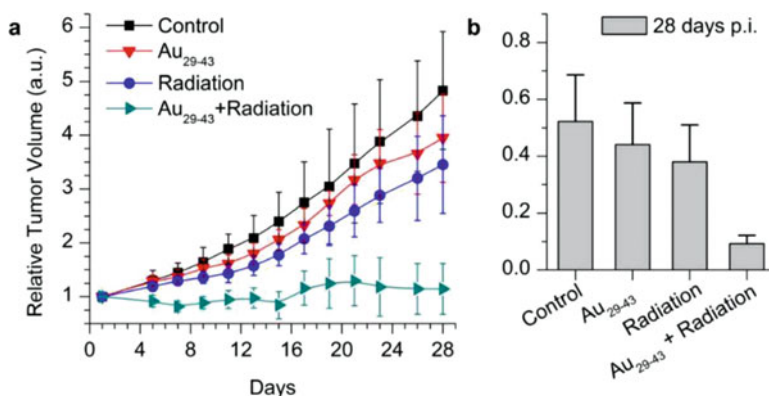


Fig. 9.35 Ultrasmall gold nanoparticles for radiation therapy. The time-course study of the tumor volume is shown in the left panel, and the right panel shows the results of weight study. The effect of enhancement is clearly visible in both studies. (Adapted from Guo and Xie et al. [200]. Used with permission under CC BY 4.0 International license.)

any physical enhancement. On the other hand, the authors observed a clear impact of the combination of X-ray radiation and the nanoparticles—after 28 days, there was almost no tumor growth among mice exposed to both ingredients, whereas the tumor grew fivefold among the mice without the treatment. Figure 9.35 shows the enhancement results, which showed a much higher enhancement than physical enhancement caused by a 10 ppm loading of gold in tissues. The calculated enhancement using Eq. 9.1 is 1.6 DEU, after taking both toxicity of the nanoclusters and X-ray damage into account.

Kunjachan and Berbeco et al. [196] reported tumor vascular damage to Panc-1 tumor xenografts using vessel-targeted gold nanoparticles. 2–3 nm gold

nanoparticles were coated with Arg-Gly-Asp ligands for targeting and imaging purposes. The overall hydrodynamic size was 8–10 nm. In vitro study results are given in Chap. 8. Animal model results are given here. The authors employed a Small Animal Radiation Research Platform to deliver localized dose at the small tumors with two orthogonal and collimated beams of X-rays. The dose was 10 Gy from 220 kVp X-rays. The local dose was about four times higher than the rest of the animal because of the irradiation configuration. 3.0 DEU enhancement in γ -H2AX assay results was observed when both gold nanomaterials and X-rays are applied. However, no quantitative biodistribution data was available, making it difficult to assess the origin of enhancement.

Xie et al. [199] studied a nanoscintillator for its X-ray-induced photodynamic therapy properties. The nanoscintillator was mechanically ground $\text{SrAl}_2\text{O}_4:\text{Eu}^{2+}$ bulk materials. The authors named the nanomaterials SAO and mesoporous SAO was called M-SAO. The luminescence was emitted from Eu^{2+} . The grinding produced approximately 80 nm nanoparticles. The nanoparticles were coated with a silica layer of different thicknesses because the nanoparticles were highly hydrolytic. The final size was near 400 nm. Photoluminescence was at 520 nm and its intensity decayed quickly to less than 10% after 3 days. Figure 9.36 shows the results. The left panel shows the results of singlet oxygen measurements, which suggested that only M-SAO produced significant amounts of singlet oxygen. The right panel shows the in vivo data. Again, only the M-SAO nanoscintillator under X-ray irradiation suppressed tumor growth. The enhancement value is significant if the volumes of tumors shown in Fig. 9.36 are used together with Eq. 7.1 or Eq. 9.1 because of the closeness of the effects of radiation or nanoparticles alone to the control.

Liu and Yang et al. [203] developed a new nanomaterial $\text{Au}@\text{MnS}@\text{ZnS}$ -PEG that was used for MRI imaging and X-ray sensitization. The nanomaterial consisted of a gold core of a few nm in diameter that was in a MnS shell followed by a coating of ZnS on the outside. The nanoparticles were then conjugated with PEG ligands.

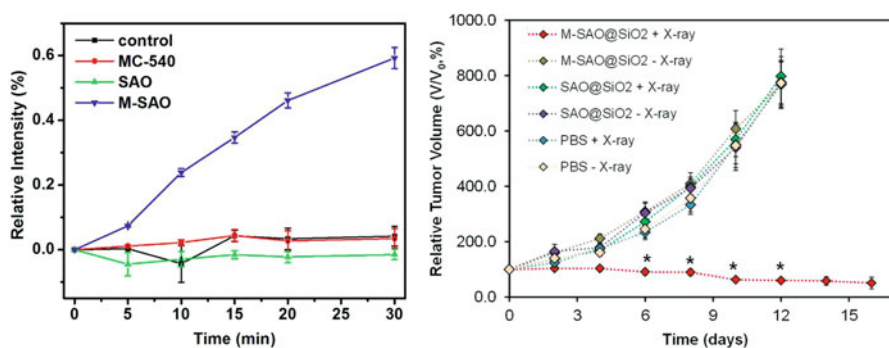


Fig. 9.36 Singlet oxygen production (left panel) and summary of in vivo radiation therapy (right panel) using M-SAO nanomaterials developed by Xie et al. An enhancement of close to 200 DEU is obtained using the data shown in right panel. (Adapted with permission from Xie et al. [199]. Copyright (2015) American Chemical Society.)

The overall size was on the order of 100 nm. Both *in vitro* and *in vivo* experiments were performed. 4T1 cells were used, and LD₅₀ was 3.5 Gy, which decreased to 2.5 Gy with the use of the nanomaterial, resulting in a 0.7 DEU enhancement. *In vivo* results showed a 1.3 DEU enhancement using a 4 Gy dose of X-ray irradiation. 6 Gy irradiation together with the nanomaterial nearly completely suppressed tumor growth. No toxicity was available for the nanomaterial.

Zhao and Yang et al. [202] synthesized silica-coated gold nanorods and employed the nanomaterial to treat tumor-bearing mice exposed to 6 MV X-ray radiation. The nanorods were 58 nm long and 14 nm in diameter and the coating thickness was 18 nm. Arginine-glycine-aspartic acid (RGD) peptides were then conjugated to the surface of the silica-coated nanorods for targeting. Both *in vitro* using MDA-MB-231 cells and *in vivo* studies were performed. Cellular survival fraction data showed improvement when RGD peptide-conjugated nanorods were used with X-rays, resulting in a moderate 0.4 DEU enhancement using X-ray doses to cause a 10% surviving fraction. *In vivo* data was more promising, reaching 2.5 DEU when RGD peptide-conjugated nanomaterials were used with X-rays compared with radiation alone.

Liu and Gu et al. [212] compared the radiosensitizing property of ca. 15 nm silver and gold nanoparticles using both *in vitro* and *in vivo* models, and the authors found that silver nanoparticles were more lethal in both models. This outcome should not be surprising as silver nanomaterials tend to disintegrate under redox and X-ray irradiation environment, as shown by Guo et al. [213].

Paquette et al. [34] investigated the effect of a tiopronin-coated gold nanoparticle on killing tumors in mice. The average X-ray energy was 26 keV. The nanoparticles were around 3 nm. Tumor volume was used to determine enhancement. Biodistribution measurements showed only 0.05 WP gold in tumor tissues, which was inadequate to cause any significant physical enhancement. Nearly 1.0 DEU was calculated using tumor volumes at the 10-day point after X-ray irradiation, which was similar to the *in vitro* enhancement in treating colorectal tumors.

Yu and Chen et al. [13] synthesized a gold nanorod core-selenium spherical shell nanomaterial covered with chitosan ligands as well as peptide targeting ligands. The authors conducted *in vitro* and *in vivo* work to determine the effect of these nanomaterials on X-ray radiotherapy. They used A375 cell line and A375-bearing mice to measure the enhancement. Based on their results, the calculated enhancement of using X-rays and the nanomaterials was approximately 0.3 DEU. The nanomaterials themselves were more than twice as toxic as 4 Gy X-rays. The cytotoxicity may be caused by dissolution of Se nanomaterials in cells.

Yang and Li et al. [71] studied the radiosensitizing properties of their 3.6 nm dia. Bismuth nanoparticles. The nanoparticles were conjugated with LyP-1 tumor targeting peptide ligands. The relative tumor volume was measured to determine the enhancement. No toxicity was found with the bismuth nanoparticles. The calculated enhancement based on the tumor size measurements was 0.8 DEU. Using contrast increase of 1193 HU and the calibrated unit mass contrast increase of 13.8 HU mM⁻¹, bismuth concentration was 86 mM, which correspond to 1.72 WP. If this amount of bismuth was accumulated in the tumor and only physical

enhancement was responsible for the increased damage observed by the authors, then up to 2.4 DEU enhancement would be seen for 33 keV X-rays.

Detappe and Berbeco et al. [165] synthesized a nanomaterial that had a Gd_2O_3 core and SiO_2 shell covered with DOTAGA ligands with Bi^{3+} ion trapping terminal groups. The final size was 4.5 nm, measured with DLS. The final nanomaterial product, called SiBiGdNP, was irradiated with 6 MV X-rays after intravenous injection into the animals infected with A549 lung tumor. Tumor growth or percentage survival data was used to estimate the enhancement. The control showed linear growth over 60 days. Radiation alone seemed to suppress tumor growth till 60 day, beyond which the volume grew exponentially. The biodistribution measurements showed small amounts of the nanomaterials in the tumor. The results again proved that biological experiments with small nanomaterials did not follow physical enhancement predictions.

As shown in Chap. 6, Liu et al. [204] developed a new nanomaterial called BM@NCP(DSP)-PEG with a bovine serum albumin protein-stabilized MnO_2 nanoparticles core that was wrapped by a polymer-linked cisplatin compound shell. This nanomaterial was then coated with dopamine and then PEG. The authors used this nanomaterial to treat 4T1 cells and measured cell damage using γ -H2AX assay for DNA damage and MTT for cell viability. 6 Gy of radiation was used. Enhanced DNA damage was observed with the nanomaterial under X-ray irradiation. However, since no data on radiation alone was available, it was impossible to calculate the enhancement. Based on the results presented by the authors, it seemed that the nanomaterial was toxic to cells. However, no such toxicity was shown in the animal model. If the result of cisplatin in combination with X-ray was used to calculate the enhancement with the nanomaterial plus X-rays, then the enhancement was approximately 1.0 DEU.

9.6.2 Preclinical and Clinical Trials

There have been only a few preclinical and clinical trials using nanomaterials to enhance the efficacy of radiotherapy. These studies are summarized here. Jain et al. [214] reviewed the preclinical trials of gold nanoparticles. The authors also discussed the gold nanoparticles as drug carriers, contrast agents, thermal drugs, and as radiosensitizers. The authors did not include certain nanoparticles such as those used by Nanobiotix in their clinical trials as discussed below.

Nanobiotix Inc. is a French company that has been developing radio-enhancers using nanomaterials. The company first reported its product NBTXR3 in 2009. NBTXR3 was claimed to contain crystalline nanomaterials that are inert and absorb X-rays and release electrons as the primary reason for its cancer treatment effectiveness. The company patented a drug platform called NanoXray Therapeutics, which includes the drug NBTXR3. The company tested the drug on several tumors including HCT116 colon cancer tumor and HT1080 fibrosarcoma tumor. Maggiorella et al. [10] investigated the radiotherapeutic effect of hafnium oxide

nanoparticles, which were NBTXR3. Negatively charged surface ligands were coated on the surface of the nanoparticles. DLS measurements suggested a 50 nm average diameter. Both in vitro measurements using HT1080 cells and clonogenic assay and in vivo studies were performed. TEM images showed aggregated nanoparticles in the cell, albeit not in the nuclei. Clonogenic assay results show higher enhancement at cobalt-60 energy than 6 MV γ -rays. The enhancement at cobalt-60 was less than 0.5 DEU. In vivo data were collected using HCT 116 tumor model. The authors claimed a ninefold or 9.0 DEU enhancement. Enhancement caused by direct X-ray absorption by nanomaterials should play a negligible role because high-energy X-rays were used. The company has been conducting a phase III clinical trial using its latest product NBTXR3. The latest news, which was shown online on July 6, 2016, indicated “promising signs of tumor volume response.” The trial used 70 Gy to treat neck cancers and the results showed shrinkage of tumor after treatment with NBTXR3 and X-ray radiation.

Sancey et al. [215] reported using gadolinium-based nanoparticles to treat brain melanoma metastases under X-ray irradiation. The authors called the study proof-of-concept before phase I trial. The idea was to use gadolinium compound surrounding nanoparticles to absorb X-rays and then release reactive oxygen species to kill tumor cells. The study included in vitro and in vivo component. Brain tumor-bearing mice were used as the animal model and skin melanoma cells were used as in the in vitro study. Radiation was 220 kVp X-rays with Al filters. The average size of the nanoparticles was 3 nm. The loading of gadolinium in the nanoparticles was 20%. The authors called the nanoparticles AGuIX. No quantitative uptake or biodistribution data was available. Dose enhancement factor using the in vitro data was 0.3 DEU with 0.6 mg/L incubation concentration of the AGuIX. In vivo data showed more than a 2.0 DEU enhancement using the survival fraction after 7 Gy and 10 mg treatment. Although this was labeled as preclinical, the scope of work was similar to many of those presented in Sect. 9.6. Long-term cytotoxicity data is not available.

Magné et al. [216] reviewed the status of field of using nanoparticles in radiation oncology. The review covered bench work as well as clinical work. The authors discussed the physical and biological aspects of nanoparticles when they interact with biological systems. Both aspects share similarities with the physical and biological enhancement discussed in this book. The review listed all the recent clinical trials in the world that employ technologies related to using nanomaterials to assist radiotherapy.

9.6.3 Summary

The in vivo enhancement results are summarized in Fig. 9.37. For the work showing uptake results, the corresponding enhancements are shown in solid symbol. The enhancement factors are clustered around 0.5 DEU, meaning that the effect is almost the same regardless of the amount of nanoparticles introduced into the animals. This

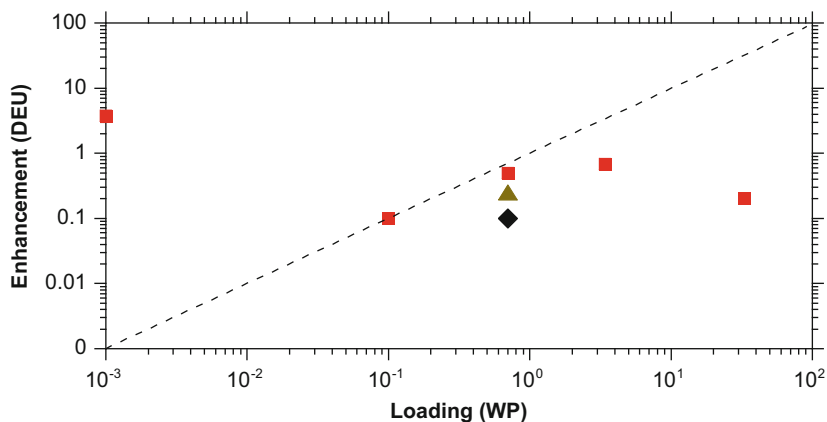


Fig. 9.37 Summary of the results of in vivo work of using nanomaterials to improve radiation therapy (red squares). The trend is similar to the in vitro results shown in Fig. 9.28, i.e., the measured enhancements are clustered around the value of 0.5–1.0 DEU regardless of the loading of the nanomaterials in the animals, which varied over five orders of magnitude. MV irradiation results are also shown here (brown triangles and black diamonds)

is similar to what is shown in Fig. 9.28 for the in vitro enhancement studies. Therefore, it is possible that the observed enhancements do not originate from physical enhancement as researchers have originally envisioned. Chemical enhancement may be more likely, and biological enhancement may be the most likely source for the observed enhancements. Although the impact of these experiments is too early to tell, it is prudent to state that animal models are a complex system, and many features such as pharmacokinetics still need to be carefully investigated. Knowing what is shown in Fig. 9.37, an immediate benefit may be that only small loadings are needed to achieve the average 0.5 DEU enhancement.

9.7 Other Methods to Improve X-Ray Treatment of Cancer with Nanomaterials

Several reports in the literature have described the results that are beyond the scope of the work discussed in the last three subsections. Here, these results are briefly discussed because they can be readily used in medical applications of X-ray nanochemistry. This part covers miscellaneous methods that can be used with nanomaterial-assisted X-ray treatment. For example, a new method is shown that can deliver hundreds and even thousands of times more dose to a target deep in the body than the surface dose using a continuous scanning focusing X-ray beam configuration.

One way to enhance the effectiveness of X-ray irradiation is to manipulate X-rays to increase the local dose at a target in the middle of an object. There were several methods reported in the literature to achieve this goal. For example, Norman et al. [220] invented a multiple beam scanner to improve X-ray therapy. These X-ray beams were on the same plane and each beam pointed at the same point on the plane. The configuration effectively focused these beams to the point, forming a focal spot a few millimeters in diameter. The dose was enhanced a few times at the focus. Uesaka et al. [218] discussed a concept using multiple 10 MeV X-ray stationary beams. The footprint of the device was relative large, around $5\text{ m} \times 5\text{ m}$. Gokeri et al. [144] used multiple parallel beams of X-rays, each with a 0.68 mm diameter and energies from 30 keV to 600 keV available at the ESRF synchrotron source. The beams delivered high dose deep in the head by pointing the beams at the same point from many directions. The authors also calculated enhancement by adding gold into the region of interest. For 7 mg/g or 0.7 WP gold loading, they observed an approximately 30% increase, which was lower than the 1.4 DEU WP^{-1} physical enhancement for 33 keV X-rays.

Jaboin et al. [190] reported a radiation-guided nanoparticle drug delivery system to treat pancreas cancer cells in mice. The authors coated the nanoparticles with HVGSSV peptides on the surface of nanoparticles, which also had several other ligands coated on the surface including an optical fluorescence label for near-infrared imaging. Upon irradiation with a 3 Gy dose of ionizing radiation, the peptide-conjugated nanoparticles were administered into mice, and it was found that these nanoparticles targeted tumors because of the selective binding between the peptide- and radiation-activated receptors. Without irradiation, there was no localization of nanoparticles at the tumors. This method may prove useful in delivering drugs only to tumor sites after being irradiated with X-rays.

Pradhan et al. [219] theoretically predicted effects of Auger processes in highly ionized gold atoms and their applications in nanotheranostics. Their work was based on resonant absorption of X-ray photons by highly ionized gold ions that allowed K to L transitions, meaning all the electrons above L shells were ionized prior to this simulated process. The authors predicted the energy deposition by electrons released from gold irradiated with 68 and 82 keV as well as 2 MeV X-rays and found a high enhancement from resonant absorption by these highly charged ions. However, in order for this to work, the gold species under investigation have to be nearly fully ionized, up to Au LXXVII or Au⁷⁷⁺. The lack of electrons for the subsequent Auger processes makes this ambitious design difficult to implement practically. An alternative may be using intense ultrafast X-ray pulses to resonantly remove just an L-shell electron, which would be similar to pulsed laser irradiation as suggested by the authors.

It is possible that other mechanisms of enhancement exist. For example, Nadeau et al. [220] demonstrated doxorubicin on small gold nanoparticles (<2.7 nm) could effectively kill even apoptosis-resistant cancer cells. The authors attributed the enhancement, which was 20 DEU, to the ability of these small nanoparticles being able to enter the nuclei. Such a process may prove to be useful in X-ray-induced enhancements.

Tu and Lo et al. [118] used gold nanoparticle contrast agents for radiotherapy planning. They compared the gold nanoparticles against a standard of Conray 60, an iodine-based contrast agent, and for the same concentration, gold nanoparticles were about 20% better. This work indirectly showed that gold nanoparticles were viable materials that could be imaged and then employed for treatment once the location is confirmed.

Welland et al. [59] used a new nanomaterial that had cisplatin conjugated to the surface of gold nanoparticles (AuNPs). They used S2 cells and three assays including the MTS cell viability assay, nuclear DNA damage γ H2AX and caspase-3 assay to determine the effectiveness of cell killing. Gold nanoparticles covered with human serum albumin (HAS) or polyethylenimine (PEI) were also used. PEI-AuNPs had much higher uptake and could cause more DNA damage than HAS-AuNPs. AuNPs with cisplatin conjugated to their surface were found to be much more effective in causing nuclear DNA damage ($>10\times$) and cell death ($\sim 3\times$) than AuNPs without cisplatin.

Guo et al. [221] showed the advantage of using a continuously rastering X-ray beam over even 65 stationary X-ray beams. The authors performed both theoretical simulations and experimental prototype work. Two possible experimental setups are shown in Fig. 9.38. The left panel shows a proposed design that employs two moving X-ray sources. The right panel shows a microfocus X-ray source mounted on the top of a lead chamber in which two rotary motors were mounted to manipulate a platform. A plastic phantom was mounted on the platform, which rotated in one direction and rocked in another, creating a truncated 3D spherical cap motion.

The simulated data of continuous scanning focusing is shown in Fig. 9.39, which displays delivered dose profiles in two directions, one along the central X-ray beam path or axial direction and another in the perpendicular direction. The left panel of Fig. 9.39 shows the dose profile in the axial direction. Three beam configurations were used: 9 beams, 65 beams, and continuous rastering beam. The results showed a clear advantage of using the continuous rastering beam, depositing most energy at the focal point deep in the tissue. The increase over the surface dose was nearly 200-fold for the X-ray spectrum shown in the inset in the top panel. Figure 9.39

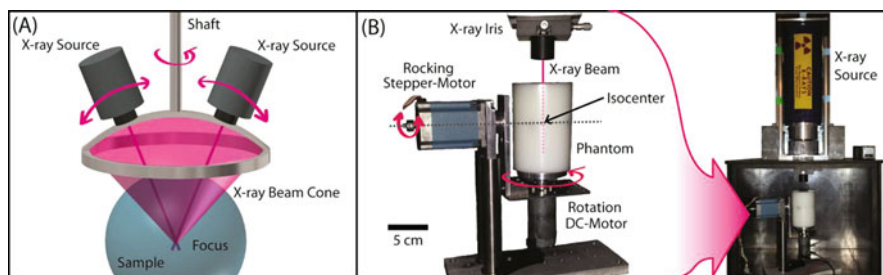
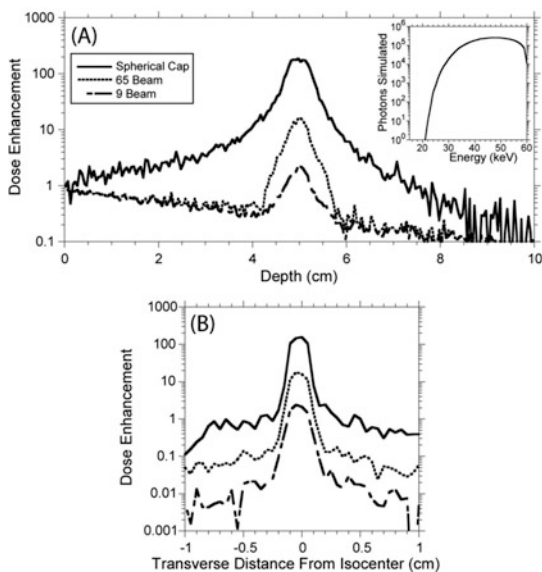


Fig. 9.38 Apparatuses of the continuous scanning focusing X-ray needle beam. The left panel shows a design using two microfocus X-ray sources and a stationary sample configuration. The right panel describes an experimental setup of a single X-ray source, a moving or rastering sample configuration using two motors. (Reprinted with permission from Guo and Davidson. [222]. Copyright (2016) by Radiation Research. All rights reserved.)

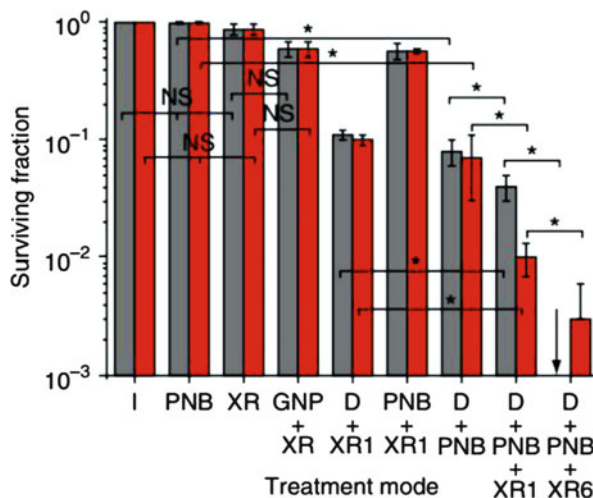
Fig. 9.39 Dose enhancement created by rastering focusing of a needle beam X-rays. Both axial (top panel) and radial (bottom panel) enhancement profiles are shown. For comparison purpose, 9 and 65 fixed X-ray beams are shown as well. Only the rastering beam produced results similar to high-energy X-rays or even protons, depositing more energy as the beam penetrates deeper till the focal point. (Reprinted with permission from Guo and Davidson. [221]. Copyright (2016) by Radiation Research. All rights reserved.)



(bottom panel) shows the dose enhancement in the radial direction. Again, the enhancement at the focus was 100-fold more than the peripheral. With the addition of gold nanoparticles, it was possible to further increase the dose deposited at the focus, and an enhancement of up to 3000 DEU was possible when scanning focusing technique was combined with multiplication of physical and chemical enhancement shown in Chap. 5. These results demonstrated the benefit of using the rastering focusing configuration to increase local dose without even using nanoparticles. For example, if only a 0.5 DEU or even 5 DEU enhancement is needed, then continuous rastering with a narrow beam of X-rays can deliver without using radiosensitizers. When higher enhancements such as 1000 DEU are needed, then nanomaterial-assisted methods may be employed in addition to the continuous rastering beam approach. If targets at shallower depths need to be treated, larger solid angle rastering focusing may be used to achieve the same effect of dose enhancement at the target.

Lapotko et al. [222] showed an interesting method which the authors claimed lowered the X-ray dose needed to treat cancer cells by 100-fold and tumors by 17-fold. Totally four modalities were used in their approach to treat cells or tumors. Gold nanoparticles were used as one of the four modalities, and the other three were X-rays, encapsulated drugs, and near-infrared laser pulses. Prior to X-ray irradiation, laser light was used to irradiate gold-loaded cells or tumors to create plasmonic nanobubbles, which can help rupture the encapsulation to release drugs. The authors then applied X-rays to work synergistically with the released drugs. The authors called the process amplification because the X-ray dose needed to kill the cells was reduced significantly, down to 2–4% of what was normally needed in X-ray radiotherapy. However, the dose employed by the authors was 4 Gy, similar to what was used to destruct cells with only X-rays, not 0.04 Gy. The amplification obtained at

Fig. 9.40 Results of combination of four methods, a drug, infrared laser light, X-rays, and gold nanoparticles, to kill tumor cells. The optimal results were obtained when all four modalities were used and X-ray irradiation occurred 6 h after laser treatment. (Reprinted by permission from Macmillan Publishers Ltd.: Nature Medicine Lapotko et al. [222], copyright (2014).)



this dose was visible in lowering the surviving fraction, which was much less than what was caused by 4 Gy of irradiation alone due to the actions of the drugs. Figure 9.40 shows their results. The authors used the term intracellular amplification, suggesting the amplification was at least partially achieved through cellular activities. As a result, the process may be understood as equivalent to biological enhancement. The authors did not explain the amplification. The loading of gold was nonuniform in the cell, and quantitative uptake data was not available. The gold nanoparticle and X-ray data suggested that the loading of gold nanoparticles was low because the enhancement from this combination (GNP+XR in Fig. 9.40) was low.

A similar method was developed by Wu and Chen et al. [42]. The nanomaterials were hollow gold nanoshells synthesized from silver seed nanoparticles. The outside diameter was ca. 60 nm. The nanoshells absorbed near-infrared (NIR) light. KB cells were used in in vitro work and mice with U14 xenograft tumors were used in in vivo work. Surviving fraction was used to determine the in vitro enhancement, and tumor size was used to determine the in vivo enhancement. No quantitative data was available for the uptake or biodistribution, so it was impossible to predict the magnitude of physical enhancement. 6 MV X-rays were used, so it was unlikely the enhancement was caused by physical enhancement. The results suggested a 0.2 DEU in vitro enhancement using the gold nanomaterials and 6 MV X-rays. Based on the tumor sizes, in vivo enhancement of 0.07 DEU was obtained. NIR together with MV X-rays produced better results, similar to what is shown in Fig. 9.40.

Shi et al. [223] studied the effect of adding nuclear targeting ligands to the surface of gold nanoparticles for enhanced X-ray irradiation damage to cells and tumors. The nanomaterials were silica-coated rare earth nanoparticles with nuclear targeting TAT ligands conjugated to the surface. The size of the nanomaterials was between 40 and 81 nm, measured with TEM and DLS, respectively. The authors claimed that these nanomaterials entered the nuclei with pores of 50–70 nm, which was different from statements in other publications. HT-1080 cells were used in in vitro work, which

showed a 0.77 DEU enhancement without TAT, and the enhancement increases to 1.2 DEU with TAT. NIR irradiation was used synergistically. Tumor volume measurements showed a 1.9 DEU enhancement. Again *in vivo* data suggested that NIR irradiation was more effective than X-rays.

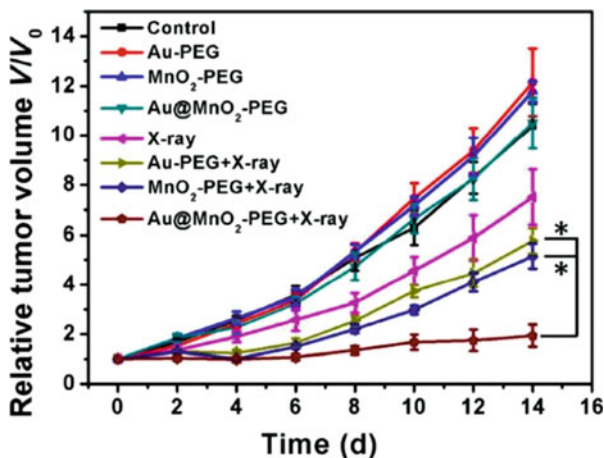
Bu and Shi et al. [197] investigated a method to release NO using X-rays, which was used to treat tumors under hypoxic conditions. The synthesis was conducted with the aid of nanochemistry because multiple step reactions were involved in constructing the nanomaterials. The authors called the rare earth nanoparticles upconversion nanoparticles (UCNPs) and mesoporous silica-covered UCNPs USMSs. When the nanoparticles contained S-nitrosothiol, an NO donor, the nanomaterial was called USMS-SNO. NO was released under X-ray irradiation. NO production was on the order of 8.5 μM over 23 h even without USMS-SNO. With irradiation of 5 Gy X-rays and in the presence of nanomaterials, the amount increased to 10 μM , representing a 30% increase. *In vivo* data was used to calculate the enhancement, and a 0.4 DEU enhancement was obtained using tumor volumes at 15-day point, which agreed well with the NO amount increase for 5 Gy irradiation. In another report, Shi et al. [224] described the results of synthesis and application of a rare earth nanoparticles core covered with porphyrin IX-embedded PEG and conjugated with TAT targeting ligands. TAT ligands significantly improved the performance of the nanomaterials in killing tumor cells and tumors.

Koger et al. [225] theoretically model the irradiation of gold nanoparticles embedded tissues similar to Guo et al. [221]. The authors called their method arc radiation therapy. PENELOPE (v 2011) was used to help predict the results, which showed a similar energy dependency as that predicted by the ratio of X-ray mass energy absorption coefficients of gold to water shown in Fig. 2.1 (right panel). With the gold nanoparticles embedded in the tissue, a much better defined spatial profile was obtained, similar to that shown in Fig. 9.39.

Yang et al. [201] found that coating a layer of MnO_2 on gold nanoparticles helped increase the amount of oxygen in hypoxic cells. MnO_2 reacted with endogenous H_2O_2 in the cell to generate oxygen, which was believed to be an important component for effective radiotherapy. The nanoparticles were then coated with PEG ligands to form $\text{Au@MnO}_2\text{-PEG}$. The gold core was 30 nm in dia., and the MnO_2 -coated gold nanoparticles had an average diameter of 50 nm. Dissolved oxygen amount increased when the nanomaterial was used with H_2O_2 . 4T1 cells were used and the best result of DNA damage using $\gamma\text{-H2AX}$ assay was achieved through using $\text{Au@MnO}_2\text{-PEG}$ and X-rays, which caused more than three times the amount of DNA damage by X-rays alone. *In vivo* results were equally encouraging. Figure 9.41 shows the results.

Ogino et al. [226] discovered a unique way to counter hypoxic conditions in tumor treatment. The idea was to treat titanium dioxide (TiO_2) nanoparticles with hydrogen peroxide (H_2O_2) so that the new nanomaterials slowly released H_2O_2 and therefore oxygen in the cells or tumors. The presence of oxygen hence sensitized the destruction of cancerous cells or tumors by X-ray irradiation. The titanium nanoparticles were first modified with polyacrylic acid and then hydrogen peroxide. The particle size characterized by DLS was on the order of 100 nm. Release of H_2O_2

Fig. 9.41 Combination of Au@MnO₂ and X-rays to kill tumor cells. The results were obtained by Yang et al. [201]. (Reprinted by permission from Macmillan Publishers.)



was measured both electrochemically and with enzyme-chemiluminescence detection. Although no direct *in vitro* or *in vivo* data was available, the method showed potential to sensitize radiotherapy under hypoxic conditions.

Wu, Hu, and Guo et al. [23] employed liposome encapsulated perfluorohexane under X-ray irradiation to treat tumors. Perfluorocarbons (PFCs) were known to supply oxygen to hypoxic locations such as tumors, and abundance of oxygen was beneficial to radiation damage of biological targets such as cells and tumors. The size of liposomes was ca. 100 nm. NIR imaging showed accumulation of approximately one-third of the liposomes in the tumor. Only a mild improvement was observed.

An interesting method was developed by Hao and Sun et al. [227] in which palladium-103 brachytherapy radioisotope was embedded in the coating of hollow gold nanoparticles. The authors called the new nanomaterial nanoseeds. The overall size of the nanoparticle was 120 nm. Both *in vitro* and *in vivo* studies were performed. Single-photon emission computed tomography (SPECT) was used to image the distribution of the nanomaterial in prostate cancer xenograft mice. Tumor suppression over 35 days was observed.

Li et al. [188] synthesized a complex nanoparticle nanomaterial that had a WS₂ nanodot core (6.1 nm dia.) and polyaniline shell covered with PDT agent chlorin e6 and hyaluronic acid targeting ligands. This nanomaterial (30 nm dia.) together with X-rays and NIR light was used to cause enhanced damage to 4T1 mouse breast tumor cells and tumors in animals. γ -H2AX assay and tumor size were used to determine the enhancement. A 0.2 DEU enhancement was observed with the nanomaterials and 6 Gy X-ray irradiation. *In vivo* results showed a similar enhancement with the use of the nanomaterials with X-rays and without NIR light. With NIR light and especially combination of 670 and 808 nm, the enhancement was much higher.

Liu et al. [228] synthesized a composite made of mesoporous tantalum oxide nanoparticles loaded with doxorubicin. The overall size was about 100 nm. The mass unit surface area was on the order of 90 m²/g, and the average pore size was

4 nm. The authors performed both *in vitro* and *in vivo* studies using 4T1 cells and tumor-bearing mice. Uptake data was not available, but biodistribution data was available. It was impossible to calculate LD₅₀ from the surviving fraction data shown in the publication, but DNA damage was minimal after 6 Gy of irradiation alone. The enhancement of using the nanomaterials and radiation was strong, which reached more than 10 DEU. *In vivo* data showed best result for doxorubicin-loaded nanomaterials under X-ray irradiation. However, enhancement was only about 2.0 DEU, much lower than the *in vitro* case.

9.8 X-Ray-Triggered Released Drugs and X-Ray Nano-Prodrugs

The biggest benefit of radiosensitizers is that they are readily used in conjunction with radiotherapy. The downside is that to date the magnitude of enhancement from using nanoparticle sensitizers is limited, and large amounts of nanomaterials are required—in many cases, these nanomaterials cause cytotoxicity. A completely different approach is to use X-rays and especially focused X-rays such as those described in the last section to trigger the release of drugs that are securely stored in delivery vehicles. Upon irradiation with the focused X-rays, the drugs are released. The biggest advantage of doing it this way is that the triggering mechanisms can be developed away from complex cellular chemistry, making it possible to use low doses of X-rays to trigger the release of a lethal dose of potent drugs. The biggest challenge is how to develop efficient triggering mechanisms to meet the low-dose requirement. Here, several publications are reviewed. It seems possible to develop efficient chemical and biological mechanisms to reach the goal of using low doses of radiation to trigger the release of large amounts of payload. The main difference between X-ray-triggered therapy and radiotherapy is that the former uses X-rays to trigger the release of drugs rather than to use X-rays to destruct cells.

X-rays have been used in conjunction with drugs to increase the efficacy of cancer treatment. Synergistic results are obtained through simultaneous or delayed X-ray irradiation with drug administration, as reported by Coppey et al. [229] who observed increased cytotoxicity from irradiation 24 h after drug administration. However, the enhancement achieved this way still depends on radiotherapy because destruction is still partially caused by radiation.

X-ray and other ionizing radiation triggered prodrugs were also studied in the past. For example, Nishimoto et al. [230] showed a fluorouracil-based prodrug activated with MeV radiation. The drug, a derivative from fluorouracil, reacted with solvated electrons produced in water by ionizing irradiation in absence of oxygen to form 5-fluorouracil, a compound of greater cytotoxicity. Less than 10 Gy was used for activation. Tumor growth delays were observed with the combination of radiation and prodrugs under hypoxic conditions, whereas cytotoxicity under aerobic conditions was much less.

When nanomaterials are used, the situation may be fundamentally changed and improved. What may prove to be revolutionary is the use of X-rays to trigger the release of an otherwise safely bound, lethal dose of chemicals in the body to annihilate tumors. Such release mechanisms using X-rays convert benign chemicals into prodrugs or on-call drugs, a process that largely eliminates radiotherapy. Using X-rays to trigger the release of drugs from nanoparticles was never attempted prior to Guo et al. [8].

The work of Guo et al. [8] was inspired by O'Brien et al. [231] and [232] in which liposome-enclosed doxorubicin (DOX) was released in water under X-ray irradiation. O'Brien's work was part of a larger body of research on photopolymerization of phospholipids, traced back to the early work in the 1980s by O'Brien et al. [233]. Two reviews on this field of research were published by Puri et al. [234] and Blumenthal et al. [235]. In some of these works, release was possible in pure water after exposure to 2 Gy of X-rays. However, the extreme scavenging environment in the cell would make this mechanism ineffective because the dose needed to create enough reactive oxygen species to break down the bilipid layer would be much higher, of the order of tens of Gy, therefore defeating the purpose of using this method to lower the side effect of radiotherapy.

Other groups have worked in this area as well. For example, Siepmann et al. [236] showed drug release from microparticles under γ -ray irradiation. However, the dose range was far above those used in radiotherapy. The authors employed between 4 and 33 kGy to release 5-fluorouracil from polylactide-glycolide microparticles. They found the initial release of drugs was accelerated by γ -ray irradiation. Benoit et al. [237] employed the triggered release system described above to treat tumor-bearing rats. Triggered release resulted in an almost 10 DEU enhancement over radiation alone. Although not exactly nanomaterials were used, this work demonstrated the potential and the results would be improved.

Xu and Zhang et al. [9] employed di-Se block copolymer constructed aggregates to trap chemo drugs and then used ionizing radiation to generate reactive oxygen species to cleave the Se-Se bond and cracked open the aggregates to release drugs. A schematic is shown in Fig. 9.42 (left panel). The authors used ^{60}Co radiation and up to 500 Gy of radiation. The authors found that nearly 70% of the drug doxorubicin trapped in the aggregates was released after a 50 Gy irradiation, beyond which the release percentage saturated. They also found that release continued after irradiation. For 50 Gy dose, release continued for nearly 5 h after irradiation. At 5 Gy, approximately 40% of the drug was released within 3 h after irradiation. HepG2 cells were used for in vitro work, and the results are shown in Fig. 9.42 (right panel). The reduction in viability was 20%, which was less than many nanoparticle-assisted radiation damage of cancer cells shown in Sect. 9.5. It is unclear whether Se-Se bond cleavage was caused by radicals generated from X-rays interacting with water around the selenide nanoparticles or produced locally through interactions between X-rays and the nanoparticles.

If reactive oxygen species such as singlet oxygen or hydroxyl radicals are considered as drugs, then nanomaterial-enhanced radiotherapy may be considered for X-ray trigger release of drugs. However, in reality these species are not treated as

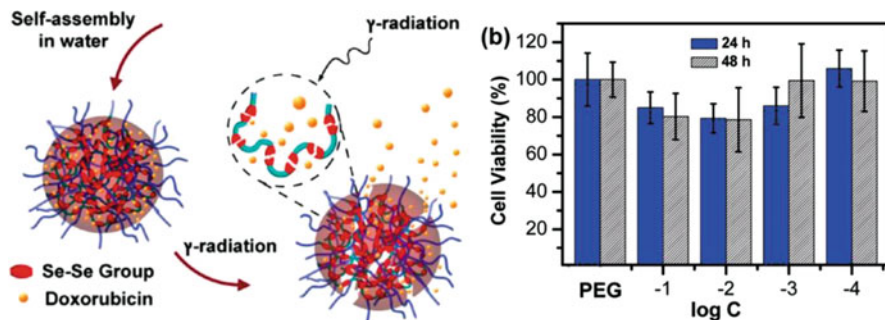


Fig. 9.42 Release of doxorubicin from diselenide block copolymer nanoparticles under ionizing irradiation for cell destruction. The left panel shows the proposed mechanism, and the right panel shows the results. (Reprinted with permission from Xu and Zhang et al. [9]. Copyright (2011) American Chemical Society.)

drugs. So here only the methods of releasing traditional forms of drugs are discussed. Photodynamic therapy does not belong to this part of discussion for the same reason.

In two patent disclosures, Fologea et al. [238] reported a method of using 6 MV X-rays to trigger the release of drugs stored in liposomes. The priority date of the issued patent was Mar 31, 2009, although no formal publication in the literature was available. The inventors used a dose of 4 Gy radiation at a 2 Gy/min dose rate. Dye molecules were trapped in liposomes to simulate drug release upon X-ray irradiation. Their work was similar to those described by O'Brien et al., which is mentioned above. The result in cells would be different because of the high scavenging nature of the cellular environment as in the case of O'Brien et al. On the other hand, this problem could be solved using the internally activatable release mechanism proposed by the inventors, although that part was not experimentally tested. The major difference, also a major advantage, was that reagents used to induce opening of liposomes were unlocked from within the liposomes. Figure 9.43 shows the proposed mechanism, which would avoid the dependency on the radicals generated by X-rays outside the liposomes. However, the experimental results cited in the patent did not fully support the proposed elegant but complex mechanism.

Yan et al. [74] developed a drug with DOX encapsulated in gold nanoparticles which also contained cancer cell targeting ligands. The average size of gold nanoparticles was 17 nm. The authors examined DNA DSBs using γ -H2AX assay in HeLa cells. DOX release was triggered by being in solution for ~ 10 h. A 1.7 DEU total enhancement was achieved with 3 Gy of 160 kVp X-ray irradiation of HeLa cells incubated with DOX-loaded gold nanoparticles. No data was available on X-ray alone.

Guo et al. [8] reported an X-ray-triggered release nanosystem in which they conjugated DOX-bound DNA strands to the surface of 15 nm diameter gold nanoparticles. The left panel of Fig. 9.44 illustrates the structure of the nanosystem and a schematic of the working mechanism. Upon X-ray irradiation of 100 kVp from a microfocus X-ray source, the results of clonogenic assay of MCF-7 breast cancer tumor cells showed a 40% reduction in cell viability after a 10 Gy dose of radiation.

Fig. 9.43 A hypothetical drug release system that could be triggered with X-rays and would not rely on species from outside. Whether this can be realized is still need to be tested experimentally [239]

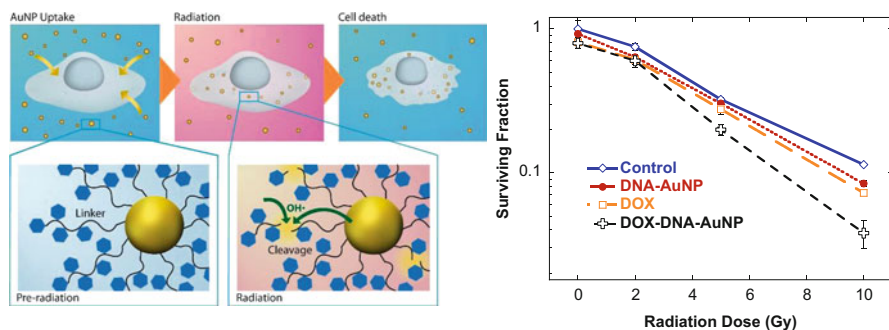
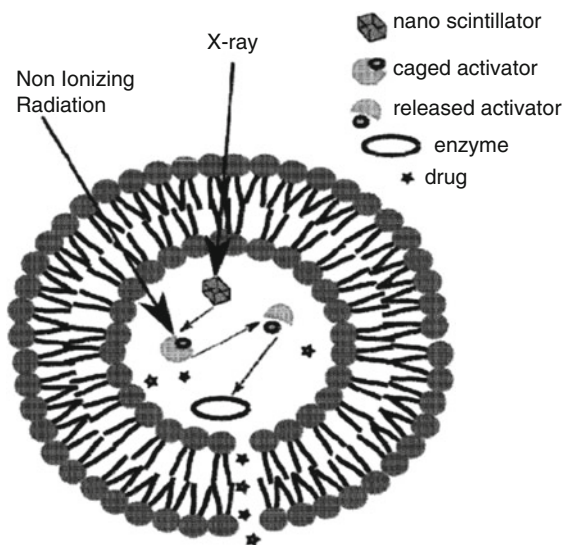


Fig. 9.44 Release of doxorubicin from gold nanoparticles under X-ray irradiation. The left panel illustrates how DOX destructs cells when the molecules are released from the gold nanoparticles. The right panel shows the surviving fraction curve as a function of X-ray dose. (Adapted with permission from Guo et al. [8]. Copyright (2013) of the Royal Society of Chemistry.)

The addition of large amounts of DNA-covered gold nanoparticles did not seem to create any enhancement, which was intriguing and might be caused by scavenging of these nanoparticles similar to that found in the gold nanotube case described in Chaps. 2 and 5. If indeed these gold nanoparticles scavenged hydroxyl radicals, then the amount of enhancement would be significantly higher when scavenging was contained or eliminated.

The triggered release can be combined with the continuous scanning focusing technique described in Sect. 9.7. Triggered release would occur at the focus when triggered release is combined scanning focusing of X-rays.

9.9 Other Reviews

Medical applications are one of the most popular topics within the discipline of X-ray nanochemistry. It is fair to state that currently medical applications of X-ray nanochemistry are a more popular topic than X-ray nanochemistry itself, which is still an obscure topic until this book is written or even after this book is published. Nonetheless, many breakthroughs in X-ray nanochemistry in the near future may change this situation, and we expect X-ray nanochemistry to become a better known topic in the near future. There are many reviews on medical applications of X-ray nanochemistry. In the following, several reviews are discussed. Readers can also refer to these reviews for special discussions that are not covered in this book.

Hainfeld et al. [189] reviewed the works of using gold nanoparticles for radiotherapy. The authors discussed many aspects related to gold nanoparticles for X-ray radiotherapy, including the choice of elements, X-ray energy, theoretically predicted dose enhancement, and requirements for nanoparticles. The authors compared enhancement by gold with iodine, a practical standard for enhancement and contrast, and found an approximately 3 DEU improvement in several energy ranges. However, the authors also noted drastic differences between mice models and human pathology. Many improvements are needed if gold nanoparticles are to be used to clinically treat cancer patients in the framework of using gold nanoparticles as radiosensitizers. For example, LD₅₀ of 1.9 nm gold nanoparticles needed for adequate dose enhancement factors is too high, near the toxic level. Many other factors such as targeting that can significantly influence the effectiveness of treatment are still under development.

Juzenas et al. [240] reviewed the field of using quantum dots and nanoparticles for radiation therapy of cancer. The review pointed out that quantum dots generally interacted with UV-Vis light to produce electron-hole pairs, which produced more singlet oxygen. X-rays also interacted with quantum dots to produce singlet oxygen, so the quantum dots functioned as a photodynamic reagent. The review summarized many of the works published in the field of X-ray nanochemistry before 2008. The article also mentioned many materials that could potentially be used for X-ray enabled photodynamic therapy as well as radiosensitizing nanomaterials. The authors mentioned the work performed on polyphenol extract as an antioxidant and radiosensitizing agent. They also showed the structure of nanoparticle scintillators covered with porphyrins. The latter produced singlet oxygen to destruct cells when the nanomaterial-porphyrin composite was irradiated with X-rays.

Kobayashi et al. [241] reviewed radiotherapy of using heavy elements for enhancement of radiation effects. The authors focused on compounds that contain high-Z elements and discussed limitations of delivering molecular chemo drugs into tumors. They noted the non-selectiveness nature of these drugs. Nanoparticles as the source of dose enhancement were discussed, but no specific limitations were mentioned by the authors. The focus was to use nanoparticles to directly sensitize radiotherapy.

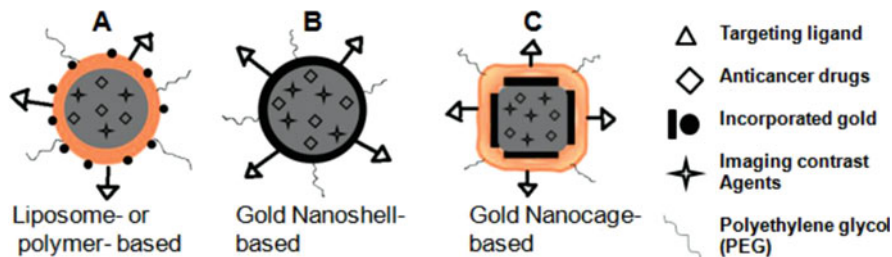


Fig. 9.45 Multiple component nanomaterials that can be used to treat tumor under X-ray irradiation. (Adapted with permission from Chithrani and Jelveh [245] under CC BY 3.0 license.)

Shortly after Chithrani et al. [35] published the results of testing gold nanoparticles as radiation sensitizers, the authors [242] reviewed the use of gold nanoparticles for combinational therapy, which included enhancement by gold nanoparticles for radiotherapy. In addition to nanomaterials for radiotherapy, the authors also reviewed the work in the areas of photodynamic therapy and photothermal therapy. The authors suggested a multifunctional nanoparticle platform for future therapeutics and imaging. Figure 9.45 shows their proposed nanostructures for therapy. The nanostructures included several components such as targeting, anticancer drugs, imaging agents, and gold nanoparticles, which were relatively small compared with the whole assembly.

Murphy and El-Sayed et al. [243] provided an extensive review on the use of gold nanoparticles in biomedicine, but did not mention applications of gold nanoparticles as radiosensitizers, suggesting that gold nanoparticle-assisted radiotherapy was not well recognized yet in 2011. Kuncic et al. [116] reviewed imaging and therapy works using nanoparticles under irradiation of light and ionizing radiation. The authors pointed out that titanium oxide nanoparticles could be a suitable image contrast agent. The unit WP contrast increase by the material is approximately 125 HU per 0.1 g/mL or 1250 HU WP^{-1} , which was higher than almost all the contrast agents shown in Fig. 9.15.

Jain et al. [214] reviewed the work of using gold nanoparticles to treat cancer. They discussed gold nanoparticles as drug carriers, contrast agents, thermal drugs, and radiosensitizers. The authors cited many papers published in the area of gold nanoparticles from 1992 to 2009 and showed an exponential growth of publications as a function of time. The review covered theory, in vitro and in vivo work. The authors also discussed clinical trials using gold nanoparticles, but did not discuss the project being conducted by Nanobiotix Inc. Jain et al. [244] published another review on prostate cancer diagnostics and treatment using metal nanoparticles and ionizing radiation. Two nanoparticles were discussed in detail: one was 15 nm gold nanoparticles and the other was sub-5 nm AGuIX@ nanoparticles that had a high loading of Gd.

Dorsey and Sun et al. [245] summarized results of using high-Z elements in the form of nanoparticles to image and treat cancer or tumor in animals. The authors discussed properties of gold nanoparticles for imaging and therapy. Both in vitro and

in vivo works were reviewed. The authors also included some of their own results in the article. They demonstrated enhancement of approximately 1.0 DEU using gold nanoparticles under 6 MV X-rays, which were much higher than the values obtained by others as shown here. The results suggested possible chemical or biological enhancement discussed in Chaps. 3 and 4. The incubation concentrations were 1 and 10 mg/mL of PEGylated gold nanoparticles.

Anant et al. [246] reviewed the work in the area of using nanoparticles to radiosensitize therapy. The authors identified three areas of (1) sensitizing, (2) reversing radiation resistance, and (3) radioprotection. Several nanomaterials, including gold nanoparticles, quantum dots, and iron oxide nanoparticles, were discussed. The focus was sensitizing while the other two factors were cursorily mentioned. Gu et al. [247] reviewed the literature of using metal nanoparticles as radiosensitizers. The review included publications in theoretical modeling of physical enhancement as well as in vitro and in vivo studies. Attention was given to silver nanoparticles.

Barberi-Heyob et al. [248] reviewed the parameters the authors considered important to radiotherapy enhanced by nanoparticles. Their intention was to critically analyze the factors that affect the transformation from preclinical to clinical applications for the nanomaterial-assisted radiation therapy. The focus was still on radiosensitization, meaning the main modality to be employed was still radiation itself. The use of nanomaterials was primarily to increase the effectiveness of damaging targets with radiation. The authors identified the main problems facing radiosensitization technology and attributed the lack of translational work to a lack of standardization. The authors provided a detailed analysis of the dose enhancement factor obtained by 64 groups using different ionizing radiation of different energies. A similar graph to what are shown in Fig. 9.28 and Fig. 9.37 is presented. Although the data showed large standard deviations, the spread of dose enhancement factors was relatively narrow, ranging from 0.1 to 1.3 for different X-ray energies and not as a function of weight percentage of gold in water. The authors indicated the desire to standardize the protocols for performing in vitro and in vivo work.

Sicard-Roselli et al. [249] reviewed the literature on studying radiosensitization by nanoparticles and discussed a few parameters such as energy dependency and biological effect that was close to what is referred to as biological enhancement in Chap. 4 of this book. The review also discussed the current deficiencies in the research area of radiosensitization using nanoparticles. A number of questions were raised in the review. The review also grouped the effects into physical, chemical, and biological, similar to the arrangement of this book in Chaps. 2, 3, and 4.

Magné et al. [216] reviewed the publications in radiotherapy with the emphasis of their impact on future clinical practice. Haume et al. [250] reviewed the literature on using gold nanoparticles for cancer treatment. The authors discussed a number of issues and parameters of gold nanoparticles that may affect the outcome of using gold nanoparticles for radiosensitization.

Rosa et al. [251] summarized the results on the literature dealing with radiosensitizing of cell damage using gold nanoparticles. The results presented by the authors pointed to a similar conclusion as shown in Chap. 4 and a few other reviews. The main point was that many publications measured similar enhancement values even though the experimental conditions were quite different. The authors

discussed several cellular activities such as cell cycles, DNA damage and repair, and the bystander effect, and discussed how these processes could be connected to enhanced damage to cells by gold nanoparticles under X-ray irradiation.

Allen et al. [252] reviewed the literature of using gold nanoparticles for cancer radiotherapy. The authors selected at least four application areas of gold nanoparticles, including imaging, diagnostics, delivery, and therapy. The authors also chose three mechanisms of radiosensitization, which were physical, chemical, and biological. Instead of sensitization, the authors called the processes effect enhancement, similar to what is given in this book. Specifically, the authors pointed to three cases of biological enhancement, which were reactive oxygen species production and oxidative stress, cell cycle effects, and inhibition of DNA repair. The authors also discussed the ideal gold nanoparticles for radiosensitization in the future, which were still largely based on using the radiotherapeutic properties of gold nanoparticles to directly damage cellular components.

Another document that is closely related to this chapter was a book published recently by Cho et al. [253]. The focus of the book was to evaluate the current status of research in several fields, including clinical radiation oncology, nanotechnology, and biomedical engineering, with the goal of providing a comprehensive survey of the current literature that facilitates clinical translation. As a result, more clinical related topics such as targeting and imaging were discussed. Also discussed in the book were regulatory issues.

9.10 Conclusions and Future Work

Medical applications of X-ray nanochemistry, including imaging, in vitro and in vivo work, have been the center of attention of X-ray nanochemistry research from the beginning. It is probably more appropriate to call this chapter X-ray nanotechnology or even X-ray nanomedicine. As this chapter has shown, the magnitude of enhancement using nanoparticles to enhance the effect of ionizing radiation to destruct cells is on the order of 1.0 DEU, regardless of the amount of nanoparticles used, and the benefits and limitations of using this concept are clear.

The main benefit of using nanoparticles is that if nanomaterials can be safely delivered to tumor sites in large enough quantities and at a reasonably low cost, then they can help increase the effectiveness of radiotherapy by nearly one DEU. This may be enough for physicians to convince patients or FDA to approve this treatment method. The use of nanomaterials, together with various X-ray focusing methods such as continuous scanning focusing method, may provide the needed modality to destruct tumors or at least temporarily stop their growth. The scanning focusing itself is worth trying, although the delivery of the focused dose needs to be guided prior to irradiation.

The most obvious limitation, however, also derives from the one DEU enhancement per one WP of gold in tissue. This means a significant enhancement can only be achieved with a large amount of gold in the targeted volume of tissue, if there is no

anti-enhancement. If approximately one DEU enhancement is acceptable, then smaller than one WP gold nanoparticles may be used.

Recognizing these benefits and limitations, the next logical step is to figure out the mechanisms of the observed enhancement so that it is possible to further improve enhancement or create new knowledge bases for various applications in the medical field. This requires a quantum leap or revolutionary paradigm shift. For example, the size of nanomaterials including nanomachines needs to be optimized for maximum uptake by tumors. If biological enhancement favors sub-10 nm diameter nanoparticles and if uptake favors 50 nm nanoparticles, then a compromise must be made. On the other hand, if triggered release can be made, then one can use 50 nm or even 500 nm diameter nanomachines to release nuclear DNA targeting drugs within or even outside the cell, therefore winning both uptake and entering the nuclei battles. These will happen only after a thorough understanding of X-ray nanochemistry.

These potentially new powerful methods of treating cancers may inspire researchers to conduct fundamental research in the discipline of X-ray nanochemistry so that one can continuously improve the sensitivity by creating newer triggering mechanisms. There are at least 10,000 organic chemical reactions and with the inclusion of transition metal complexes and catalysis, as discussed in Chap. 10, it seems extremely possible that one can discover many sensitive and efficient reactions that can help develop effective chemical systems to respond to X-ray irradiation and release drugs in cells to treat cancer anywhere in the body.

X-ray nanochemistry will advance in all fronts. The most important discoveries will happen at the fundamental chemical and nanochemical levels. Many clinical works may happen with fruitful collaborations between chemists and doctors. This iteration between advancing basic and applied sciences is like developing semiconductor materials and modern electronics. One needs to improve the materials and the devices in a concerted effort to make breakthroughs. Therefore, it is critical to have close collaborations between medical doctors and physical scientists. Such collaborations will help accelerate the advancement of the field and improve the overall productivity so that patients can enjoy the best care at the earliest times.

References

1. Kassis, A. I. (2003). Cancer therapy with Auger electrons: Are we almost there? *Journal of Nuclear Medicine*, 44, 1479–1481.
2. Sung, W., Jung, S., & Ye, S. J. (2016). Evaluation of the microscopic dose enhancement for nanoparticle-enhanced Auger therapy. *Physics in Medicine and Biology*, 61, 7522–7535.
3. Guo, T. (2004, August). Nanoparticle enhanced X-ray therapy. ACS Annual Meeting, Philadelphia.
4. Guo, T. (2006). Nanoparticle radiosensitizers. US patent application number: US 11/728,943; publication number: US20080003183 A1 and WO2006037081A2.
5. Hainfeld, J. F., Slatkin, D. N., & Smilowitz, H. M. (2004). The use of gold nanoparticles to enhance radiotherapy in mice. *Physics in Medicine and Biology*, 49, N309–N315.
6. Foley, E., Carter, J., Shan, F., & Guo, T. (2005). Enhanced relaxation of nanoparticle-bound supercoiled DNA in X-ray radiation. *Chemical Communications*, 3192–3194.

7. Roco, M. C., & Tech, N. S. E. (2004). Nanoscale science and engineering: Unifying and transforming tools. *AIChE Journal*, *50*, 890–897.
8. Starkewolf, Z. B., Miyachi, L., Wong, J., & Guo, T. (2013). X-ray triggered release of doxorubicin from nanoparticle drug carriers for cancer therapy. *Chemical Communications*, *49*, 2545–2547.
9. Ma, N., Xu, H. P., An, L. P., Li, J., Sun, Z. W., & Zhang, X. (2011). Radiation-sensitive diselenide block co-polymer micellar aggregates: Toward the combination of radiotherapy and chemotherapy. *Langmuir*, *27*, 5874–5878.
10. Maggiorella, L., Barouch, G., Devaux, C., Pottier, A., Deutsch, E., Bourhis, J., Borghi, E., & Levy, L. (2012). Nanoscale radiotherapy with hafnium oxide nanoparticles. *Future Oncology*, *8*, 1167–1181.
11. Chen, J., Li, M. F., Yi, X., Zhao, Q., Chen, L., Yang, C., Wu, J. C., & Yang, K. (2017). Synergistic effect of thermo-radiotherapy using au@FeS Core-Shell nanoparticles as multifunctional therapeutic nanoagents. *Particle and Particle Systems Characterization*, *34*.
12. Stewart, C., Konstantinov, K., McKinnon, S., Guatelli, S., Lerch, M., Rosenfeld, A., Tehei, M., & Corde, S. (2016). First proof of bismuth oxide nanoparticles as efficient radiosensitizers on highly radioresistant cancer cells. *Physica Medica*, *32*, 1444–1452.
13. Chang, Y. Z., He, L. Z., Li, Z. B., Zeng, L. L., Song, Z. H., Li, P. H., Chan, L., You, Y. Y., Yu, X. F., Chu, P. K., et al. (2017). Designing core-shell gold and selenium nanocomposites for cancer radiochemotherapy. *ACS Nano*, *11*, 4848–4858.
14. Leach, J. K., Van Tuyle, G., Lin, P. S., Schmidt-Ullrich, R., & Mikkelsen, R. B. (2001). Ionizing radiation-induced, mitochondria-dependent generation of reactive oxygen/nitrogen. *Cancer Research*, *61*, 3894–3901.
15. Zhang, X. M., Yang, H. J., Gu, K., Chen, J. A., Rui, M. J., & Jiang, G. L. (2011). In vitro and in vivo study of a nanoliposomal cisplatin as a radiosensitizer. *International Journal of Nanomedicine*, *6*, 437–444.
16. Li, X., Zhou, H. Y., Yang, L., Du, G. Q., Pai-Panandiker, A. S., Huang, X. F., & Yan, B. (2011). Enhancement of cell recognition in vitro by dual-ligand cancer targeting gold nanoparticles. *Biomaterials*, *32*, 2540–2545.
17. Rahman, W. N., Corde, S., Yagi, N., Aziz, S. A. A., Annabell, N., & Geso, M. (2014). Optimal energy for cell radiosensitivity enhancement by gold nanoparticles using synchrotron-based monoenergetic photon beams. *International Journal of Nanomedicine*, *9*, 2459–2467.
18. Regulla, D. F., Hieber, L. B., & Seidenbusch, M. (1998). Physical and biological interface dose effects in tissue due to X-ray-induced release of secondary radiation from metallic gold surfaces. *Radiation Research*, *150*, 92–100.
19. Gara, P. M. D., Garabano, N. I., Portoles, M. J. L., Moreno, M. S., Dodat, D., Casas, O. R., Gonzalez, M. C., & Kotler, M. L. (2012). ROS enhancement by silicon nanoparticles in X-ray irradiated aqueous suspensions and in glioma C6 cells. *Journal of Nanoparticle Research*, *14*, 741.
20. Herold, D. M., Das, I. J., Stobbe, C. C., Iyer, R. V., & Chapman, J. D. (2000). Gold microspheres: A selective technique for producing biologically effective dose enhancement. *International Journal of Radiation Biology*, *76*, 1357–1364.
21. Choi, G. H., Seo, S. J., Kim, K. H., Kim, H. T., Park, S. H., Lim, J. H., & Kim, J. K. (2012). Photon activated therapy (PAT) using monochromatic synchrotron x-rays and iron oxide nanoparticles in a mouse tumor model: Feasibility study of PAT for the treatment of superficial malignancy. *Radiation Oncology*, *7*, 184.
22. Liu, C. J., Wang, C. H., Chien, C. C., Yang, T. Y., Chen, S. T., Leng, W. H., Lee, C. F., Lee, K. H., Hwu, Y., Lee, Y. C., et al. (2008). Enhanced x-ray irradiation-induced cancer cell damage by gold nanoparticles treated by a new synthesis method of polyethylene glycol modification. *Nanotechnology*, *19*(295104), 1–5.
23. Xu, L. F., Qiu, X. F., Zhang, Y. T., Cao, K., Zhao, X. Z., Wu, J. H., Hu, Y. Q., & Guo, H. Q. (2016). Liposome encapsulated perfluorohexane enhances radiotherapy in mice without additional oxygen supply. *Journal of Translational Medicine*, *14*, 268.

24. Kleinauskas, A., Rocha, S., Sahu, S., Sun, Y. P., & Juzenas, P. (2013). Carbon-core silver-shell nanodots as sensitizers for phototherapy and radiotherapy. *Nanotechnology*, *24*, 325103.
25. Youkhana, E., Feltis, B., Blencowe, A., & Geso, M. (2017). Titanium dioxide nanoparticles as radiosensitizers: An in vitro and phantom-based study. *International Journal of Medical Sciences*, *14*, 602–614.
26. Taggart, L. E., McMahon, S. J., Butterworth, K. T., Currell, F. J., Schettino, G., & Prise, K. M. (2016). Protein disulphide isomerase as a target for nanoparticle-mediated sensitisation of cancer cells to radiation. *Nanotechnology*, *27*, 215101.
27. Pan, C. L., Chen, M. H., Tung, F. I., & Liu, T. Y. (2017). A nanovehicle developed for treating deep-seated bacteria using low-dose X-ray. *Acta Biomaterialia*, *47*, 159–169.
28. Liu, C. J., Wang, C. H., Chen, S. T., Chen, H. H., Leng, W. H., Chien, C. C., Wang, C. L., Kempson, I. M., Hwu, Y., Lai, T. C., et al. (2010). Enhancement of cell radiation sensitivity by pegylated gold nanoparticles. *Physics in Medicine and Biology*, *55*, 931–945.
29. Lim, S. N., Pradhan, A. K., Barth, R. F., Nahar, S. N., Nakkula, R. J., Yang, W. L., Palmer, A. M., Turro, C., Weldon, M., Bell, E. H., et al. (2015). Tumoricidal activity of low-energy 160-KV versus 6-MV X-rays against platinum-sensitized F98 glioma cells. *Journal of Radiation Research*, *56*, 77–89.
30. Bhattacharai, S. R., Derry, P. J., Aziz, K., Singh, P. K., Khoo, A. M., Chadha, A. S., Liopo, A., Zubarev, E. R., & Krishnan, S. (2017). Gold nanotriangles: Scale up and X-ray radiosensitization effects in mice. *Nanoscale*, *9*, 5085–5093.
31. Diaz, R., Hariri, G., Passarella, R. J., Wu, H., Fu, A., & Hallahan, D. E. (2008). Radiation-guided platinum drug delivery using recombinant peptides. *International Journal of Radiation Oncology, Biology, Physics*, *72*, S1–S1.
32. Wang, G. D., Nguyen, H. T., Chen, H. M., Cox, P. B., Wang, L. C., Nagata, K., Hao, Z. L., Wang, A., Li, Z. B., & Xie, J. (2016). X-ray induced photodynamic therapy: A combination of radiotherapy and photodynamic therapy. *Theranostics*, *6*, 2295–2305.
33. Yang, W. S., Read, P. W., Mi, J., Baisden, J. M., Reardon, K. A., Larner, J. M., Helmke, B. P., & Sheng, K. (2008). Semiconductor nanoparticles as energy mediators for photosensitizer-enhanced radiotherapy. *International Journal of Radiation Oncology, Biology, Physics*, *72*, 633–635.
34. Shi, M. H., Paquette, B., Thippayamontri, T., Gendron, L., Guerin, B., & Sanche, L. (2016). Increased radiosensitivity of colorectal tumors with intra-tumoral injection of low dose of gold nanoparticles. *International Journal of Nanomedicine*, *11*, 5323–5333.
35. Chithrani, D. B., Jelveh, S., Jalali, F., van Prooijen, M., Allen, C., Bristow, R. G., Hill, R. P., & Jaffray, D. A. (2010). Gold nanoparticles as radiation sensitizers in cancer therapy. *Radiation Research*, *173*, 719–728.
36. Yong, Y., Zhang, C. F., Gu, Z. J., Du, J. F., Guo, Z., Dong, X. H., Xie, J. N., Zhang, G. J., Liu, X. F., & Zhao, Y. L. (2017). Polyoxometalate-based radiosensitization platform for treating hypoxic tumors by attenuating radioresistance and enhancing radiation response. *ACS Nano*, *11*, 7164–7176.
37. Liu, X., Liu, Y., Zhang, P. C., Jin, X. D., Zheng, X. G., Ye, F., Chen, W. Q., & Li, Q. (2016). The synergistic radiosensitizing effect of tirapazamine-conjugated gold nanoparticles on human hepatoma HepG2 cells under X-ray irradiation. *International Journal of Nanomedicine*, *11*, 3517–3530.
38. Al Zaki, A., Joh, D., Cheng, Z. L., De Barros, A. L. B., Kao, G., Dorsey, J., & Tsourkas, A. (2014). Gold-loaded polymeric micelles for computed tomography-guided radiation therapy treatment and radiosensitization. *ACS Nano*, *8*, 104–112.
39. Saberi, A., Shahbazi-Gahrouei, D., Abbasian, M., Fesharaki, M., Baharlouei, A., & Arab-Bafarani, Z. (2017). Gold nanoparticles in combination with megavoltage radiation energy increased radiosensitization and apoptosis in colon cancer HT-29 cells. *International Journal of Radiation Biology*, *93*, 315–323.

40. Kim, S. R., & Kim, E. H. (2017). Gold nanoparticles as dose-enhancement agent for kilovoltage X-ray therapy of melanoma. *International Journal of Radiation Biology*, *93*, 517–526.
41. Zhang, P. P., Qiao, Y., Xia, J. F., Guan, J. J., Ma, L. Y., & Su, M. (2015). Enhanced radiation therapy with multilayer microdisks containing radiosensitizing gold nanoparticles. *ACS Applied Materials & Interfaces*, *7*, 4518–4524.
42. Ma, N. N., Jiang, Y. W., Zhang, X. D., Wu, H., Myers, J. N., Liu, P. D., Jin, H. Z., Gu, N., He, N. Y., Wu, F. G., et al. (2016). Enhanced radiosensitization of gold Nanospikes via hyperthermia in combined cancer radiation and photothermal therapy. *ACS Applied Materials & Interfaces*, *8*, 28480–28494.
43. Fang, X., Wang, Y. L., Ma, X. C., Li, Y. Y., Zhang, Z. L., Xiao, Z. S., Liu, L. J., Gao, X. Y., & Liu, J. (2017). Mitochondria-targeting Au nanoclusters enhance radiosensitivity of cancer cells. *Journal of Materials Chemistry B*, *5*, 4190–4197.
44. Li, Y. J., Perkins, A. L., Su, Y., Ma, Y. L., Colson, L., Horne, D. A., & Chen, Y. (2012). Gold nanoparticles as a platform for creating a multivalent poly-SUMO chain inhibitor that also augments ionizing radiation. *Proceedings of the National Academy of Sciences of the United States of America*, *109*, 4092–4097.
45. Butterworth, K. T., Coulter, J. A., Jain, S., Forker, J., McMahon, S. J., Schettino, G., Prise, K. M., Currell, F. J., & Hirst, D. G. (2010). Evaluation of cytotoxicity and radiation enhancement using 1.9 nm gold particles: Potential application for cancer therapy. *Nanotechnology*, *21* (295101), 1–9.
46. Klein, S., Sommer, A., Distel, L. V. R., Hazemann, J. L., Kroner, W., Neuhuber, W., Muller, P., Proux, O., & Kryschi, C. (2014). Superparamagnetic iron oxide nanoparticles as novel X-ray enhancer for low-dose radiation therapy. *The Journal of Physical Chemistry. B*, *118*, 6159–6166.
47. Ito, S., Miyoshi, N., Degraff, W. G., Nagashima, K., Kirschenbaum, L. J., & Riesz, P. (2009). Enhancement of 5-Aminolevulinic acid-induced oxidative stress on two cancer cell lines by gold nanoparticles. *Free Radical Research*, *43*, 1214–1224.
48. Lee, S. M., Tsai, D. H., Hackley, V. A., Brechbiel, M. W., & Cook, R. F. (2013). Surface-engineered nanomaterials as X-ray absorbing adjuvant agents for Auger-mediated chemoradiation. *Nanoscale*, *5*, 5252–5256.
49. Huang, P., Bao, L., Zhang, C. L., Lin, J., Luo, T., Yang, D. P., He, M., Li, Z. M., Gao, G., Gao, B., et al. (2011). Folic acid-conjugated silica-modified gold nanorods for X-ray/CT imaging-guided dual-mode radiation and photo-thermal therapy. *Biomaterials*, *32*, 9796–9809.
50. Jain, S., Coulter, J. A., Hounsell, A. R., Butterworth, K. T., McMahon, S. J., Hyland, W. B., Muir, M. F., Dickson, G. R., Prise, K. M., Currell, F. J., et al. (2011). Cell-specific radiosensitization by gold nanoparticles at megavoltage radiation energies. *International Journal of Radiation Oncology, Biology, Physics*, *79*, 531–539.
51. McMahon, S. J., Hyland, W. B., Muir, M. F., Coulter, J. A., Jain, S., Butterworth, K. T., Schettino, G., Dickson, G. R., Hounsell, A. R., O'Sullivan, J. M., et al. (2011). Biological consequences of nanoscale energy deposition near irradiated heavy atom nanoparticles. *Scientific Reports*, *1*. <https://doi.org/10.1038/srep00018>.
52. Latimer, C. L. (2013). Octaarginine labelled 30 nm gold nanoparticles as agents for enhanced radiotherapy. Department of Medical Biophysics, University of Toronto, Toronto, Vol. Master of Science, p. 81.
53. Seo, S. J., Han, S. M., Cho, J. H., Hyodo, K., Zaboronok, A., You, H., Peach, K., Hill, M. A., & Kim, J. K. (2015). Enhanced production of reactive oxygen species by gadolinium oxide nanoparticles under core-inner-shell excitation by proton or monochromatic X-ray irradiation: Implication of the contribution from the interatomic de-excitation-mediated nanoradiator effect to dose enhancement. *Radiation and Environmental Biophysics*, *54*, 423–431.
54. Hwu, J. R., Lin, Y. S., Josephrajan, T., Hsu, M. H., Cheng, F. Y., Yeh, C. S., Su, W. C., & Shieh, D. B. (2009). Targeted paclitaxel by conjugation to iron oxide and gold nanoparticles. *Journal of the American Chemical Society*, *131*, 66–68.

55. Liu, Y. F., Zhang, Y. B., Wang, S. P., Pope, C., & Chen, W. (2008). Optical behaviors of ZnO-porphyrin conjugates and their potential applications for cancer treatment. *Applied Physics Letters*, *92*, 143901.
56. Clement, S., Deng, W., Camilleri, E., Wilson, B. C., & Goldys, E. M. (2016). X-ray induced singlet oxygen generation by nanoparticle-photosensitizer conjugates for photodynamic therapy: Determination of singlet oxygen quantum yield. *Scientific Reports*, *6*, 19954.
57. Scaffidi, J. P., Gregas, M. K., Laully, B., Zhang, Y., & Vo-Dinh, T. (2011). Activity of psoralen-functionalized nanoscintillators against cancer cells upon X-ray excitation. *ACS Nano*, *5*, 4679–4687.
58. Rahman, W. N., Davidson, R., Yagi, N., Bansal, V., Geso, M., & Darby, I. (2011). Influence of gold nanoparticles on radiation dose enhancement and cellular migration in microbeam-irradiated cells. *BioNanoScience*, *1*, 4–13 4.
59. Setua, S., Ouberai, M., Piccirillo, S. G., Watts, C., & Welland, M. (2014). Cisplatin-tethered gold nanospheres for multimodal chemo-radiotherapy of glioblastoma. *Nanoscale*, *6*, 10865–10873.
60. Wu, H., Lin, J., Liu, P. D., Huang, Z. H., Zhao, P., Jin, H. Z., Ma, J., Wen, L. P., & Gu, N. (2016). Reactive oxygen species acts as executor in radiation enhancement and autophagy inducing by AgNPs. *Biomaterials*, *101*, 1–9.
61. Retif, P., Reinhard, A., Paquot, H., Jouan-Hureau, V., Chateau, A., Sancey, L., Barberi-Heyob, M., Pinel, S., & Bastogne, T. (2016). Monte Carlo simulations guided by imaging to predict the in vitro ranking of radiosensitizing nanoparticles. *International Journal of Nanomedicine*, *11*, 6169–6179.
62. Wang, G. N., Gao, W., Zhang, X. J., & Mei, X. F. (2016). Au nanocage functionalized with ultra-small Fe₃O₄ nanoparticles for targeting T-1-T-2 dual MRI and CT imaging of tumor. *Scientific Reports*, *6*, 28258.
63. Chithrani, B. D., Ghazani, A. A., & Chan, W. C. W. (2006). Determining the size and shape dependence of gold nanoparticle uptake into mammalian cells. *Nano Letters*, *6*, 662–668.
64. Zhang, X. J., Xing, J. Z., Chen, J., Ko, L., Amanie, J., Gulavita, S., Pervez, N., Yee, D., Moore, R., & Roa, W. (2008). Enhanced radiation sensitivity in prostate cancer by gold-nanoparticles. *Clinical and Investigative Medicine*, *31*, E160–E167.
65. Kong, T., Zeng, J., Wang, X. P., Yang, X. Y., Yang, J., McQuarrie, S., McEwan, A., Roa, W., Chen, J., & Xing, J. Z. (2008). Enhancement of radiation cytotoxicity in breast-cancer cells by localized attachment of gold nanoparticles. *Small*, *4*, 1537–1543.
66. Roa, W., Zhang, X. J., Guo, L. H., Shaw, A., Hu, X. Y., Xiong, Y. P., Gulavita, S., Patel, S., Sun, X. J., Chen, J., et al. (2009). Gold nanoparticle sensitize radiotherapy of prostate cancer cells by regulation of the cell cycle. *Nanotechnology*, *20*(375101), 1–9.
67. Antosh, M. P., Wijesinghe, D. D., Shrestha, S., Lanou, R., Huang, Y. H., Hasselbacher, T., Fox, D., Neretti, N., Sun, S., Katenka, N., et al. (2015). Enhancement of radiation effect on cancer cells by gold-pHLIP. *Proceedings of the National Academy of Sciences of the United States of America*, *112*, 5372–5376.
68. Her, S., Cui, L., Bristow, R. G., & Allen, C. (2016). Dual action enhancement of gold nanoparticle radiosensitization by pentamidine in triple negative breast cancer. *Radiation Research*, *185*, 549–562.
69. Yu, B., Liu, T., Du, Y., Luo, Z., Zheng, W., & Chen, T. (2016). X-ray-responsive selenium nanoparticles for enhanced cancer chemo-radiotherapy. *Colloid Surface B*, *139*, 180–189.
70. McMahon, S. J., Hyland, W. B., Muir, M. F., Coulter, J. A., Jain, S., Butterworth, K. T., Schettino, G., Dickson, G. R., Hounsell, A. R., O'Sullivan, J. M., et al. (2011). Nanodosimetric effects of gold nanoparticles in megavoltage radiation therapy. *Radiotherapy and Oncology*, *100*, 412–416.
71. Yu, X. J., Li, A., Zhao, C. Z., Yang, K., Chen, X. Y., & Li, W. W. (2017). Ultrasmall semimetal nanoparticles of bismuth for dual-modal computed tomography/photoacoustic imaging and synergistic thermoradiotherapy. *ACS Nano*, *11*, 3990–4001.

72. Liu, J. X., Du, Y. H., Liu, J., Zhao, Z., Cheng, K., Chen, Y. S., Wei, Y. C., Song, W. Y., & Zhang, X. (2017). Design of MoFe/Beta@CeO₂ catalysts with a core-shell structure and their catalytic performances for the selective catalytic reduction of NO with NH₃. *Applied Catalysis B: Environmental*, *203*, 704–714.
73. Khoshgard, K., Hashemi, B., Arbabi, A., Rasaei, M. J., & Soleimani, M. (2014). Radiosensitization effect of folate-conjugated gold nanoparticles on HeLa cancer cells under orthovoltage superficial radiotherapy techniques. *Physics in Medicine and Biology*, *59*, 2249–2263.
74. Zhou, H. Y., Zhang, Y., Su, G. X., Zhai, S. M., & Yan, B. (2013). Enhanced cancer cell killing by a targeting gold nanoconstruct with doxorubicin payload under X-ray irradiation. *RSC Advances*, *3*, 21596–21603.
75. Chithrani, B. D., & Chan, W. C. W. (2007). Elucidating the mechanism of cellular uptake and removal of protein-coated gold nanoparticles of different sizes and shapes. *Nano Letters*, *7*, 1542–1550.
76. Dou, Y., Guo, Y. Y., Li, X. D., Li, X., Wang, S., Wang, L., Lv, G. X., Zhang, X. N., Wang, H. J., Gong, X. Q., et al. (2016). Size-tuning ionization to optimize gold nanoparticles for simultaneous enhanced CT imaging and radiotherapy. *ACS Nano*, *10*, 2536–2548.
77. Roa, W., Yang, A., Li, P., Kong, T., Yang, J., Pervez, N., McQuarrie, S., McEwan, A., Chen, J., & Xing, J. (2007). Functional gold nanoparticles enhance radiation cytotoxicity in breast and prostate cancer cells. *Radiotherapy and Oncology*, *84*, S83–S83.
78. Kudgus, R. A., Szabolcs, A., Khan, J. A., Walden, C. A., Reid, J. M., Robertson, J. D., Bhattacharya, R., & Mukherjee, P. (2013). Inhibiting the growth of pancreatic adenocarcinoma in vitro and in vivo through targeted treatment with designer gold nanotherapeutics. *PLoS One*, *8*, e57522.
79. Zhang, P. P., Qiao, Y., Wang, C. M., Ma, L. Y., & Su, M. (2014). Enhanced radiation therapy with internalized polyelectrolyte modified nanoparticles. *Nanoscale*, *6*, 10095–10099.
80. Zhu, Z. J., Tang, R., Yeh, Y. C., Miranda, O. R., Rotello, V. M., & Vachet, R. W. (2012). Determination of the intracellular stability of gold nanoparticle monolayers using mass spectrometry. *Analytical Chemistry*, *84*, 4321–4326.
81. Subiel, A., Ashmore, R., & Schettino, G. (2016). Standards and methodologies for characterizing radiobiological impact of high-Z nanoparticles. *Theranostics*, *6*, 1651–1671.
82. Hariri, G., Yan, H. P., Wang, H. L., Han, Z. Z., & Hallahan, D. E. (2010). Radiation-guided drug delivery to mouse models of lung cancer. *Clinical Cancer Research*, *16*, 4968–4977.
83. Kang, B., Mackey, M. A., & El-Sayed, M. A. (2010). Nuclear targeting of gold nanoparticles in cancer cells induces DNA damage, causing cytokinesis arrest and apoptosis. *Journal of the American Chemical Society*, *132*, 1517–1519.
84. Nativo, P., Prior, I. A., & Brust, M. (2008). Uptake and intracellular fate of surface-modified gold nanoparticles. *ACS Nano*, *2*, 1639–1644.
85. Yu, M. K., Park, J., & Jon, S. (2012). Targeting strategies for multifunctional nanoparticles in cancer imaging and therapy. *Theranostics*, *2*, 3–44.
86. Ng, S. K., Ma, L., Qiu, Y., Xun, X., Webster, T. J., & Su, M. (2016). Enhancing cancer radiation therapy with cell penetrating peptide modified gold nanoparticles. *Austin Journal of Biomedical Engineering*, *3*(id1033), 1031–1038.
87. Hainfeld, J. F., & Smilowitz, H. M. (2015). Nuclear targeted gold nanoparticles for radiation enhancement. *Cancer Research*, *75*, Abstract 1807.
88. Cormode, D. P., Naha, P. C., & Fayad, Z. A. (2014). Nanoparticle contrast agents for computed tomography: A focus on micelles. *Contrast Media & Molecular Imaging*, *9*, 37–52.
89. Xu, C. J., Tung, G. A., & Sun, S. H. (2008). Size and concentration effect of gold nanoparticles on X-ray attenuation as measured on computed tomography. *Chemistry of Materials*, *20*, 4167–4169.
90. Cheong, S. K., Jones, B. L., Siddiqi, A. K., Liu, F., Manohar, N., & Cho, S. H. (2010). X-ray fluorescence computed tomography (XFCT) imaging of gold nanoparticle-loaded objects using 110 kVp x-rays. *Physics in Medicine and Biology*, *55*, 647–662.

91. Jones, B. L., & Cho, S. H. (2011). The feasibility of polychromatic cone-beam x-ray fluorescence computed tomography (XFCT) imaging of gold nanoparticle-loaded objects: A Monte Carlo study. *Physics in Medicine and Biology*, *56*, 3719–3730.
92. Jones, B., Manohar, N., Karellas, A., & Cho, S. (2012). Polychromatic cone-beam X-ray fluorescence computed tomography of gold nanoparticle-loaded objects. *Medical Physics*, *39*, 3986–3987.
93. Manohar, N., Reynoso, F. J., & Cho, S. H. (2013). Experimental demonstration of direct L-shell x-ray fluorescence imaging of gold nanoparticles using a benchtop x-ray source. *Medical Physics*, *40*, 080702.
94. Manohar, N., Jones, B. L., & Cho, S. H. (2014). Improving x-ray fluorescence signal for benchtop polychromatic cone-beam x-ray fluorescence computed tomography by incident x-ray spectrum optimization: A Monte Carlo study. *Medical Physics*, *41*, 101906.
95. Meng, L., Fu, G., Li, N., Newville, M., Eng, P., & La Riviere, P. (2010). X-ray fluorescence tomography using imaging detectors. *Proceedings of SPIE*, *7804*, B1–B9.
96. Wen, H., Bennett, E. E., Hegedus, M. A., & Carroll, S. C. (2008). Spatial harmonic imaging of X-ray scattering initial results. *IEEE Transactions on Medical Imaging*, *27*, 997–1002.
97. Bazalova, M., Kuang, Y., Prax, G., & Xing, L. (2012). Investigation of X-ray fluorescence computed tomography (XFCT) and K-edge imaging. *IEEE Transactions on Medical Imaging*, *31*, 1620–1627.
98. Bazalova, M., Weil, M. D., Wilfley, B., & Graves, E. E. (2012). Monte Carlo model of the scanning beam digital x-ray (SBDX) source. *Physics in Medicine and Biology*, *57*, 7381–7394.
99. Kuang, Y., Prax, G., Bazalova, M., Meng, B. W., Qian, J. G., & Xing, L. (2013). First demonstration of multiplexed X-ray fluorescence computed tomography (XFCT) imaging. *IEEE Transactions on Medical Imaging*, *32*, 262–267.
100. Guo, R., Wang, H., Peng, C., Shen, M. W., Pan, M. J., Cao, X. Y., Zhang, G. X., & Shi, X. Y. (2010). X-ray attenuation property of dendrimer-entrapped gold nanoparticles. *Journal of Physical Chemistry C*, *114*, 50–56.
101. Hariri, G., Wellons, M. S., Morris, W. H., Lukehart, C. M., & Hallahan, D. E. (2011). Multifunctional FePt nanoparticles for radiation-guided targeting and imaging of cancer. *Annals of Biomedical Engineering*, *39*, 946–952.
102. Luo, T., Huang, P., Gao, G., Shen, G. X., Fu, S., Cui, D. X., Zhou, C. Q., & Ren, Q. S. (2011). Mesoporous silica-coated gold nanorods with embedded indocyanine green for dual mode X-ray CT and NIR fluorescence imaging. *Optics Express*, *19*, 17030–17039.
103. Rand, D., Ortiz, V., Liu, Y. A., Derdak, Z., Wands, J. R., Taticek, M., & Rose-Petrucci, C. (2011). Nanomaterials for X-ray imaging: Gold nanoparticle enhancement of X-ray scatter imaging of hepatocellular carcinoma. *Nano Letters*, *11*, 2678–2683.
104. Guo, T., & Davidson, R. A. (2016). Nanoparticle assisted scanning focusing X-ray fluorescence imaging and enhanced treatment. *Radiat Res*. *185*, 87–95.
105. Guo, T., & Davidson, R. A. (2015). Nanoparticle assisted scanning focusing X-ray fluorescence imaging and enhanced treatment. Patent publication number: WO/2015/031675; international application number: PCT/US2014/053259. Publication date: May 03, 2015.
106. Boote, E., Fent, G., Kattumuri, V., Casteel, S., Katti, K., Chanda, N., Kannan, R., Katti, K., & Churchill, R. (2010). Gold nanoparticle contrast in a phantom and juvenile swine: Models for molecular imaging of human organs using X-ray computed tomography. *Academic Radiology*, *17*, 410–417.
107. Hainfeld, J. F., Slatkin, D. N., Focella, T. M., & Smilowitz, H. M. (2006). Gold nanoparticles: A new X-ray contrast agent. *The British Journal of Radiology*, *79*, 248–253.
108. Hainfeld, J. F., Smilowitz, H. M., O'Connor, M. J., Dilmanian, F. A., & Slatkin, D. N. (2013). Gold nanoparticle imaging and radiotherapy of brain tumors in mice. *Nanomedicine*, *8*, 1601–1609.
109. Alric, C., Taleb, J., Le Duc, G., Mandon, C., Billotey, C., Le Meur-Herland, A., Brochard, T., Vocanson, F., Janier, M., Perriat, P., et al. (2008). Gadolinium chelate coated gold

- nanoparticles as contrast agents for both X-ray computed tomography and magnetic resonance imaging. *Journal of the American Chemical Society*, *130*, 5908–5915.
110. Yusa, N., Jiang, M., Mizuno, K., & Uesaka, M. (2009). Numerical evaluation of the effectiveness of colloidal gold as a contrast agent. *Radiological Physics and Technology*, *2*, 33–39.
 111. Jones, B. L., Manohar, N., Reynoso, F., Karellas, A., & Cho, S. H. (2012). Experimental demonstration of benchtop x-ray fluorescence computed tomography (XFCT) of gold nanoparticle-loaded objects using lead- and tin-filtered polychromatic cone-beams. *Physics in Medicine and Biology*, *57*, N457–N467.
 112. Kim, D., Jeong, Y. Y., & Jon, S. (2010). A drug-loaded aptamer-gold nanoparticle bioconjugate for combined CT imaging and therapy of prostate cancer. *ACS Nano*, *4*, 3689–3696.
 113. van Schooneveld, M. M., Cormode, D. P., Koole, R., van Wijngaarden, J. T., Calcagno, C., Skajaa, T., Hilhorst, J., 't Hart, D. C., Fayad, Z. A., Mulder, W. J. M., et al. (2010). A fluorescent, paramagnetic and PEGylated gold/silica nanoparticle for MRI, CT and fluorescence imaging. *Contrast Media & Molecular Imaging*, *5*, 231–236.
 114. Manohar, N. (2011). Effect of source X-ray energy spectra on the detection of fluorescence photons from gold nanoparticles. *Medical Physics*, Georgia Institute of Technology, Atlanta, Vol. M.S., p. 38.
 115. Le Duc, G., Miladi, I., Alric, C., Mowat, P., Brauer-Krisch, E., Bouchet, A., Khalil, E., Billotey, C., Janier, M., Lux, F., et al. (2011). Toward an image-guided microbeam radiation therapy using gadolinium-based nanoparticles. *ACS Nano*, *5*, 9566–9574.
 116. Smith, L., Kuncic, Z., Ostrikov, K., & Kumar, S. (2012). Nanoparticles in cancer imaging and therapy. *Journal of Nanomaterials*, 891318, 1–7.
 117. Kunzel, R., Okuno, E., Levenhagen, R. S., & Umisedo, N. K. (2013). Evaluation of the X-ray absorption by gold nanoparticles solutions. *Nanotechnology*, *5*(865283), 203.
 118. Tu, S. J., Yang, P. Y., Hong, J. H., & Lo, C. J. (2013). Quantitative dosimetric assessment for effect of gold nanoparticles as contrast media on radiotherapy planning. *Radiation Physics and Chemistry*, *88*, 14–20.
 119. Rivera, E. J., Tran, L. A., Hernandez-Rivera, M., Yoon, D., Mikos, A. G., Rusakova, I. A., Cheong, B. Y., Cabreira-Hansen, M. D., Willerson, J. T., Perin, E. C., et al. (2013). Bismuth@US-tubes as a potential contrast agent for X-ray imaging applications. *Journal of Materials Chemistry B*, *1*, 4792–4800.
 120. Cole, L. E., Vargo-Gogola, T., & Roeder, R. K. (2014). Contrast-enhanced X-ray detection of breast microcalcifications in a murine model using targeted gold nanoparticles. *ACS Nano*, *8*, 7486–7496.
 121. Deyhimighighi, N., Mohd Noor, N., Soltani, N., Jorfi, R., Erfani Haghiri, M., Adenan, M. Z., Saion, E., & Khandaker, M. U. (2014). Contrast enhancement of magnetic resonance imaging (MRI) of polymer gel dosimeter by adding Platinum nano-particles. *Journal of Physics: Conference Series*, *546*, 012013.
 122. Xia, H. X., Yang, X. Q., Song, J. T., Chen, J., Zhang, M. Z., Yan, D. M., Zhang, L., Qin, M. Y., Bai, L. Y., Zhao, Y. D., et al. (2014). Folic acid-conjugated silica-coated gold nanorods and quantum dots for dual-modality CT and fluorescence imaging and photothermal therapy. *Journal of Materials Chemistry B*, *2*, 1945–1953.
 123. Wathen, C. A., Caldwell, C., Chanda, N., Upendran, A., Zambre, A., Afrasiabi, Z., Chapaman, S. E., Foje, N., Leevy, W. M., & Kannan, R. (2015). Selective X-ray contrast enhancement of the spleen of living mice mediated by gold nanorods. *Contrast Media & Molecular Imaging*, *10*, 188–193.
 124. Rand, D., Derdak, Z., Carlson, R., Wands, J. R., & Rose-Petrucci, C. (2015). X-ray scatter imaging of hepatocellular carcinoma in a mouse model using nanoparticle contrast agents. *Scientific Reports*, *5*, 15673.
 125. McQuade, C., Al Zaki, A., Desai, Y., Vido, M., Sakhujia, T., Cheng, Z. L., Hickey, R. J., Joh, D., Park, S. J., Kao, G., et al. (2015). A multifunctional nanoplatform for imaging, radiotherapy, and the prediction of therapeutic response. *Small*, *11*, 834–843.

126. Elmenoufy, A. H., Tang, Y. A., Hu, J., Xu, H. B., & Yang, X. L. (2015). A novel deep photodynamic therapy modality combined with CT imaging established via X-ray stimulated silica-modified lanthanide scintillating nanoparticles. *Chemical Communications*, *51*, 12247–12250.
127. Lv, R. C., Yang, P. P., He, F., Gai, S. L., Li, C. X., Dai, Y. L., Yang, G. X., & Lin, J. (2015). A yolk-like multifunctional platform for multimodal imaging and synergistic therapy triggered by a single near-infrared light. *ACS Nano*, *9*, 1630–1647.
128. Kim, T., Lee, N., Arifin, D. R., Shats, I., Janowski, M., Walczak, P., Hyeon, T., & Bulte, J. W. M. (2017). In vivo micro-CT imaging of human mesenchymal stem cells labeled with gold-poly-l-lysine nanocomplexes. *Advanced Functional Materials*, *27*, 1604213.
129. Duan, S., Yang, Y. J., Zhang, C. L., Zhao, N. N., & Xu, F. J. (2017). NIR-responsive polycationic gatekeeper-cloaked hetero-nanoparticles for multimodal imaging-guided triple-combination therapy of cancer. *Small*, *13*, 1603133.
130. Wathen, C. A., Foje, N., van Avermaete, T., Miramontes, B., Chapaman, S. E., Sasser, T. A., Kannan, R., Gerstler, S., & Leevy, W. M. (2013). In vivo X-ray computed tomographic imaging of soft tissue with native, intravenous, or oral contrast. *Sensors*, *13*, 6957–6980.
131. Liu, X., Zhang, X., Zhu, M., Lin, G. H., Liu, J., Zhou, Z. F., Tian, X., & Pan, Y. (2017). PEGylated au@Pt nanodendrites as novel theranostic agents for computed tomography imaging and photothermal/radiation synergistic therapy. *ACS Applied Materials & Interfaces*, *9*, 279–285.
132. Mieszawska, A. J., Mulder, W. J. M., Fayad, Z. A., & Cormode, D. P. (2013). Multifunctional gold nanoparticles for diagnosis and therapy of disease. *Molecular Pharmaceutics*, *10*, 831–847.
133. Jakhmola, A., Anton, N., & Vandamme, T. F. (2012). Inorganic nanoparticles based contrast agents for X-ray computed tomography. *Advanced Healthcare Materials*, *1*, 413–431.
134. Cole, L. E., Ross, R. D., Tilley, J. M. R., Vargo-Gogola, T., & Roeder, R. K. (2015). Gold nanoparticles as contrast agents in x-ray imaging and computed tomography. *Nanomedicine*, *10*, 321–341.
135. Liu, Y. L., Liu, J. H., Ai, K. L., Yuan, Q. H., & Lu, L. H. (2014). Recent advances in ytterbium-based contrast agents for in vivo X-ray computed tomography imaging: Promises and prospects. *Contrast Media & Molecular Imaging*, *9*, 26–36.
136. Gao, Y. P., & Li, Y. S. (2016). Gold nanostructures for cancer imaging and therapy. In Z. Dai (Ed.), *Advances in nanotheranostics I, Springer Series in Biomaterials Science and Engineering* (Vol. 6, pp. 53–101). Berlin/Heidelberg: Springer.
137. Patel, L. N., Zaro, J. L., & Shen, W. C. (2007). Cell penetrating peptides: Intracellular pathways and pharmaceutical perspectives. *Pharmaceutical Research*, *24*, 1977–1992.
138. Cesbron, Y., See, V., Free, P., Nativo, P., Shaheen, U., Rigden, D. J., Spiller, D. G., Fernig, D. G., White, M. R. H., Prior, I. A., et al. (2010). Intracellular delivery and fate of peptide-capped gold nanoparticles. *Biophysical Journal*, *98*, 203a.
139. Popovtzer, R., Agrawal, A., Kotov, N. A., Popovtzer, A., Balter, J., Carey, T. E., & Kopelman, R. (2008). Targeted gold nanoparticles enable molecular CT imaging of cancer. *Nano Letters*, *8*, 4593–4596.
140. Cole, L. E., Vargo-Gogola, T., & Roeder, R. K. (2014). Bisphosphonate-functionalized gold nanoparticles for contrast-enhanced X-ray detection of breast microcalcifications. *Biomaterials*, *35*, 2312–2321.
141. Zhang, X. D., Wu, D., Shen, X., Chen, J., Sun, Y. M., Liu, P. X., & Liang, X. J. (2012). Size-dependent radiosensitization of PEG-coated gold nanoparticles for cancer radiation therapy. *Biomaterials*, *33*, 6408–6419.
142. Cho, S. H. (2005). Estimation of tumor dose enhancement due to gold nanoparticles during typical radiation treatments: A preliminary Monte Carlo study. *Medical Physics*, *32*, 2162–2162.

143. McMahon, S. J., Mendenhall, M. H., Jain, S., & Currell, F. (2008). Radiotherapy in the presence of contrast agents: A general figure of merit and its application to gold nanoparticles. *Physics in Medicine and Biology*, *53*, 5635–5651.
144. Gokeri, G., Kocar, C., & Tombakoglu, M. (2010). Monte Carlo simulation of microbeam radiation therapy with an interlaced irradiation geometry and an Au contrast agent in a realistic head phantom. *Physics in Medicine and Biology*, *55*, 7469–7487.
145. Lechtman, E., Chattopadhyay, N., Cai, Z., Mashouf, S., Reilly, R., & Pignol, J. P. (2011). Implications on clinical scenario of gold nanoparticle radiosensitization in regards to photon energy, nanoparticle size, concentration and location. *Physics in Medicine and Biology*, *56*, 4631–4647.
146. Martinez-Rovira, I., & Prezado, Y. (2011). Monte Carlo dose enhancement studies in microbeam radiation therapy. *Medical Physics*, *38*, 4430–4439.
147. Ngwa, W., Makrigiorgos, G. M., & Berbeco, R. I. (2012). Gold nanoparticle enhancement of stereotactic radiosurgery for neovascular age-related macular degeneration. *Physics in Medicine and Biology*, *57*, 6371–6380.
148. Lechtman, E., Mashouf, S., Chattopadhyay, N., Keller, B. M., Lai, P., Cai, Z., Reilly, R. M., & Pignol, J. P. (2013). A Monte Carlo-based model of gold nanoparticle radiosensitization accounting for increased radiobiological effectiveness. *Physics in Medicine and Biology*, *58*, 3075–3087.
149. Amato, E., Italiano, A., Leotta, S., Pergolizzi, S., & Torrisi, L. (2013). Monte Carlo study of the dose enhancement effect of gold nanoparticles during X-ray therapies and evaluation of the anti-angiogenic effect on tumour capillary vessels. *Journal of X-Ray Science and Technology*, *21*, 237–247.
150. Mesbahi, A., Jamali, F., & Gharehaghaji, N. (2013). Effect of photon beam energy, gold nanoparticle size and concentration on the dose enhancement in radiation therapy. *BiolImpacts: BI*, *29-35(29)*, 3.
151. Jeynes, J. C. G., Merchant, M. J., Spindler, A., Wera, A. C., & Kirkby, K. J. (2014). Investigation of gold nanoparticle radiosensitization mechanisms using a free radical scavenger and protons of different energies. *Physics in Medicine and Biology*, *59*, 6431–6443.
152. Li, W. B., Müllner, M., Greiter, M. B., Bissardon, C., Xie, W. Z., Schlattl, H., Oeh, U., Li, J. L., & Hoeschen, C. (2014). Monte Carlo simulations of dose enhancement around gold nanoparticles used as X-ray imaging contrast agents and radiosensitizers. *Medical Imaging 2014: Physics of Medical Imaging. Proceedings of SPIE*, *9033*, 90331K.
153. Wardlow, N., Polin, C., Villagomez-Bernabe, B., & Currell, F. (2015). A simple model to quantify radiolytic production following electron emission from heavy-atom nanoparticles irradiated in liquid suspensions. *Radiation Research*, *184*, 518–532.
154. Xie, W. Z., Friedland, W., Li, W. B., Li, C. Y., Oeh, U., Qiu, R., Li, J. L., & Hoeschen, C. (2015). Simulation on the molecular radiosensitization effect of gold nanoparticles in cells irradiated by x-rays. *Physics in Medicine and Biology*, *60*, 6195–6212.
155. Ferrero, V., Visona, G., Dalmasso, F., Gobbato, A., Cerello, P., Strigari, L., Visentin, S., & Attili, A. (2017). Targeted dose enhancement in radiotherapy for breast cancer using gold nanoparticles, part 1: A radiobiological model study. *Medical Physics*, *44*, 1983–1992.
156. Sung, W. M., Ye, S. J., McNamara, A. L., McMahon, S. J., Hainfeld, J., Shin, J., Smilowitz, H. M., Paganetti, H., & Schuemann, J. (2017). Dependence of gold nanoparticle radiosensitization on cell geometry. *Nanoscale*, *9*, 5843–5853.
157. Zabihzadeh, M., Moshirian, T., Ghorbani, M., Knaup, C., & Behrooz, M. A. (2016). A Monte Carlo study on dose enhancement by homogenous and inhomogeneous distributions of gold nanoparticles in radiotherapy with low energy X-rays. *Journal of Biomedical Physics and Engineering*, I–XVI.
158. Zygmanski, P., & Sajo, E. (2016). Nanoscale radiation transport and clinical beam modeling for gold nanoparticle dose enhanced radiotherapy (GNPT) using X-rays. *The British Journal of Radiology*, *89*, 20150200.
159. Oliver, P. A. K., & Thomson, R. M. (2017). A Monte Carlo study of macroscopic and microscopic dose descriptors for kilovoltage cellular dosimetry. *Physics in Medicine and Biology*, *62*, 1417–1437.

160. Lee, C., Cheng, N. N., Davidson, R. A., & Guo, T. (2012). Geometry enhancement of nanoscale energy deposition by X-rays. *Journal of Physical Chemistry C*, *116*, 11292–11297.
161. Ma, L., Zou, X. J., Bui, B., Chen, W., Song, K. H., & Solberg, T. (2014). X-ray excited ZnS: Cu,Co afterglow nanoparticles for photodynamic activation. *Applied Physics Letters*, *105*, 013702.
162. Huang, F. K., Chen, W. C., Lai, S. F., Liu, C. J., Wang, C. L., Wang, C. H., Chen, H. H., Hua, T. E., Cheng, Y. Y., Wu, M. K., et al. (2010). Enhancement of irradiation effects on cancer cells by cross-linked dextran-coated iron oxide (CLIO) nanoparticles. *Physics in Medicine and Biology*, *55*, 469–482.
163. Zou, X. J., Yao, M. Z., Ma, L., Hossu, M., Han, X. M., Juzenas, P., & Chen, W. (2014). X-ray-induced nanoparticle-based photodynamic therapy of cancer. *Nanomedicine*, *9*, 2339–2351.
164. McQuaid, H. N., Muir, M. F., Taggart, L. E., McMahon, S. J., Coulter, J. A., Hyland, W. B., Jain, S., Butterworth, K. T., Schettino, G., Prise, K. M., et al. (2016). Imaging and radiation effects of gold nanoparticles in tumour cells. *Scientific Reports*, *6*, 19442.
165. Detappe, A., Thomas, E., Tibbitt, M. W., Kunjachan, S., Zavidij, O., Parnandi, N., Reznichenko, E., Lux, F., Tillemen, O., & Berbeco, R. (2017). Ultrasmall silica-based bismuth gadolinium nanoparticles for dual magnetic resonance-computed tomography image guided radiation therapy. *Nano Letters*, *17*, 1733–1740.
166. Stefancikova, L., Lacombe, S., Salado, D., Porcel, E., Pagacova, E., Tillement, O., Lux, F., Depes, D., Kozubek, S., & Falk, M. (2016). Effect of gadolinium-based nanoparticles on nuclear DNA damage and repair in glioblastoma tumor cells. *Journal of Nanobiotechnology*, *14*, 63.
167. Clement, S., Chen, W. J., Anwer, A. G., & Goldys, E. M. (2017). Verteporfin conjugated to gold nanoparticles for fluorescent cellular bioimaging and X-ray mediated photodynamic therapy. *Microchimica Acta*, *184*, 1765–1771.
168. Ghaemi, B., Mashinchian, O., Mousavi, T., Karimi, R., Kharrazi, S., & Amani, A. (2016). Harnessing the cancer radiation therapy by lanthanide-doped zinc oxide based theranostic nanoparticles. *ACS Applied Materials & Interfaces*, *8*, 3123–3134.
169. Khoei, S., Mahdavi, S. R., Fakhimikabir, H., Shakeri-Zadeh, A., & Hashemian, A. (2014). The role of iron oxide nanoparticles in the radiosensitization of human prostate carcinoma cell line DU145 at megavoltage radiation energies. *International Journal of Radiation Biology*, *90*, 351–356.
170. Brown, R., Tehei, M., Oktaria, S., Briggs, A., Stewart, C., Konstantinov, K., Rosenfeld, A., Corde, S., & Lerch, M. (2014). High-Z nanostructured ceramics in radiotherapy: First evidence of Ta₂O₅-induced dose enhancement on radioresistant cancer cells in an MV photon field. *Particle and Particle Systems Characterization*, *31*, 500–505.
171. Kumar, R., Korideck, H., Ngwa, W., Berbeco, R. I., Makrigiorgos, G. M., & Sridhar, S. (2013). Third generation gold nanoplatfrom optimized for radiation therapy. *Translational Cancer Research*, *2*, 228–239.
172. Yousef, I., Seksek, O., Gil, S., Prezado, Y., Sule-Susoe, J., & Martinez-Rovira, I. (2016). Study of the biochemical effects induced by X-ray irradiations in combination with gadolinium nanoparticles in F98 glioma cells: First FTIR studies at the Emira laboratory of the SESAME synchrotron. *Analyst*, *141*, 2238–2249.
173. Takahashi, J., & Misawa, M. (2007). Analysis of potential radiosensitizing materials for X-ray-induced photodynamic therapy. *NanoBiotechnology*, *3*, 116–126 116.
174. Ngwa, W., Korideck, H., Kassis, A. I., Kumar, R., Sridhar, S., Makrigiorgos, G. M., & Cormack, R. A. (2013). In vitro radiosensitization by gold nanoparticles during continuous low-dose-rate gamma irradiation with I-125 brachytherapy seeds. *Nanomedicine-Nanotechnology*, *9*, 25–27.
175. Bao, Z. R., He, M. Y., Quan, H., Jiang, D. Z., Zheng, Y. H., Qin, W. J., Zhou, Y. F., Ren, F., Guo, M. X., & Jiang, C. Z. (2016). FePt nanoparticles: A novel nanoprobe for enhanced HeLa cells sensitivity to chemoradiotherapy. *RSC Advances*, *6*, 35124–35134.

176. Kraščakovā, S., Giuliani, A., Lacerda, S., Pallier, A., Mercere, P., Toth, E., & Refregiers, M. (2015). X-ray-induced radiophotodynamic therapy (RPDT) using lanthanide micelles: Beyond depth limitations. *Nano Research*, 8, 2373–2379.
177. Rossi, F., Bedogni, E., Bigi, F., Rimoldi, T., Cristofolini, L., Pinelli, S., Alinovi, R., Negri, M., Dhanabalan, S. C., Attolini, G., et al. (2015). Porphyrin conjugated SiC/SiO_x nanowires for X-ray-excited photodynamic therapy. *Scientific Reports*, 5, 7606.
178. Nakayama, M., Sasaki, R., Ogino, C., Tanaka, T., Morita, K., Umetsu, M., Ohara, S., Tan, Z. Q., Nishimura, Y., Akasaka, H., et al. (2016). Titanium peroxide nanoparticles enhanced cytotoxic effects of X-ray irradiation against pancreatic cancer model through reactive oxygen species generation in vitro and in vivo. *Radiation Oncology*, 11, 91.
179. Huang, C. W., Kearney, V., Moeendarbari, S., Jiang, R. Q., Christensen, P., Tekade, R., Sun, X. K., Mao, W. H., & Hao, Y. W. (2015). Hollow gold nanoparticles as biocompatible radiosensitizer: An in vitro proof of concept study. *Journal of Nano Research*, 32, 106–U140.
180. Jiang, X. Y., Du, B. J., Yu, M. X., Jia, X., & Zheng, J. (2016). Surface-ligand effect on radiosensitization of ultrasmall luminescent gold nanoparticles. *Journal of Innovative Optical Health Sciences*, 9, 1642003.
181. Zhang, X. D., Guo, M. L., Wu, H. Y., Sun, Y. M., Ding, Y. Q., Feng, X., & Zhang, L. A. (2009). Irradiation stability and cytotoxicity of gold nanoparticles for radiotherapy. *International Journal of Nanomedicine*, 4, 165–173.
182. Levy, L., Pottier, A., Rouet, A., Marill, J., Devaux, C., & Germain, M. (2009). Inorganic nanoparticles of high density to destroy cells in-vivo, WO2009 147214 A1.
183. Geng, F., Song, K., Xing, J. Z., Yuan, C. Z., Yan, S., Yang, Q. F., Chen, J., & Kong, B. H. (2011). Thio-glucose bound gold nanoparticles enhance radio-cytotoxic targeting of ovarian cancer. *Nanotechnology*, 22(285101), 1–8.
184. Yang, C., Neshatian, M., van Prooijen, M., & Chithrani, D. B. (2014). Cancer nanotechnology: Enhanced therapeutic response using peptide-modified gold nanoparticles. *Journal of Nanoscience and Nanotechnology*, 14, 4813–4819.
185. Carter, J. D., Cheng, N. N., Qu, Y. Q., Suarez, G. D., & Guo, T. (2007). Nanoscale energy deposition by x-ray absorbing nanostructures. *The Journal of Physical Chemistry. B*, 111, 11622–11625.
186. Hossain, M., Luo, Y., Sun, Z. Y., Wang, C. M., Zhang, M. H., Fu, H. Y., Qiao, Y., & Su, M. (2012). X-ray enabled detection and eradication of circulating tumor cells with nanoparticles. *Biosensors & Bioelectronics*, 38, 348–354.
187. Detappe, A., Rottmann, J., Kunjachan, S., Tillement, O., & Berbeco, R. (2015). Theranostic gadolinium-based AGuIX nanoparticles for MRI-guided radiation therapy. *Medical Physics*, 42, 3566–3566.
188. Wang, J. P., Pang, X. J., Tan, X. X., Song, Y. L., Liu, L., You, Q., Sun, Q., Tan, F. P., & Li, N. (2017). A triple-synergistic strategy for combinational photo/radiotherapy and multimodality imaging based on hyaluronic acid-hybridized polyaniline-coated WS₂ nanodots. *Nanoscale*, 9, 5551–5564.
189. Hainfeld, J. F., Dilmanian, F. A., Slatkin, D. N., & Smilowitz, H. M. (2008). Radiotherapy enhancement with gold nanoparticles. *The Journal of Pharmacy and Pharmacology*, 60, 977–985.
190. Jaboin, J. I., Fu, A., Hariri, G., Han, Z., & Hallahan, D. (2007). Novel radiation-guided nanoparticle drug delivery system for prostate cancer. *International Journal of Radiation Oncology, Biology, Physics*, 69, S111–S111.
191. Chang, M. Y., Shiau, A. L., Chen, Y. H., Chang, C. J., Chen, H. H. W., & Wu, C. L. (2008). Increased apoptotic potential and dose-enhancing effect of gold nanoparticles in combination with single-dose clinical electron beams on tumor-bearing mice. *Cancer Science*, 99, 1479–1484.
192. Popovtzer, A., Mizrachi, A., Motiei, M., Bragilovski, D., Lubimov, L., Levi, M., Hilly, O., Ben-Aharon, I., & Popovtzer, R. (2016). Actively targeted gold nanoparticles as novel radiosensitizer agents: An in vivo head and neck cancer model. *Nanoscale*, 8, 2678–2685.

193. Tseng, S. J., Chien, C. C., Liao, Z. X., Chen, H. H., Kang, Y. D., Wang, C. L., Hwu, Y., & Margaritondo, G. (2012). Controlled hydrogel photopolymerization inside live systems by X-ray irradiation. *Soft Matter*, *8*, 1420–1427.
194. Anijdan, S. H. M., Mahdavi, S. R., Shirazi, A., Zarrinfard, M. A., & Hajati, J. (2013). Megavoltage X-ray dose enhancement with gold nanoparticles in tumor bearing mice. *International Journal of Molecular and Cellular Medicine (IJMCM)*, *3*, 118–124.
195. Krishnan, S., Diagaradjane, P., Goudrich, G. P., & Payne, J. D. (2013). Enhancement of radiation therapy by targeted high-Z nanoparticles. US 2013/0225901 A1.
196. Kunjachan, S., Detappe, A., Kumar, R., Ireland, T., Cameron, L., Biancur, D. E., Motto-Ros, V., Sancey, L., Sridhar, S., Makrigiorgos, G. M., et al. (2015). Nanoparticle mediated tumor vascular disruption: A novel strategy in radiation therapy. *Nano Letters*, *15*, 7488–7496.
197. Fan, W. P., Bu, W. B., Zhang, Z., Shen, B., Zhang, H., He, Q. J., Ni, D. L., Cui, Z. W., Zhao, K. L., Bu, J. W., et al. (2015). X-ray radiation-controlled NO-release for on-demand depth-independent hypoxic radiosensitization. *Angewandte Chemie, International Edition*, *54*, 14026–14030.
198. Chen, N., Yang, W. T., Bao, Y., Xu, H. L., Qin, S. B., & Tu, Y. (2015). BSA capped Au nanoparticle as an efficient sensitizer for glioblastoma tumor radiation therapy. *RSC Advances*, *5*, 40514–40520.
199. Chen, H. M., Wang, G. D., Chuang, Y. J., Zhen, Z. P., Chen, X. Y., Biddinger, P., Hao, Z. L., Liu, F., Shen, B. Z., Pan, Z. W., et al. (2015). Nanoscintillator-mediated X-ray inducible photodynamic therapy for in vivo cancer treatment. *Nano Letters*, *15*, 2249–2256.
200. Zhang, X. D., Luo, Z. T., Chen, J., Song, S. S., Yuan, X., Shen, X., Wang, H., Sun, Y. M., Gao, K., Zhang, L. F., et al. (2015). Ultrasmall glutathione-protected gold nanoclusters as next generation radiotherapy sensitizers with high tumor uptake and high renal clearance. *Scientific Reports*, *5*.
201. Yi, X., Chen, L., Zhong, X. Y., Gao, R. L., Qian, Y. T., Wu, F., Song, G. S., Chai, Z. F., Liu, Z., & Yang, K. (2016). Core-shell Au@MnO₂ nanoparticles for enhanced radiotherapy via improving the tumor oxygenation. *Nano Research*, *9*, 3267–3278.
202. Zhao, N., Yang, Z. R., Li, B. X., Meng, J., Shi, Z. L., Li, P., & Fu, S. (2016). RGD-conjugated mesoporous silica-encapsulated gold nanorods enhance the sensitization of triple-negative breast cancer to megavoltage radiation therapy. *International Journal of Nanomedicine*, *11*, 5595–5610.
203. Li, M. F., Zhao, Q., Yi, X., Zhong, X. Y., Song, G. S., Chai, Z. F., Liu, Z. A., & Yang, K. (2016). Au@MnS@ZnS core/shell/shell nanoparticles for magnetic resonance imaging and enhanced cancer radiation therapy. *ACS Applied Materials & Interfaces*, *8*, 9557–9564.
204. Liu, J. J., Chen, Q., Zhu, W. W., Yi, X., Yang, Y., Dong, Z. L., & Liu, Z. (2017). Nanoscale-coordination-polymer-shelled manganese dioxide composite nanoparticles: A multistage redox/pH/H₂O₂-responsive cancer theranostic nanoplatform. *Advanced Functional Materials*, *27*, 1605926.
205. Smilowitz, H. M., Hainfeld, J. F., Dilmanian, F. A., Zhong, Z., Slatkin, D. N., & Kalef-Ezra, J. A. (2010). Gold nanoparticles enhance the radiation therapy of a murine squamous cell carcinoma. *Physics in Medicine and Biology*, *55*, 3045–3059.
206. Chen, W., & Zhang, J. (2006). Using nanoparticles to enable simultaneous radiation and photodynamic therapies for cancer treatment. *Journal of Nanoscience and Nanotechnology*, *6*, 1159–1166.
207. Davidson, R. A., Sugiyama, C., & Guo, T. (2014). Determination of absolute quantum efficiency of X-ray nano phosphors by thin film photovoltaic cells. *Analytical Chemistry*, *86*, 10492–10496.
208. Alric, C., Serduc, R., Mandon, C., Taleb, J., Le Duc, G., Le Meur-Herland, A., Billotey, C., Perriat, P., Roux, S., & Tillement, O. (2008). Gold nanoparticles designed for combining dual modality imaging and radiotherapy. *Gold Bulletin*, *41*, 90–97.
209. Hebert, E. M., Deboutiere, P. J., Lepage, M., Sanche, L., & Hunting, D. J. (2010). Preferential tumour accumulation of gold nanoparticles, visualised by magnetic resonance imaging:

- Radiosensitisation studies in vivo and in vitro. *International Journal of Radiation Biology*, *86*, 692–700.
210. Townley, H. E., Rapa, E., Wakefield, G., & Dobson, P. J. (2012). Nanoparticle augmented radiation treatment decreases cancer cell proliferation. *Nanomedicine-Nanotechnology*, *8*, 526–536.
211. Townley, H. E., Kim, J., & Dobson, P. J. (2012). In vivo demonstration of enhanced radiotherapy using rare earth doped titania nanoparticles. *Nanoscale*, *4*, 5043–5050.
212. Liu, P. D., Jin, H. Z., Guo, Z. R., Ma, J., Zhao, J., Li, D. D., Wu, H., & Gu, N. (2016). Silver nanoparticles outperform gold nanoparticles in radiosensitizing U251 cells in vitro and in an intracranial mouse model of glioma. *International Journal of Nanomedicine*, *11*, 5003–5013.
213. Lien, J., Peck, K. A., Su, M. Q., & Guo, T. (2016). Sub-monolayer silver loss from large gold nanospheres detected by surface plasmon resonance in the sigmoidal region. *Journal of Colloid and Interface Science*, *479*, 173–181.
214. Jain, S., Hirst, D. G., & O'Sullivan, J. M. (2012). Gold nanoparticles as novel agents for cancer therapy. *The British Journal of Radiology*, *85*, 101–113.
215. Kotb, S., Detappe, A., Lux, F., Appaix, F., Barbier, E. L., Tran, V. L., Plissonneau, M., Gehan, H., Lefranc, F., Rodriguez-Lafrasse, C., et al. (2016). Gadolinium-based nanoparticles and radiation therapy for multiple brain melanoma metastases: Proof of concept before phase I trial. *Theranostics*, *6*, 418–427.
216. Rancoule, C., Magne, N., Vallard, A., Guy, J. B., Rodriguez-Lafrasse, C., Deutsch, E., & Chargari, C. (2016). Nanoparticles in radiation oncology: From bench-side to bedside. *Cancer Letters*, *375*, 256–262.
217. Norman, A., & Iwamoto, K. S. (1991). Therapy X-ray scanner, 5,008,907.
218. Uesaka, M., Mizumo, K., Sakumi, A., Meiling, J., Yusa, N., Nishiyama, N., & Nakagawa, K. (2007). Pinpoint KEV/MEV X-ray sources for X-ray drug delivery system. PAC, IEEE, Albuquerque, Vol. THPMN035, p. 2793.
219. Montenegro, M., Nahar, S. N., Pradhan, A. K., Huang, K., & Yu, Y. (2009). Monte Carlo simulations and atomic calculations for auger processes in biomedical nanotheranostics. *The Journal of Physical Chemistry. A*, *113*, 12364–12369.
220. Zhang, E., Ntumba, K., & Nadeau, J. (2010). Enhanced cytotoxicity of doxorubicin conjugated to ultrasmall au nanoparticles. *Nanotechnology*, *3*, 316–319.
221. Davidson, R. A., & Guo, T. (2016). Nanoparticle-assisted scanning focusing X-ray therapy with needle beam X rays. *Radiation Research*, *185*, 87–95.
222. Lukianova-Hleb, E. Y., Ren, X. Y., Sawant, R. R., Wu, X. W., Torchilin, V. P., & Lapotko, D. O. (2014). On-demand intracellular amplification of chemoradiation with cancer-specific plasmonic nanobubbles. *Nature Medicine*, *20*, 778–784.
223. Fan, W. P., Shen, B., Bu, W. B., Zheng, X. P., He, Q. J., Cui, Z. W., Zhao, K. L., Zhang, S. J., & Shi, J. L. (2015). Design of an intelligent sub-50 nm nuclear-targeting nanotheranostic system for imaging guided intranuclear radiosensitization. *Chemical Science*, *6*, 1747–1753.
224. Fan, W. P., Shen, B., Bu, W. B., Zheng, X. P., He, Q. J., Cui, Z. W., Ni, D. L., Zhao, K. L., Zhang, S. J., & Shi, J. L. (2015). Intranuclear biophotonics by smart design of nuclear-targeting photo-/radio-sensitizers co-loaded upconversion nanoparticles. *Biomaterials*, *69*, 89–98.
225. Koger, B., & Kirkby, C. (2016). Optimization of photon beam energies in gold nanoparticle enhanced arc radiation therapy using Monte Carlo methods. *Physics in Medicine and Biology*, *61*, 8839–8853.
226. Morita, K., Miyazaki, S., Numako, C., Ikeno, S., Sasaki, R., Nishimura, Y., Ogino, C., & Kondo, A. (2016). Characterization of titanium dioxide nanoparticles modified with polyacrylic acid and H₂O₂ for use as a novel radiosensitizer. *Free Radical Research*, *50*, 1319–1328.
227. Moeendarbari, S., Tekade, R., Mulgaonkar, A., Christensen, P., Ramezani, S., Hassan, G., Jiang, R., Oz, O. K., Hao, Y. W., & Sun, X. K. (2016). Theranostic nanoseeds for efficacious internal radiation therapy of unresectable solid tumors. *Scientific Reports*, *6*, 20614.

228. Chen, Y. Y., Song, G. S., Dong, Z. L., Yi, X., Chao, Y., Liang, C., Yang, K., Cheng, L., & Liu, Z. (2017). Drug-loaded mesoporous tantalum oxide nanoparticles for enhanced synergistic chemoradiotherapy with reduced systemic toxicity. *Small*, *13*, 1602869.
229. Chevillard, S., Vielh, P., Campana, F., Bastian, G., & Coppey, J. (1992). Cytotoxic effects and pharmacokinetic analysis of combined Adriamycin and X-ray treatments in human organotypic cell-cultures. *Anti-Cancer Drugs*, *3*, 133–137.
230. Shibamoto, Y., Zhou, L., Hatta, H., Mori, M., & Nishimoto, S. (2000). A novel class of antitumor prodrug, 1-(2'-oxopropyl)-5-fluorouracil (OFU001), that releases 5-fluorouracil upon hypoxic irradiation. *Japanese Journal of Cancer Research*, *91*, 433–438.
231. Mueller, A., Bondurant, B., & O'Brien, D. F. (2000). Visible-light-stimulated destabilization of PEG-liposomes. *Macromolecules*, *33*, 4799–4804.
232. Spratt, T., Bondurant, B., & O'Brien, D. F. (2003). Rapid release of liposomal contents upon photoinitiated destabilization with UV exposure. *Biochimica et Biophysica Acta-Biomembranes*, *1611*, 35–43.
233. Lopez, E., O'Brien, D. F., & Whitesides, T. H. (1982). Structural effects on the photopolymerization of bilayer-membranes. *Journal of the American Chemical Society*, *104*, 305–307.
234. Yavlovich, A., Smith, B., Gupta, K., Blumenthal, R., & Puri, A. (2010). Light-sensitive lipid-based nanoparticles for drug delivery: Design principles and future considerations for biological applications. *Molecular Membrane Biology*, *27*, 364–381.
235. Puri, A., & Blumenthal, R. (2011). Polymeric lipid assemblies as novel theranostic tools. *Accounts of Chemical Research*, *44*, 1071–1079.
236. Faisant, N., Siepmann, J., Oury, P., Laffineur, V., Bruna, E., Haffner, J., & Benoit, J. P. (2002). The effect of gamma-irradiation on drug release from bioerodible microparticles: A quantitative treatment. *International Journal of Pharmaceutics*, *242*, 281–284.
237. Roullin, V. G., Mege, M., Lemaire, L., Cueyssac, J. P., Venier-Julienne, M. C., Menei, P., Gamelin, E., & Benoit, J. P. (2004). Influence of 5-fluorouracil-loaded microsphere formulation on efficient rat glioma radiosensitization. *Pharmaceutical Research*, *21*, 1558–1563.
238. Fologea, E., Salamo, G., Henry, R., Borrelli, M. J., & Corry, P. M. (2010). Method of controlling drug release from a liposome carrier. US patent application number: US20120041357A1; priority date: Mar. 31, 2009.
239. Fologea, D., Salamo, G., Henry, R., Borrelli, M. J., & Corry, P. M. (2010). Method of controlled drug release from a liposome carrier, United State Patent: US 8808733 B2. Issued date: Aug. 19, 2014.
240. Juzenas, P., Chen, W., Sun, Y. P., Coelho, M. A. N., Generalov, R., Generalova, N., & Christensen, I. L. (2008). Quantum dots and nanoparticles for photodynamic and radiation therapies of cancer. *Advanced Drug Delivery Reviews*, *60*, 1600–1614.
241. Kobayashi, K., Usami, N., Porcel, E., Lacombe, S., & Le Sech, C. (2010). Enhancement of radiation effect by heavy elements. *Mutation Research, Reviews in Mutation Research*, *704*, 123–131.
242. Jelveh, S., & Chithrani, D. B. (2011). Gold nanostructures as a platform for combinational therapy in future cancer therapeutics. *Cancer*, *3*, 1081–1110.
243. Dreaden, E. C., Alkilany, A. M., Huang, X. H., Murphy, C. J., & El-Sayed, M. A. (2012). The golden age: Gold nanoparticles for biomedicine. *Chemical Society Reviews*, *41*, 2740–2779.
244. Coulter, J. A., Butterworth, K. T., & Jain, S. (2015). Prostate cancer radiotherapy: Potential applications of metal nanoparticles for imaging and therapy. *The British Journal of Radiology*, *88*, 20150256.
245. Dorsey, J. F., Sun, L., Joh, D. Y., Witztum, A., Al Zaki, A., Kao, G. D., Alonso-Basanta, M., Avery, S., Tsourkas, A., & Hahn, S. M. (2013). Gold nanoparticles in radiation research: Potential applications for imaging and radiosensitization. *Translational Cancer Research*, *2*, 280–291.
246. Kwatra, D., Venugopal, A., & Anant, S. (2013). Nanoparticles in radiation therapy: A summary of various approaches to enhance radiosensitization in cancer. *Translational Cancer Research*, *2*, 330–342.

247. Su, X. Y., Liu, P. D., Wu, H., & Gu, N. (2014). Enhancement of radiosensitization by metal-based nanoparticles in cancer radiation therapy. *Cancer Biology & Medicine*, *11*, 86–91.
248. Retif, P., Pinel, S., Toussaint, M., Frochot, C., Chouikrat, R., Bastogne, T., & Barberi-Heyob, M. (2015). Nanoparticles for radiation therapy enhancement: The key parameters. *Theranostics*, *5*, 1030–1045.
249. Brun, E., & Sicard-Roselli, C. (2016). Actual questions raised by nanoparticle radiosensitization. *Radiation Physics and Chemistry*, *128*, 134–142.
250. Haume, K., Rosa, S., Grellet, S., Smialek, M. A., Butterworth, K. T., Solov'yov, A. V., Prise, K. M., Golding, J., & Mason, N. J. (2016). Gold nanoparticles for cancer radiotherapy: A review. *Cancer Nanotechnology*, *7*, 8.
251. Rosa, S., Connolly, C., Schettino, G., Butterworth, K. T., & Prise, K. (2017). Biological mechanisms of gold nanoparticle radiosensitization. *Cancer Nanotechnology*, *8*(1).
252. Her, S., Jaffray, D. A., & Allen, C. (2017). Gold nanoparticles for applications in cancer radiotherapy: Mechanisms and recent advancements. *Advanced Drug Delivery Reviews*, *109*, 84–101.
253. Cho, S. H., & Krishnan, S. (2013). *Cancer nanotechnology: Principles and applications of radiation oncology*, W. R. Hendee (p. 284). Boca Raton: CRC Press.